

Universidade do Minho  
Escola de Engenharia

Pedro Filipe Lima Marques

Frictional Contacts in  
Multibody Dynamics





Universidade do Minho  
Escola de Engenharia

Pedro Filipe Lima Marques

## Frictional Contacts in Multibody Dynamics

Dissertação de Mestrado  
Ciclo de Estudos Integrados Conducentes ao  
Grau de Mestre em Engenharia Mecânica

Trabalho efectuado sob a orientação do  
Professor Doutor João Paulo Flores Fernandes

## DECLARAÇÃO

Nome: Pedro Filipe Lima Marques

Endereço eletrónico: a62055@alunos.uminho.pt    Telefone: 915034366

Cartão do Cidadão: 14043235

Título da dissertação: Frictional Contacts in Multibody Dynamics

Orientador:

Professor Doutor João Paulo Flores Fernandes

Ano de conclusão: 2015

Mestrado Integrado em Engenharia Mecânica

É AUTORIZADA A REPRODUÇÃO INTEGRAL DESTA DISSERTAÇÃO APENAS PARA EFEITOS DE INVESTIGAÇÃO, MEDIANTE DECLARAÇÃO ESCRITA DO INTERESSADO, QUE A TAL SE COMPROMETE.

Universidade do Minho, \_\_\_\_/\_\_\_\_/\_\_\_\_

Assinatura:

*“Feeling gratitude and not expressing it is like wrapping a present and not giving it.”*

William Arthur Ward

## ACKNOWLEDGMENTS

Reached the culmination of this work, I would like to leave a word of appreciation to those who contributed to its prosperity. My commitment was fundamental, but it would not have been possible to realize this work alone.

To Professor Paulo Flores, Full Professor in the Mechanical Engineering Department in University of Minho and my supervisor, I want to express my deep gratitude for his dedication, commitment and willingness to convey his knowledge and guide me through this journey. The dedication and rigor which he imposes on his work and requires from his co-workers will be, for me, an example for the future. I would also like to thank his friendship demonstrated along this path, which I will never forget.

My gratitude is extended to everyone who contributed to my success through their support and motivation, and some of them should be highlighted. To my parents, for the education they provided me, they will always be an example. To my sister, Inês, who sometimes drives me crazy, but, at the end, is always there. Finally, I want to thank Ana for all the confidences, for saying to me what I needed to hear and for being always very patient. She was undoubtedly a major support.



## ABSTRACT

This work has as primary goal to study the influence of friction modeling on the dynamic behavior of mechanical systems.

In this sense, an extensive literature review was conducted in order to present the main phenomena due to friction generated between two contacting surfaces. Furthermore, a comprehensive study of different friction modeling approaches was carried in order to explain the main characteristics of the most relevant static and dynamic friction models.

The comparison between different methodologies of friction modelling is presented in two distinct phases. The first consists in a simple system with one degree of freedom where friction plays a major role in the behavior of the system. The second phase involves more complex three-dimensional mechanical systems, where just a small part of the presented models is employed. In the latter phase, it is analyzed a kinematic translational joint with friction, where the friction force is implicitly calculated in the resolution of the equations of motion, and a spatial revolute joint with axial and radial clearance where friction is treated as an external force acting on the system.

Due to the use of multibody systems in the mentioned examples, it was necessary to introduce the three-dimensional formulation for their dynamic analysis, which in this case is based on the Newton-Euler equations. Some methods for solving the equations of motion are also discussed, as well as their efficiency and accuracy. The dynamic simulations of multibody systems performed in the context of this work were carried out using MUBODYNA (Flores, 2012).

The main conclusion of this study is that friction plays a key role in the behavior of multibody systems due to its energy dissipation properties. The main differences between the existing models are in the vicinity of zero relative velocity, thus the disparities occur during motion reversal.

**Keywords:**

- Friction;
- Multibody systems;
- Contacts;
- Simulation.



## RESUMO

Este trabalho tem como objetivo principal estudar a influência da modelação do atrito no comportamento dinâmico de sistemas mecânicos com múltiplos corpos.

Nesse sentido, uma vasta pesquisa bibliográfica foi efetuada, de modo a apresentar quais os principais fenómenos produzidos devido ao atrito gerado entre duas superfícies em contacto. Para além disso, um estudo abrangente sobre diferentes abordagens para o cálculo da força de atrito foi realizado de modo a explicar as características dos modelos de atrito mais importantes.

A comparação entre as diferentes metodologias de modelação de atrito é apresentada em duas fases distintas. A primeira consiste na utilização de um sistema simples com um grau de liberdade onde o atrito tem papel preponderante no comportamento sistema. A segunda fase considera sistemas mecânicos tridimensionais mais complexos, onde apenas é estudada uma pequena parte dos modelos apresentados. Nesta fase, analisa-se uma junta cinemática de translação com atrito, onde o atrito é calculado implicitamente na resolução das equações do movimento, e uma junta de revolução com folga radial e axial onde o atrito é tratado como uma força externa que atua no sistema.

Devido à utilização de sistemas multicorpo nos exemplos apresentados, foi necessário introduzir a formulação tridimensional para a sua análise dinâmica, que neste caso tem por base as equações Newton-Euler. Alguns métodos para a resolução das equações do movimento também são discutidos, bem como as suas eficiência e precisão. As simulações dinâmicas realizadas no âmbito deste trabalho foram executadas usando o código MUBODYNA (Flores, 2012).

A principal conclusão deste trabalho é de que o atrito tem um papel fundamental no comportamento de sistemas multicorpo devido às suas propriedades de dissipação de energia. As principais diferenças entre os modelos existentes encontram-se na vizinhança da velocidade relativa nula, posto isto, estas acontecem durante inversões de sentido.

**Palavras-Chave:**

- Atrito;
- Sistemas multicorpo;
- Contactos;
- Simulação.

# TABLE OF CONTENTS

Acknowledgments .....	iii
Abstract.....	v
Resumo .....	vii
List of Figures.....	xi
List of Tables.....	xv
List of Symbols.....	xvii
1. Introduction .....	1
1.1 Motivation and Objectives.....	1
1.2 Literature Review .....	3
1.3 Structure of the Dissertation .....	14
1.4 Contributions .....	15
2. Spatial Multibody Dynamics .....	17
2.1 Concepts and Formulations of Multibody Systems.....	17
2.2 Equations of Motion for Constrained Systems.....	20
2.3 Methods to Solve Equations of Motion.....	29
2.4 Example of Application.....	41
2.5 Summary and Conclusions .....	46
3. Friction Models for Multibody Dynamics.....	47
3.1 General Issues on Friction .....	47
3.2 Static Friction Models .....	51
3.3 Dynamic Friction Models .....	63
3.4 Example of Application.....	75
3.5 Summary and Conclusions .....	81
4. Demonstrative Examples of Application.....	83

4.1 Translational Joints with Friction .....	83
4.2 Spatial Revolute Joint with Axial and Radial Clearance.....	88
4.3 Spatial Revolute Joint with Clearance and Friction .....	104
4.4 Summary and Conclusions .....	110
5. Concluding Remarks .....	113
References .....	117

## LIST OF FIGURES

<b>Figure 1.1</b> - Differences between an elastic and a viscoelastic force models.....	9
<b>Figure 2.1</b> - Abstract representation of a multibody system.....	18
<b>Figure 2.2</b> - Representation of the Euler parameters. ....	21
<b>Figure 2.3</b> - (a) Holonomic constraint (revolute joint); (b) Nonholonomic constraint (wheel rolling over a plane).....	23
<b>Figure 2.4</b> - Four-bar mechanism with redundant constraints.....	23
<b>Figure 2.5</b> - Flowchart of dynamic analysis of multibody systems (Flores, 2012). ....	31
<b>Figure 2.6</b> - Spatial slider-crank mechanism. ....	41
<b>Figure 2.7</b> - Positions constraints violation ( $\Phi^T \Phi$ ). ....	43
<b>Figure 2.8</b> - Velocities constraints violation ( $\dot{\Phi}^T \dot{\Phi}$ ). ....	44
<b>Figure 2.9</b> - Variation of mechanical energy. ....	45
<b>Figure 2.10</b> - Comparison of computation time for different methods.....	45
<b>Figure 3.1</b> - The friction-velocity relation for a hysteresis loop.....	49
<b>Figure 3.2</b> - Pre-sliding displacement behavior.....	50
<b>Figure 3.3</b> - Relation between rate of force and break-away force. ....	51
<b>Figure 3.4</b> - Representation of Coulomb friction for 1D case. ....	52
<b>Figure 3.5</b> - Representation of the Coulomb model with stiction for 1D case. ....	53
<b>Figure 3.6</b> - Representation of Coulomb model with linear viscous friction for 1D case. .....	54
<b>Figure 3.7</b> - Representation of the Stribeck curve without viscous friction. ....	55
<b>Figure 3.8</b> - Representation of Karnopp model with Coulomb friction for 1D case. ....	56
<b>Figure 3.9</b> - Representation of Coulomb model with linear friction modification for 1D case. ....	57

<b>Figure 3.10</b> - Representation of Threlfall model for 1D case.....	58
<b>Figure 3.11</b> - Representation of the linear model with stiction for 1D case. ....	59
<b>Figure 3.12</b> - Representation of the Bengisu and Akay model for 1D case. ....	59
<b>Figure 3.13</b> - Representation of Ambrósio friction model for 1D case. ....	60
<b>Figure 3.14</b> - Representation of the Awrejcewicz et al. model for 1D case. ....	62
<b>Figure 3.15</b> - Physical interpretation of LuGre model.....	68
<b>Figure 3.16</b> - Physical interpretation of the elastic and plastic displacements. ....	69
<b>Figure 3.17</b> - Representation of the generalized Maxwell slip model.....	72
<b>Figure 3.18</b> - Representation of the Liang et al. bristle model. ....	74
<b>Figure 3.19</b> - Representation of the 1DoF spring-mass model.....	76
<b>Figure 3.20</b> - Results for static models without stiction. ....	77
<b>Figure 3.21</b> - Results for static models with stiction. ....	78
<b>Figure 3.22</b> - Results for dynamic models.....	79
<b>Figure 3.23</b> - Dynamic models behavior: friction force versus displacement. ....	80
<b>Figure 3.24</b> - Dynamic models behavior: friction force versus relative velocity. ....	81
<b>Figure 4.1</b> - Distinction of friction force acting on (a) an inner slider and (b) an outer slider. ....	85
<b>Figure 4.2</b> - Spatial slider-crank mechanism. ....	86
<b>Figure 4.3</b> - Comparison of the motion of the slider for different friction models: (a) position; (b) velocity; (c) acceleration; (d) detail of the acceleration...	87
<b>Figure 4.4</b> - Typical configuration of a spatial revolute joint with clearance.....	88
<b>Figure 4.5</b> - General configuration of a spatial revolute joint. ....	89
<b>Figure 4.6</b> - General configuration of a spatial revolute joint with clearance. ....	91
<b>Figure 4.7</b> - Representation of the different contact scenarios. ....	93
<b>Figure 4.8</b> - Configuration of a spatial revolute joint aligned with axial and radial contact.....	94
<b>Figure 4.9</b> - Configuration of a spatial revolute joint misaligned with axial and radial	

contact.....	96
<b>Figure 4.10</b> - Motion of the slider for simulation 1: (a) position; (b) velocity; (c) acceleration.....	101
<b>Figure 4.11</b> – Phase portraits for simulation 1: (a) Position-Velocity; (b) Velocity-Acceleration.....	101
<b>Figure 4.12</b> - Motion of the slider for simulation 2: (a) position; (b) velocity; (c) acceleration.....	102
<b>Figure 4.13</b> – Phase portraits for simulation 2: (a) Position-Velocity; (b) Velocity-Acceleration.....	102
<b>Figure 4.14</b> - Motion of the slider for simulation 3: (a) position; (b) velocity; (c) acceleration.....	103
<b>Figure 4.15</b> – Phase portraits for simulation 3: (a) Position-Velocity; (b) Velocity-Acceleration.....	103
<b>Figure 4.16</b> - Comparison of the variation of mechanical energy for the three simulations.....	104
<b>Figure 4.17</b> - Motion of the slider for Coulomb friction: (a) position; (b) velocity; (c) acceleration.....	106
<b>Figure 4.18</b> – Phase portraits for Coulomb friction: (a) Position-Velocity; (b) Velocity-Acceleration.....	106
<b>Figure 4.19</b> - Motion of the slider for Stribeck model: (a) position; (b) velocity; (c) acceleration.....	107
<b>Figure 4.20</b> – Phase portraits for Stribeck model: (a) Position-Velocity; (b) Velocity-Acceleration.....	107
<b>Figure 4.21</b> - Motion of the slider for Dahl model: (a) position; (b) velocity; (c) acceleration.....	108
<b>Figure 4.22</b> – Phase portraits for Dahl model: (a) Position-Velocity; (b) Velocity-Acceleration.....	108
<b>Figure 4.23</b> - Motion of the slider for LuGre model: (a) position; (b) velocity; (c) acceleration.....	109

<b>Figure 4.24</b> – Phase portraits for LuGre model: (a) Pos-Vel; (b) Vel-Acc. ....	109
<b>Figure 4.25</b> - Comparison of the variation of mechanical energy for the different friction models. ....	110



## LIST OF TABLES

<b>Table 2.1</b> - Dimensional and inertia properties of each body. ....	42
<b>Table 2.2</b> - Initial conditions for the dynamic analysis.....	42
<b>Table 2.3</b> - Parameters used for the dynamic simulation.....	43
<b>Table 3.1</b> - Simulation parameters for the spring-mass model. ....	76
<b>Table 3.2</b> - Parameters considered for the different friction models. ....	76
<b>Table 4.1</b> - Parameters considered for the different friction models. ....	87
<b>Table 4.2</b> – Geometric parameters of the joint for each simulation.....	100
<b>Table 4.3</b> - General parameters for simulation .....	100
<b>Table 4.4</b> - Parameters considered for the different friction models. ....	105



# LIST OF SYMBOLS

## Chapter 1

### Latin Symbols

Symbol	Unit (SI)	Description
$F_N$	N	Normal contact force
$K$	N/m <sup>3/2</sup>	Contact stiffness
$m$	-	Contact force damping exponent
$n$	-	Hertz's contact force exponent

### Greek Symbols

Symbol	Unit (SI)	Description
$\delta$	m	Penetration depth
$\dot{\delta}$	m/s	Penetration velocity
$\chi$	N/m <sup>5/2</sup>	Hysteresis damping factor

## Chapter 2

### Latin Symbols

Symbol	Unit (SI)	Description
$\mathbf{C}$	-	Auxiliary matrix for Moore-Penrose generalized inverse
$\mathbf{D}$	-	Jacobian matrix of the constraints equations
$e_0, e_1, e_2, e_3$	-	Euler parameters
$\mathbf{f}$	N	Vector of forces acting on a body
$\mathbf{G}$	-	Transformation matrix for Euler parameters
$\mathbf{g}$	N, N.m	Vector of generalized forces
$\mathbf{g}^{(c)}$	N, N.m	Vector of constraint reaction forces
$\mathbf{J}$	kg.m <sup>2</sup>	Inertia tensor

$k$	-	Total number of constraints
$L$	J	Lagrangian
$\mathbf{M}$	kg, kg.m <sup>2</sup>	Global mass matrix
$m$	-	Number of independent constraints
$m_b$	kg	Mass of a body
$m_c, d_c, k_c$	-	Mass, damping and stiffness coefficients for Penalty and Augmented method
$n$	-	Number of generalized coordinates
$\mathbf{n}$	N.m	Vector of moments acting on a body
$n_b$	-	Number of bodies
$n_{\text{DoF}}$	-	Number of degrees of freedom
$\mathbf{p}$	-	Euler parameters vector
$\mathbf{q}$	-	Vector of generalized coordinates
$\mathbf{R}$	-	Transformation matrix for independent velocities
$\mathbf{r}$	-	Global position vector
$T$	J	Kinetic energy
$t$	s	Time
$\mathbf{u}$	-	Dependent coordinates vector
$\mathbf{u}_e$	-	Unit vector to define Euler parameters
$V$	J	Potential energy
$\mathbf{v}$	m/s, rad/s	Generalized velocities vector
$\dot{\mathbf{v}}$	m/s <sup>2</sup> , rad/s <sup>2</sup>	Generalized accelerations vector
$\mathbf{w}$	-	Independent coordinates vector
$xyz$	-	Global coordinate system
$\mathbf{y}$	-	Auxiliary vector for integration

#### Greek Symbols

Symbol	Unit (SI)	Description
$\alpha, \beta$	-	Baumgarte stabilization coefficients
$\alpha, \mu, \omega$	-	Coefficients for Penalty and Augmented method
$\gamma$	-	Right hand side vector of accelerations constraint

		equations
$\Delta t$	s	Time step
$\varepsilon$	-	Tolerance for solving the equations of motion
$\Phi$	-	Vector of kinematic constraints
$\phi$	rad	Angle to define Euler parameters
$\xi\eta\zeta$	-	Body-fixed coordinate system
$\omega$	rad/s	Angular velocities vector

### Chapter 3

#### Latin Symbols

Symbol	Unit (SI)	Description
$C$	-	Attraction parameter
$c_b$	N.s/m	Bristle damping
$D_v$	m/s	Tolerance velocity
$F_b$	N	Hysteresis friction force at the beginning of a transition curve
$F_C$	N	Magnitude of Coulomb friction
$F_d$	N	Transition curve of hysteresis friction force
$\mathbf{F}_e$	N	External tangential force
$f$	-	Function for viscous effect
$F_h$	N	Hysteresis friction force
$F_N$	N	Normal contact force
$F_S$	N	Magnitude of static friction
$F_{S,a}$	N	Magnitude of static friction at the end of the previous sliding period
$F_{S,\infty}$	N	Magnitude of static friction after a long time at rest
$F_v$	N.s/m	Coefficient of viscosity
$g$	-	Function for the Stribeck effect
$k_b$	N/m	Bristle stiffness

$k_i$	N/m	Bristle stiffness
$k_s$	N/m	Spring stiffness
$m$	kg	Mass
$s$	-	Space variable for the relative displacement (Bli-man-Sorine)
$s$	-	Auxiliary variable to define friction regime (Gonthier)
$s_{dw}$	-	State variable to control frictional lag
$t_d$	s	Dwell-time
$\mathbf{v}_b$	m/s	Velocity of the belt
$v_0, v_1$	m/s	Tolerance velocities
$v_c$	m/s	Tolerance velocity
$v_d$	m/s	Threshold velocity
$v_S$	m/s	Stribeck velocity
$\mathbf{v}_T$	m/s	Relative tangential velocity
$\mathbf{x}$	m	Displacement vector
$\mathbf{z}$	m	Average bristle deflection
$z_{ba}$	m	Break-away bristle deflection
$z_{\max}$	m	Maximum bristle deflection

### Greek Symbols

Symbol	Unit (SI)	Description
$\alpha_i$	-	Scaling parameter
$\gamma$	s	Temporal parameter of the rising static friction
$\delta_\sigma$	-	Exponent to define the shape of Stribeck curve
$\mu_k$	-	Kinetic friction coefficient
$\mu_s$	-	Static friction coefficient
$\sigma_0$	N/m	Stiffness coefficient
$\sigma_1$	N.s/m	Damping coefficient
$\sigma_2$	N.s/m	Coefficient of viscosity

$\tau_{br}$	s	Bristle dynamics time constant
$\tau_{dw}$	s	Dwell-time dynamics time constant
$\tau_L$	s	Time constant of frictional memory

## Chapter 4

### Latin Symbols

Symbol	Unit (SI)	Description
<b>a</b>	-	Unit vector in bearing and journal axis
$c_a$	m	Axial clearance size
$c_r$	m	Radial clearance size
$c_e$	-	Coefficient of restitution
<b>D</b>	-	Jacobian matrix of the constraints equations
<b>F</b>	-	Matrix with relation between reaction and friction forces
<b>f</b>	N	Vector of forces acting on a body
<b>f<sub>F</sub></b>	N	Vector of friction forces
$F_N$	N	Normal contact force
<b>g</b>	N, N.m	Vector of generalized forces
$K$	N/m <sup>3/2</sup>	Contact stiffness
$L$	m	Length of bearing or journal
<b>M</b>	kg, kg.m <sup>2</sup>	Global mass matrix
$n$	-	Hertz's contact force exponent
<b>n</b>	N.m	Vector of moments acting on a body
<b>n<sub>d</sub></b>	-	Auxiliary vector to contact detection
<b>n<sub>v</sub></b>	-	Unit vector normal to the contact
$R$	m	Radius of bearing or journal
<b>r</b>	-	Global position vector
<b>s</b>	-	Global position vector on body coordinate system
<b>v</b>	m/s, rad/s	Generalized velocities vector
<b><math>\dot{v}</math></b>	m/s <sup>2</sup> , rad/s <sup>2</sup>	Generalized accelerations vector

$v_s$	m/s	Stribeck velocity
$\mathbf{v}_T$	m/s	Relative tangential velocity
$xyz$	-	Global coordinate system

#### Greek Symbols

Symbol	Unit (SI)	Description
$\gamma$	-	Right hand side vector of accelerations constraint equations
$\delta$	m	Penetration depth
$\dot{\delta}$	m/s	Penetration velocity
$\dot{\delta}^{(-)}$	m/s	Initial impact velocity
$\delta_\sigma$	-	Exponent to define the shape of Stribeck curve
$\lambda$	-	Lagrange multipliers vector
$\mu_k$	-	Kinetic friction coefficient
$\mu_s$	-	Static friction coefficient
$\xi\eta\zeta$	-	Body-fixed coordinate system
$\sigma_0$	N/m	Stiffness coefficient
$\sigma_1$	N.s/m	Damping coefficient
$\sigma_2$	N.s/m	Coefficient of viscosity
$\chi$	N/m <sup>5/2</sup>	Hysteresis damping factor
$\omega$	rad/s	Angular velocities vector



*“Live as if you were to die tomorrow. Learn as if you were to live forever.”*

Mahatma Gandhi

## **1. INTRODUCTION**

The rapid development of computer power led to the introduction of new methodologies for design and validation of mechanical systems. Nowadays, the market competitiveness demands the product optimization and cost saving which makes improper the utilization of trial and error procedures due to their money and time consuming. Moreover, more complex systems have been developed, and, therefore, difficulties of performing analytical analyzes arose. The Computer Aided Engineering (CAE) and Manufacturing (CAM) play an increasingly important role in the product development which requires that computational studies become more reliable. In order to have more realistic simulations, it is necessary to take into account all the effects that have a significant impact in the final results. This line of thought is applied in any engineering field, including multibody systems dynamics which is in the context of this work. This area involves the analysis of the motion and the forces generated in different mechanical systems. Bearing that in mind, this work intends to understand the influence of the frictional phenomena in dynamic simulation of multibody systems.

### **1.1 Motivation and Objectives**

The main objective of the current work is to study the influence of friction modeling on the dynamic behavior of mechanical systems. The friction forces can be found in all real mechanical systems that contain contacting surfaces with relative velocity. In most of the situations, these forces are not desired due to their dissipative effect and

wear production (Flores, 2009; Ylinen et al., 2014), while sometimes they are preponderant to the correct operation of the system (Teixeira et al., 2015; Park and Gschwendtner, 2015). Both situations require a rigorous evaluation of friction forces in order to obtain an accurate dynamic response of the system.

Several techniques are frequently employed to minimize the influence of friction forces, namely utilize a pair of materials with low friction coefficient, improve surface finishing, add fluid lubricant, or use intermediary elements as bearings. However, these procedures cannot completely eliminate the generation of friction forces and their effects during contact events. Thus, several researchers have been devoted to the study of friction phenomena and how to model the resultant behavior in the dynamic analysis of a mechanical system (Amontons, 1699; Coulomb, 1785).

The advances on technology allowed the scientists to perform more sophisticated experiments which contributed to the identification of several issues associated with friction. The investigation on frictional effects led to the development of several mathematical methodologies to describe its behavior. Due to the high complexity of this phenomenon, the researchers aspire to provide a model that fully describes the friction characteristics and, at the same time, can be easily implemented for the simulation of mechanical systems without requiring significant extra effort. The techniques available in the literature present distinct degrees of complexity, and it is of paramount importance to identify the most suitable approaches to use in the modelling of different systems.

One of the most important characteristics of friction force consists on being proportional to the normal contact forces. Since the collision between bodies generates high normal force levels, this feature reveals the importance of taking into account the frictional effects in mechanical systems with impacts. In this sense, the correct prediction of frictional behavior is highly dependent of the accurate evaluation of the contact forces. Therefore, this work aims to include the analysis of mechanical systems with impacts which involves dealing with the contact detection and selection of contact law.

To sum up, this work intends to deliver a general and comprehensive literature review in the multibody dynamics formulation, contact problems and, mainly, friction modelling. The comparison between different methodologies to evaluate the friction force will be undergone with utilization of simple multibody systems. The application examples represent distinct situations in which friction has different influence.

## 1.2 Literature Review

Multibody dynamics had a huge growth in the last century due to the advent of computational power. In that sense, several methodologies have been proposed to perform more efficient and accurate simulations. One of the most important issues in multibody dynamics is the interaction between the different bodies, therefore, the contact problems has had special attention by this community. The evaluation of the generated forces has supreme relevance in the response of the system. Among the different types contact forces, friction plays a significant role since it is a complex phenomenon which origins energy dissipation.

This section aim to provide a contextualization of these topics with a broad review of past work, including the most relevant landmarks in each field as well as a brief explanation of different approaches.

### 1.2.1 Multibody Dynamics

The field of study of multibody systems has its primordial origin in the Ancient Greece. At that time, most of the studies was carried only by the static analysis of very simple systems. Throughout the following centuries, some advances were performed in the dynamic analysis of mechanical systems, several fundamental concepts were introduced such as inertia, momentum, work of a force, among others. Although, these developments were mainly based on empirical knowledge of the researchers.

The emergence of classical mechanics<sup>1</sup> was a paramount breakthrough for this field of expertise. Newton (1686) introduced the law of universal gravitation and the laws of motion, which enabled the analytical study of the motion of a free particle that is the most basic element in a MBS. The equations of the dynamics of a rigid body were found by Euler (1776), who extended Newton's work with rotational motion.

A system of constrained rigid bodies was considered originally by d'Alembert (1743), who used the principle of the virtual work to present the concept of dynamic equilibrium. Thus, d'Alembert stated that the sum of the external forces acting on a system and its inertial forces must be zero. A mathematical formulation based on energy analysis from the d'Alembert principle by Lagrange (1788). Hence, the Lagrange's equations of the first and second kind emerged. The former represents a set of differen-

---

<sup>1</sup> Classical mechanics is often called Newtonian mechanics since most of studies developed in this field is based on the work of Isaac Newton (1642-1727).

tial algebraic equations (DAE) which treats the constraints explicitly, while the latter expresses a set of ordinary differential equations (ODE) with smaller number of equations. This formulation was developed by Hamilton with the principle of least action.

In the subsequent years, several other researchers have been devoted to the study of the dynamic of multibody systems, although the computational limitations prevented a faster development of this area. The systems under study had to be widely simplified.

The increase of computational power along with the need of creating models for more complex mechanical systems led to the development of computer algorithms based on the classical mechanics formulation. Since then, the multibody simulation field has two main goals. The first consists in the increase of simulation speed by developing more efficient methods to solve the equations of motion and using more adequate numerical integrators. The second ambition is including more complex issues in order to have more realistic simulations, i.e., taking into account contacts, impacts, fluid interaction, etc.

In order to solve the equations of motion of a constrained multibody system, the standard Lagrange multipliers technique can be employed. However, during the integration process, this method cannot guarantee the fulfillment of constraints of positions and velocities. To overcome this problem several methodologies have been presented, their objectives are the elimination or stabilization of the violation of constraints, handling redundant constraints and dealing with singular positions.

Baumgarte (1972) proposed a method to stabilize the constraints by adding feedback terms during the resolution of the equations of motion, which became the most used technique. From this approach, some other methodologies to stabilize the constraints appeared, as the work of Park and Chiou (1988) or Weijia et al. (2000). Bayo et al. (1988) presented two alternative formulations to stabilize the constraints, the penalty method and the augmented Lagrangian formulation. These two approaches are also based on the utilization of penalty terms to stabilize the constraints. However, these techniques have to solve a smaller number of equations, can handle redundant constraints and deal with singular configurations.

The coordinate partitioning method (Wehage and Haug, 1982) is also a popular technique to eliminate the violation of the constraints. In this approach, only the independent coordinates are integrated, since the dependent coordinates can be evaluated from them.

Another typology of methods to deal with constraints violation is the direct cor-

rection formulations, these approaches eliminate the violations after the integration process by forcing the positions and velocities to fulfill their constraints. Some examples of these methods can be found in the literature (Yoon et al., 1994; Blajer, 1995; Yu and Chen, 2000; Flores, 2013).

Another methodologies to solve the equations of motion which do not handle the violation of constraints have been proposed. García de Jalón and Bayo (1994) described a method based on the transformation matrix from the independent velocities to the generalized velocities. This approach requires to solve a small number of equations and, since it uses independent quantities, it is indicated for inverse dynamic analysis. Arabian and Wu (1998) introduced a methodology to solve equations of motion with redundant constraints or singular configurations. Recently, García de Jalón and Gutierrez-Lopez (2013) studied some issues of the analysis of multibody systems in the presence of redundant constraints and singular mass matrix.

The rapid growth of the multibody systems dynamic community generated the need of having the knowledge and information gathered. Thus, a set of textbooks had been published about this topic. The first textbook was written by Wittenburg (1977). Some years later, Roberson and Schwertassek (1988) presented the kinematic and dynamic analyzes of one and several rigid bodies. Nikravesh (1988) and Haug (1989) gave more emphasis to the computer aided analysis. Shabana (1989) studied flexible multibody systems, Huston (1990) also covered this topic. The numerical methods for multibody dynamics were treated by Amirouche (1992). García de Jalón and Bayo (1994) focused on efficient methods to achieve real time simulation.

A considerable number of computational programs were developed deliberately for the kinematic and dynamic analyzes of MBS. Schiehlen (1990) gathered contributions on the most relevant software for multibody dynamics at the epoch. Nowadays, several computational programs capable of automatic generation and integration of the equations of motion have been developed are used to perform dynamic analysis of multibody systems, their main advantages are the easiness of implementing the system and its constraints, when compared with dedicated codes. Some examples of commercial programs are Adams, SIMPACK, SimWise 4D, COMSOL, RecurDyn or NEW-EUL.

The kinematic and dynamic analyzes of multibody systems have a comprehensive scope. This area of expertise has extended its influence to a wide range of applications, such as railway vehicles (Pombo and Ambrósio, 2008), road vehicles (Ambrósio and

Verissimo, 2009), robotics (Ben Horin et al., 2006), mechanisms (Flores, 2011), spacecrafts (Xu et al., 2014) or biomechanics (Aoustin and Formalskii, 2013).

### 1.2.2 Contact Problems

During the dynamic analysis of a multibody system, it is frequent to deal with contacts or impacts between two or more bodies. The contact and impact modelling is a fundamental issue when studying MBS since the selected constitutive force laws affect significantly its motion. Impact is a complex phenomenon characterized by a very short duration, high force levels, rapid energy dissipation, and large changes in the velocity of the bodies. In turn, contact is a continuous process which occurs during a finite time. The contact mechanics problems are still an open field in several engineering areas, such as biomechanics (Machado, 2013), railway dynamics (Pombo and Ambrósio, 2012), crashworthiness (Sousa et al., 2008) or mechanisms (Flores et al., 2010).

The resolution of contact problems involve two main phases. The first is the contact detection which can be a straightforward task and solved analytically if the colliding geometries have a simple shape, as in the case of two spheres (Kim et al., 2005). However, in the general case, the contact detection is a very complex assignment due to the assumption of contact between arbitrary surfaces (Nassauer and Kuna, 2013). This type of contact evaluation can be divided into polygonal and non-polygonal models. In turn, the former divides in structured and Polygon soups, while the latter comprises constructive solid geometry, implicit surfaces and parametric surfaces (Lin and Gottschalk, 1998). Further review of the geometric contact detection can be found in the work of Machado (2013). The second phase consists on the evaluation of the contact forces. This step depends on the selected approach to model the contact problem, the force law has a paramount influence in the dynamic response of a system and it is chosen based on the geometry, the kinematics of the bodies and their materials.

A real collision between two bodies is a dissipative phenomenon, therefore, the kinetic energy immediately before and after the impact is not equal. In order to measure this effect, it is used the coefficient of restitution which gives the ratio of the relative normal velocity before and after collision (Seifried et al., 2010; Jackson et al., 2010). The value of this parameter is typically a real number bounded by 0 and 1, and it defines the type of collision. A null coefficient of restitution represents a fully plastic contact, while a coefficient of restitution equal to one denotes a perfectly elastic contact.

During a contact event between two or more bodies, two main types of normal

forces can be generated, they are attractive or repulsive. The attractive forces have their origin in the adhesion of the contacting surfaces, they are modelled based on van der Waals forces (Hamaker, 1937) or surface energy approaches, such as JKR model (Johnson et al., 1971), DMT model (Derjaguin et al., 1975) or Maugis adhesion theories (Maugis, 1992). This type of contact problems is out of the scope of the present work, therefore, the attractive forces will not have any further mention. In turn, the repulsive forces aim to separate the contacting bodies, and they can be evaluated based on two approaches: nonsmooth dynamics and regularized contact models (Johnson, 1985; Pfeiffer, 2008; Flores, 2010).

The Linear Complementary Problem (LCP) is one of the most well-known approaches within the nonsmooth dynamics context (Pfeiffer and Glocker, 1996). This technique is built in the assumption that the contacting bodies are truly rigid and, therefore, local deformations cannot happen. Thus, this method uses unilateral constraints to solve the contact dynamics and determine the impulses that prevent the penetration of the surfaces. The Signorini's condition (Signorini, 1933) was among the first contributions to the resolution of contact problems with LCP formulation. The main foundation of this approach is considering two quantities, the distance of the potential contact points and the normal contact force, which must be non-negative values in the sense that it cannot occur interpenetration and the forces are not attractive, respectively. Moreover, the product of these variables must always be zero, i.e., either the distance is zero or the normal force is zero. The employment of a LCP formulation in the modelling of contact-impact events requires the adoption of different methods to solve the equations of motion during contact (Glocker and Studer, 2005).

Alternatively to the nonsmooth approaches, the regularized contact models are also a widely used technique to evaluate the contact forces for multibody dynamics formulation (Koshy et al., 2013). These contact models allow the local deformation of the bodies and their interpretation. The magnitude of normal contact forces is calculated as a continuous function of the penetration depth. These approaches evaluate the contact loads as the bodies contain a spring-damper connection. The employment of regularized contact models in multibody dynamics simulation do not consider any kinematic constraint, instead, the contact forces are treated as external forces acting on the colliding bodies in opposite directions. The contact modeled by these continuous approaches comprehends two main phases, the compression and the restitution. The former corresponds with the approximation of the bodies until the relative normal velocity is zero

and the indentation depth reaches its maximum. During the restitution phase, the bodies are separating and some of the energy absorbed in the compression phase is restored. An accurate identification of the instant of the impact has supreme importance to the correct evaluation of the contact forces, otherwise the initial contact force may be exceedingly large due to initial high penetration (Flores and Ambrósio, 2010). One of the main shortcomings of these techniques is the selection of parameters of each model, such as the stiffness or the degree of nonlinearity. The choice of these parameters can embrace different methodologies, for simple geometries, analytical expressions can be used, though, for an arbitrary shape, experimental or computational methods (as Finite Element Method) can be adopted (Brutti et al., 2011; Bai and Zhao, 2012).

In the present work, only regularized contact force models will be further mentioned, since the author adopted this methodology to model the impacts in the upcoming chapters.

The first main contribution for the study of dynamic contacts was made by Hertz (1881) who analyzed the contact stresses between two perfectly elastic bodies. Hertz's law describe the normal contact force as a nonlinear function of indentation and can be stated as

$$F_N = K\delta^n \quad (1.1)$$

where  $\delta$  expresses the relative penetration,  $K$  denotes the stiffness of the contact and  $n$  is an exponent that defines the degree of nonlinearity. This exponent is usually defined as 1.5 for the case where there is a parabolic distribution of contact stresses, according Hertzian approach. The value of this parameter can adjusted for different materials or geometries in order to meet the experimental data. When this exponent is equal to one, it is said that is a Hookean relation due to the similarities with Hooke's law. That is the case of Kelvin-Voigt approach which models the contact as a linear spring and a linear damper associated in parallel which have in consideration the energy loss during the impact. Although, this model contains some physical impossibilities, since, at the beginning of the contact, the force is not continuous and, at the end of the restitution phase, the force is negative which implies the attraction of the bodies.

The Hertz's contact law was the basis for the development of the large set of impact force models. However, this approach does not consider energy dissipation which plays an important role in contact impact events. In that sense, Hunt and Crossley (1975) proposed a more realistic contact force model that improves Hertz's law with the



introduction of a nonlinear damping term which should be proportional to the power of the indentation. These contact force laws are known as viscoelastic, and can be distinguished from the elastic models by having different behavior during loading and unloading phases, as it is represented in Figure 1.1. This methodology was an important breakthrough in the impact of modelling, and for, a generic contact model, it can be expressed in the following form

$$F_N = K\delta^n + \chi\delta^m\dot{\delta} \quad (1.2)$$

where  $\chi$  is the hysteresis damping factor,  $\dot{\delta}$  represents the indentation velocity,  $m$  is an exponent that defines the behavior of the damping term, and the remaining parameters were already defined. The Hunt and Crossley (1975) model considers that  $n=m$  which means that the damping term is weighted by the elastic force. This characteristic was followed by several other contact laws (Herbert and McWhannell, 1977; Lee and Wang, 1983; Lankarani and Nikravesh, 1990; Gonthier et al., 2004; Zhiying and Qishao, 2006; Flores et al., 2011a). The main difference between these approaches is the determination of the hysteresis damping factor. This parameter is usually calculated based on the initial impact velocity, the contact stiffness and the coefficient of restitution. The relation between the latter and the hysteresis damping factor is the major distinction among the contact models which can be divided in two main categories (Alves et al., 2015): (i) the energy based approaches, as it is the case of the methodologies presented by Hunt and Crossley (1975), Lankarani and Nikravesh (1990), and Flores et al. (2011a); and (ii) the direct inclusion of equation of motion, such as the approach of Helbert and McWhannell (1977), Lee and Wang (1983), and Gonthier et al. (2004).

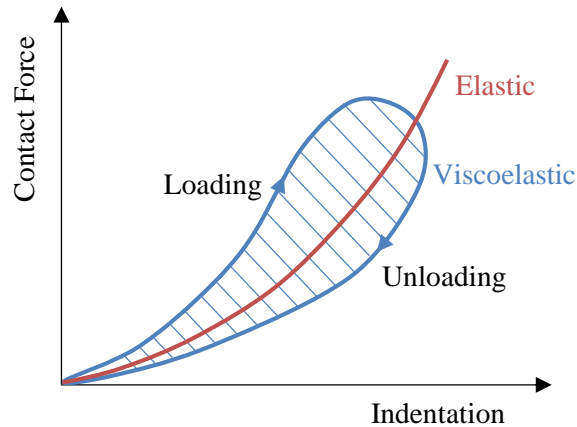


**Figure 1.1** - Differences between an elastic and a viscoelastic force models.

Most of the abovementioned models are only valid for high coefficients of restitu-

tion (larger than 0.7), since the hysteresis damping factor does not increase significantly with the decreasing of the coefficient of restitution. In turn, the approaches proposed by Gonthier et al. (2004) and Flores et al. (2011a) can be employed in the full range of the coefficient of restitution.

Nearly all of the previous presented models were originally derived for contacts between spherical bodies, i.e., for ellipsoidal contact areas. However, several of these models are used in other types of geometries, such as in cylindrical contacts. Although, there are some contact laws specially developed to model the contact between two cylinders (Radzimovsky, 1953; Goldsmith, 1960; Dubowsky and Freudenstein, 1971; ESDU-78035 Tribology Series, 1978; Johnson, 1985). Most of these approaches express the contact force as an implicit function of indentation, which, in the context of a forward dynamic analysis, it is necessary to apply an iterative method to evaluate the contact force. More detailed explanation on the cylinder contact force models can be found in the work of Pereira et al. (2011).

The contact force models discussed earlier do not consider any permanent deformation, ergo they are only accurate for low impact velocities since, in this case, the energy dissipation is related to internal damping or heat. Thus, these models are only valid if the impact velocity is lower than  $10^{-5}(E/\rho)^{1/2}$  and, therefore, negligible when compared with the propagation speed of deformation waves across the bodies. For high impact velocities, the main mechanism for energy dissipation is the plastic deformation of the surfaces. Goldschmidt (1960) proposed an alternative contact law based on Hertz's approach that includes permanent indentation. Lankarani and Nikravesh (1994) also studied this methodology and the identification of the parameters.

The selection of the contact law to evaluate the normal force has paramount importance, since it highly affects the dynamic response of the system (Flores et al., 2006a). Further description and explanation of the contact force models can be found in the review papers of Gilardi and Sharf (2002), Machado et al. (2012), and Alves et al. (2015).

### **1.2.3 Frictional Contacts**

Friction is generally related to the resistance to the relative motion between different surfaces in contact. There are different phenomena associated with friction, such as the dry friction and the lubricated friction. Friction is a highly complex phenomenon, which occurs in all mechanical systems. In some cases the presence of friction is desira-

ble, e.g. while walking or braking a car. However, friction has in general provided resistance and could have negative effects.

Due to its importance, friction has been studied over the centuries. One of the first works appeared in the 16th century resulting from Leonardo da Vinci's work, who stated that the friction force is proportional to normal load, opposes to the motion, and is independent of the contact area. Later, Amontons (1699) corroborated with da Vinci. Coulomb (1785) stated that friction was independent of velocity magnitude, and developed the first friction model.

Coulomb friction law was the predecessor for all of the friction models. This approach is very simple and only needs one parameter to be implemented, the coefficient of friction. However, it fails on describing most of the frictional effects, and presents a discontinuity for the friction force at zero velocity since the force is dependent on the direction of the relative velocity. This discontinuity is an important issue for dynamic simulations because it introduces numerical instability in the system.

Further researches on frictional behavior suggested the existence of higher friction forces at rest (Morin, 1833; Rabinowicz, 1951), which led to consider two different friction coefficients, one for static friction and another for kinetic friction. These differences on the friction force provoke the occurrence of the stick-slip phenomenon (Rabinowicz, 1956; Dieterich, 1978). Several researchers have experimentally verified the influence of this phenomenon on the mechanical systems response (Awrejcewicz and Olejnik, 2007; Chatelet et al., 2008; Berger and Mackin, 2014).

Stribeck (1902) proposed a steady state curve for the friction force as a function of relative sliding velocity. The continuous decreasing of friction force from static to kinetic friction is the main characteristic of the Stribeck effect. This dependence contradicts the Coulomb's law which considers that friction force magnitude is not affected by changes of relative velocity. However, Coulomb friction is still widely used due to its simplicity, and, for that reason, several friction models were developed based on modifications of Coulomb's approach (Threlfall, 1978; Ambrósio, 2003; Andersson et al.; 2007). Most of these models aim to eliminate the discontinuity at zero velocity.

The primal friction models were very simple, although the complexity associated to frictional effects introduced the need to develop models more robust. These models seek to capture several phenomena, such as viscous friction, stick-slip, frictional lag, among others (Berger, 2002).

A significant number of friction models can be found in the literature. In order to

perform a comparative analysis, they are usually classified. This division can be done by complexity or chronology, although the most utilized criterion consists on the separation between static and dynamic models (Olsson et al., 1998; Iurian et al., 2005; Andersson et al., 2007; Marques et al., 2015). On the one hand, the static models usually describe the steady state behavior of the friction force, and are, in general, simpler. On the other hand, the dynamic models aim to describe friction more realistically due to the introduction of extra state variables.

Since Coulomb friction model is not capable of describing most of friction characteristics, other static models have been suggested. Several researchers proposed different mathematical expressions to describe the Stribeck curve (Tustin, 1947; Hess and Soom, 1990; Popp and Stelter, 1990; Armstrong-Hélouvry, 1991; Makkar et al., 2005), although the exponential approximation presented by Bo and Pavelescu (1982) showed greater acceptance. Karnopp (1985) suggested an approach in which the friction force is evaluated as the relative velocity is null within a velocity range. This model eliminates the discontinuity at zero velocity, and it is capable to capture stick-slip motion. In order to overcome some numerical instability of Karnopp model, Leine et al. (1998) proposed the switch model. Armstrong-Hélouvry et al. (1994) presented a survey on friction models, and introduced the seven parameter model which is constituted by two state equations, one for sliding and another for sticking. More recently, Wojewoda et al. (2008) proposed a model which describes the hysteretic behavior of friction, and Awrejcewicz et al. (2008) modelled the friction force as a function of the external tangential force for low velocities.

The dynamic models emerged along with the need of capturing some friction characteristics that the static models were not able to describe. Dahl (1968, 1976) introduced the first dynamic model based on the stress-strain curve to model the frictional behavior of bearing balls. Comparing to Coulomb friction law, both models do not capture stick-slip motion, but it was shown Dahl model presents better results (Pennestrì et al., 2007; Ksentini et al., 2012), since this model is capable to describe the pre-sliding displacement.

Most of the dynamic friction models are based on the physical interaction between the surfaces asperities, such as the bristle model (Haessig and Friedland, 1991), the reset integrator (Haessig and Friedland, 1991), the LuGre (Canudas de Wit et al., 1995), the Elasto-Plastic (Dupont et al., 2000), among others (Swevers et al., 2000; Lampaert et al., 2003; Al-Bender et al., 2004; Gonthier et al., 2004; De Moerlooze et al., 2010;

Oleksowicz and Mruk, 2011; Liang et al., 2012). Generally, these approaches consider an extra state variable related to the bristles deflection. Haessig and Friedland (1991) proposed a bristle model that considers several simultaneous contacts between bristles which introduces a random behavior. The same authors had presented the reset integrator model which models the friction force as a function of the average bristle deflection. Later, Canudas de Wit et al. (1995) developed the LuGre model based on the work of Dahl (1968) and Haessig and Friedland (1991). Swevers et al. (2000) introduced Leuven model which consists on a modification of LuGre with the inclusion of pre-sliding hysteresis. The same authors (Lampaert et al., 2003; Al-Bender et al., 2005) proposed the generalized Maxwell slip (GMS) model which similarly to the bristle model considers more than one contacting element. Dupont et al (2000) presented the elasto-plastic friction model as an improvement of LuGre, since its capacity of capturing stiction is enhanced. Gonthier et al. (2004) also introduced a modification of LuGre model by considering dwell-time dependence. Liang et al. (2012) proposed a three-dimensional bristle model which is an extension of the reset integrator.

Bliman and Sorine (1995) presented a family of friction models based on Dahl model. Harnoy and Friedland (1994) studied the frictional behavior of lubricated journal bearings, and proposed a dynamic model to estimate the friction force taking into account the hydrodynamics effects.

There are several studies providing the comparison between different friction models with the objective of deciding which is more suitable for a certain application. Hensen et al. (2003) showed that LuGre and switch model present a similar behavior. Hassan and Rogers (2005) investigated different friction models to simulate the contact between a preloaded tube and its support. Garcia (2008) compared several models on the simulation of a control valve. A two state elasto-plastic model was presented by Ruderman and Bertram (2013) and its behavior was compared with LuGre and GMS model.

One of the most important reasons in the choice of the model to adopt, it is the easiness to establish the parameters to be used on the simulation and its quantity. Dahl (1977) proposed an experimental methodology to determine the parameters of his model (Dahl, 1968). The selection of the static and kinetic friction coefficients was addressed by Borsotto et al. (2009). The parameters for Karnopp friction model have been also studied (Liu et al., 2009; Bicakci et al., 2014). Wu et al. (2011) introduced an experimental procedure to the identification of the parameters of LuGre model to simulate tire

friction. Piatkowski (2014a) studied parameters selection for Dahl and LuGre, and concluded that a certain set of parameters is only valid for a normal external force range.

The experimental validation of friction modelling is of paramount importance to ensure the proficiency to model the several phenomena associated with friction. Lamparter et al. (2002) provide a comparison between a static model with Stribeck curve, Dahl, LuGre and Leuven, they showed that Leuven model has a better agreement with experimental results. Tjahjowidodo et al. (2005) used a DC motor to provide a comparison between Coulomb, Stribeck static friction, LuGre and GMS approaches, and the results present a better fit for GMS model. They also saw that for high velocities the Coulomb and Stribeck models also provide good results. Liang et al. (2012) used two experimental test rigs to validate the friction model proposed. More recently, Liu et al. (2015) performed a study where the behavior modelled by Coulomb, Stribeck, Dahl, LuGre and Elasto-Plastic approaches has been compared with the experimental measurements, and the results showed that LuGre presents a more similar behavior.

### **1.3 Structure of the Dissertation**

This work aims to deliver a comprehensive study on the analysis of frictional contacts in multibody systems dynamics. Bearing that in mind, the most important issues about multibody dynamics, contact problems and friction modelling have to be addressed. For that purpose, this dissertation was divided in five chapters that will be explained hereinafter.

In Chapter One, an overview of the entire dissertation is provided, and a broad review of literature is presented to recognize the scope of the current work.

Chapter Two introduces the most basic concepts for the dynamic analysis of multibody systems, and presents the Newton-Euler formulation to build the equations of motion for constrained multibody systems. Several methodologies can be employed to solve the equations of motion, some of those techniques are described in this chapter as well as their aptitude to deal with the violation of constraints or redundant constraints. Finally, a spatial slider-crank mechanism is utilized to compare the accuracy and efficiency of different methods in a forward dynamic analysis.

Chapter Three focuses on the friction modelling and the associated issues. Since friction is a complex phenomenon, its main characteristics should be correctly described, in that sense, stick-slip motion, viscous friction, frictional lag, pre-sliding dis-

placement and break-away force are explained. The friction force models are divided in two groups, and the most relevant static and dynamic friction models are presented. In order to compare these models, the well-known example of a single degree of freedom mass-spring model is employed.

In Chapter Four, some examples are performed to study the influence of different friction models in the dynamic response of a multibody system. The first situation consists on the inclusion of friction to a kinematic translational joint. The second example deals with a spatial revolute joint with clearance which introduces impact problems. The third, and last, involves the introduction of friction modelling in the previous case.

Finally, Chapter Five summarizes the most relevant conclusion of this work and presents some perspectives for future work.

## **1.4 Contributions**

A general overview of spatial multibody systems formulation was introduced. The most relevant methods for solving the equations of motion were described and compared through the dynamic analysis of a mechanism.

This work provides a comprehensive review of the literature about friction modelling in multibody systems. In this sense, it is presented a detailed description of the most relevant friction force models. A fair comparison between the different friction models is delivered recurring, at first, to a simple system with one-dimensional motion and, then, to a spatial slider-crank mechanism.

Furthermore, a new methodology to deal with spatial revolute joints with both axial and radial clearance has been proposed. The contact detection technique and the contact forces evaluation were presented, and this model is used to study the influence of friction.





*“Laziness is the mother of progress.*

*If man had not been too lazy to walk, he would not have invented the wheel.”*

Mário Quintana

## **2. SPATIAL MULTIBODY DYNAMICS**

Multibody system dynamics relies on the study of a set of different bodies which are interconnected by kinematic joints and undergone to the action of force elements. The multibody systems analysis dates back to Newton (1687), who derived the equations of motion for a free particle. However, with the increase in computational power during the past decades, several researchers have been devoted to this subject due to the wide range of applications on the science and engineering fields. They developed a new branch of computer programs, extended the number of existing formulations, and augmented the range of influence of this field of knowledge.

In this chapter, the main formulations for MBS will be discussed. The equations of motion for a constrained multibody system will be defined, and several methods to solve them will be considered. Then, a 3D slider-crank mechanism will be used as an illustrative example for the comparison of the presented methods.

### **2.1 Concepts and Formulations of Multibody Systems**

The bodies that constitute the multibody system represent mechanical components, and they generally can describe large translational and rotational displacements. These bodies can be considered either rigid either flexible. All bodies present a finite deformation when they are on duty, although, in some situations, that deformation can be negligible compared to the global motion of the system. In those cases, it is fair considering the assumption of a rigid body, which can be fully described by six coordinates

since it cannot change its shape. In turn, flexible bodies have an elastic structure, and beyond the same six coordinates, to be fully described, they need one extra coordinate per degree of freedom of deformation. For a large number of applications, it is fair to assume a system with rigid bodies, which makes the problem simpler and faster to solve. In the scope of the present work, it will only be considered rigid bodies.

The joints are responsible for connect different bodies in a multibody system. There are several types of joints, being spherical, revolute or translational joints, which are, in practice, represented by mechanical components such as bearings, sliders, wheels, among others. The joints can be treated as perfect or imperfect joints. For one hand, the perfect or ideal joints are defined by kinematic constraint equations which introduce restrictions on the kinematical degrees of freedom. For the other hand, imperfect joints take into account some physical phenomena, such as clearance, friction or lubrication, which produces an analysis with more similarities with its real behavior. In this case, the joints are, in general, defined by force constraints instead of kinematic constraints.

Taking into account force elements is what distinguish a dynamic analysis from a kinematic. There are several types of force elements which can be classified according to their source, such as contact-impact forces, gravitational forces, spring-damper-actuator forces, among others.

Bodies, joints and forces are the three main elements of a multibody system, as it is presented in the abstract representation in Figure 2.1.

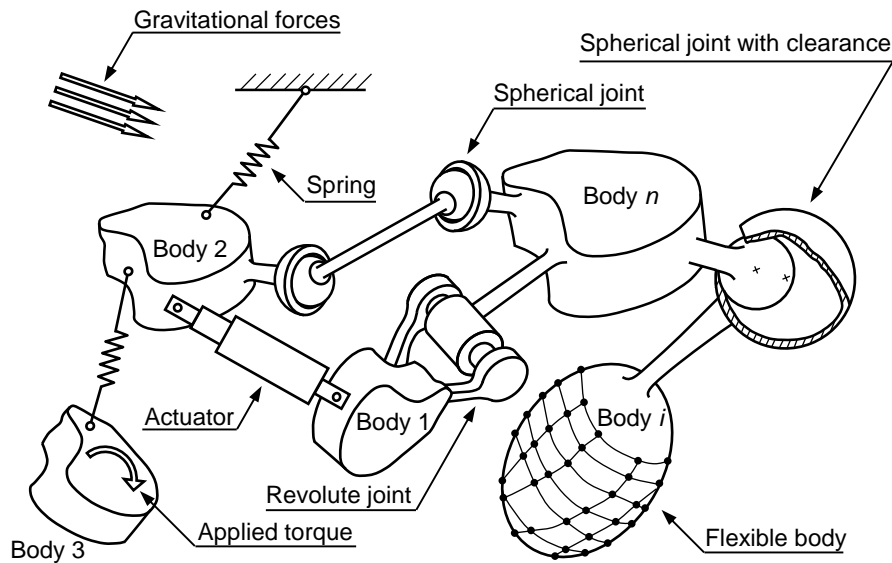


**Figure 2.1** - Abstract representation of a multibody system.

One of first steps in the study of a multibody system is the determination of the number of degrees of freedom (DoF), which is the minimum number of variables necessary to fully describe the system configuration. If the constraint relations are not taking into account, each body has six degrees of freedom. However, the introduction of kinematic joint will restrict number of DoF, which will depend on the type of the joint. For a general multibody system, the number of DoF can be calculated by

$$n_{\text{DoF}} = 6n_b - m \quad (2.1)$$

where  $n_b$  denotes the number of bodies that constitute the system and  $m$  is number of independent constraints. When the number of DoF is null or negative, the system is a structure.

Regardless of the used formulation, the equations of motion express the relation between motion and forces. Hence, they can be solved for each of them. Using the forces as an input information, it is possible perform a direct analysis of the system in order to calculate its motion. Nevertheless, if it is known the motion of the system, the force elements acting on the bodies can be determined solving equations of motion, called inverse analysis. In the scope of this work, only direct dynamic analysis will be performed.

Before performing a dynamic analysis of a multibody system, it is of paramount importance to choose the formulation to be implemented, which is deeply associated with the type of coordinates adopted.

A straightforward approach is considering a system as a group of connected free bodies using Newton-Euler method (Nikravesh, 1988). There are introduced three equations for translational accelerations and three equations for the rotational accelerations. The kinematic joints are included by adding an additional set of algebraic constraint equations, which is used along the Lagrange multipliers technique to find the reaction forces. This method will have a more detailed explanation later on this chapter. This approach is based on body-coordinate formulation (absolute coordinates), and it is easy to implement. However, it involves the construction of a large set of equations which leads to computational inefficiency. This drawback makes it more suitable for systems with a small number of bodies.

Alternatively, it can be used a point-coordinate formulation (natural coordinates) which considers each body as collection of points and vector. In this case, most of the constraints do not arise from the kinematic joints, but rather from the bodies. As the

previous formulation, point-coordinate formulation also yields a large set of equations (Nikravesh, 2004).

Beyond the aforementioned formulations, there is the joint-coordinate formulation (relative coordinates), which uses the Lagrange method based on the principle of virtual power (Shabana, 1989). This formulation is not straightforward, yet it involves a smaller number of equations that is related to the number of degrees of freedom which makes it much efficient. To understand this method, let introduce the concept of the Lagrangian of mechanism which is the difference between its kinetic and potential energy ( $L=T-V$ ). The Hamilton's principle states that the motion of mechanism has to lead that the integral of the Lagrangian over time is minimal. With this principle, and some mathematical manipulation, it can be written

$$\frac{d}{dt} \left( \frac{\partial L}{\partial \dot{\mathbf{q}}} \right) - \frac{\partial L}{\partial \mathbf{q}} = \mathbf{g} \quad (2.2)$$

where  $L$  is the Lagrangian,  $\mathbf{q}$  is the vector of generalized coordinates, and  $\mathbf{g}$  denotes the vector of generalized forces acting on the system. Eq. (2.2) is commonly referred as the Lagrange's equation. Kane developed equations of motion using Lagrange's equation combined with d'Alembert's principle<sup>2</sup>, also known as Kane's method (Kane and Levinson, 1985).

Basically, there are three main methodologies to derive the equations of motion, namely, Newton-Euler's method, Lagrange's method, and Kane's method.

The body-coordinate formulation along with the Newton-Euler equations was adopted for this work. The reason for this choice concerns its simplicity, and the analysis of systems with a small number of bodies.

## 2.2 Equations of Motion for Constrained Systems

The configuration of a multibody system can be described by a set  $n$  of variables called generalized coordinates, which are gathered in a vector  $\mathbf{q} = \{q_1, q_2, \dots, q_n\}^T$ . There are necessary six coordinates to fully describe the position and orientation of each body in space, as it has six degrees of freedom. They can be divided into three coordinates to specify the body's position, and three extra coordinates to establish its angular orienta-

---

<sup>2</sup> The d'Alembert's principle states that the sum of the forces applied on a system and its inertial forces is zero.

tion. Nevertheless, in this work, the angular orientation of a body is defined using Euler parameters, which uses four coordinates. This is an alternative formulation for angular representation based on Euler's theorem on finite rotation, which states that a rotation in the three-dimensional space can always be described by a rotation along a certain axis over a certain angle.

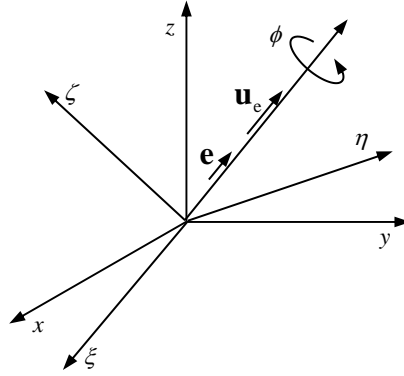


**Figure 2.2** - Representation of the Euler parameters.

Normally, the angular orientation can be described by a technique as Euler angles or Bryant angles, however, these formulations present singularities for some configurations of the bodies. Hence, the vector of generalized coordinates for a body  $i$  can be defined as follows

$$\mathbf{q}_i = \begin{Bmatrix} \mathbf{r}_i \\ \mathbf{p}_i \end{Bmatrix} \quad (2.3)$$

where  $\mathbf{r}_i$  denotes the vector of the translational coordinates of body  $i$  in global coordinates and  $\mathbf{p}_i$  is the vector of Euler parameters for body  $i$ . The vector  $\mathbf{r}_i$  is defined in Cartesian coordinates

$$\mathbf{r}_i = \begin{Bmatrix} x_i \\ y_i \\ z_i \end{Bmatrix} \quad (2.4)$$

The Euler parameters are fully defined by an angle  $\phi$  and a unit vector  $\mathbf{u}_e$  which represents the unique axis that if the body is rotated about an angle  $\phi$  its reference frame would be parallel to the global reference frame, as it is shown in Figure 2.2. Thus, the vector of Euler parameters is given by

$$\mathbf{p} = \{e_0 \quad e_1 \quad e_2 \quad e_3\}^T = \left\{ \cos \frac{\phi}{2} \quad \mathbf{u}_e \sin \frac{\phi}{2} \right\}^T \quad (2.5)$$

Therefore, the number of generalized coordinates for each body becomes seven.

For sake of simplicity, the generalized velocities and generalized accelerations are not defined as the time derivative of Eq. (2.3). Thus, applying the concept of angular velocity (Nikravesh, 1988), the velocity vector can be written as

$$\mathbf{v}_i = \begin{Bmatrix} \dot{\mathbf{r}}_i \\ \boldsymbol{\omega}_i \end{Bmatrix} \quad (2.6)$$

where  $\boldsymbol{\omega}_i$  denotes the vector angular velocities of body  $i$ , and is defined as

$$\boldsymbol{\omega}_i = \begin{Bmatrix} \omega_x \\ \omega_y \\ \omega_z \end{Bmatrix} \quad (2.7)$$

Hence, the vector of the generalized accelerations can be obtained yielding the time derivative of Eq. (2.6) and written as follows

$$\dot{\mathbf{v}}_i = \begin{Bmatrix} \ddot{\mathbf{r}}_i \\ \dot{\boldsymbol{\omega}}_i \end{Bmatrix} \quad (2.8)$$

Since the velocities vector does not yield the time of Eq. (2.3), it must be defined the transformation between the time derivative of the Euler parameters and the angular velocities which can be expressed as

$$\boldsymbol{\omega} = 2\mathbf{G}\dot{\mathbf{p}} \quad (2.9)$$

where the matrix  $\mathbf{G}$  is defined as

$$\mathbf{G} = \begin{bmatrix} -e_1 & e_0 & -e_3 & e_2 \\ -e_2 & e_3 & e_0 & -e_1 \\ -e_3 & -e_2 & e_1 & e_0 \end{bmatrix} \quad (2.10)$$

The inverse transformation is given by

$$\dot{\mathbf{p}} = \frac{1}{2}\mathbf{G}^T \boldsymbol{\omega} \quad (2.11)$$

The generalized coordinates of the system are usually divided into the independent (can vary arbitrarily) and dependent (have to satisfy the equations of constraints) coordinates. The set of constraint equations is denoted by  $\boldsymbol{\Phi}$ , and represents the kinematic relations between different coordinates of the system.

Each kinematic constraint introduces a different number of equations, this number will depend on the amount of degrees of freedom that are restricted, i.e., a revolute joint involves five equations while a spherical joint only implies three equations.

Beyond the number of independent constraints, the kinematic constraints can have different classifications. They can be derived from geometric constraints and, in that

case, be integrable into a form involving only coordinate, and, in that sense, called holonomic constraints. Contrarily, nonholonomic constraints cannot be integrable. For instance, Figure 2.3 shows a wheel rolling over a plane in which the constraints set that the relative velocity in the contact point is null, since it is a constraint at velocity level, it is not possible to be written in coordinate form. The constraints can also be distinguished for being or not an explicit function of time, called rheonomic or scleronomic constraints, respectively.

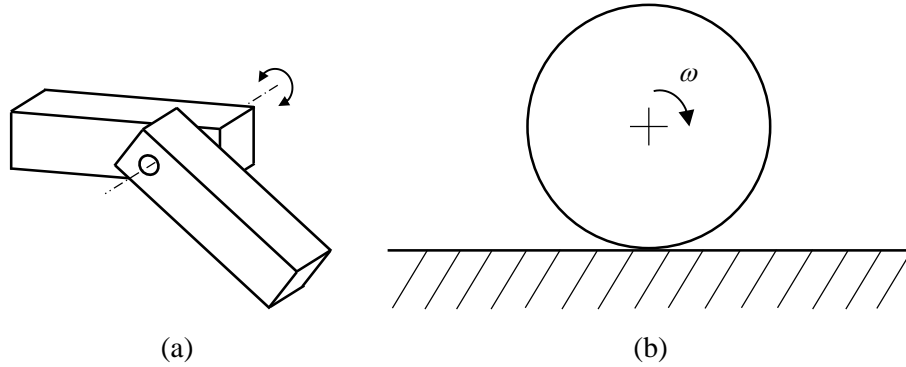


**Figure 2.3** - (a) Holonomic constraint (revolute joint); (b) Nonholonomic constraint (wheel rolling over a plane).

In the scope of this work, it will be treated only holonomic and scleronomic constraints. Thus, the kinematic constraints considered are geometrical restriction, and do not depend explicitly of time.

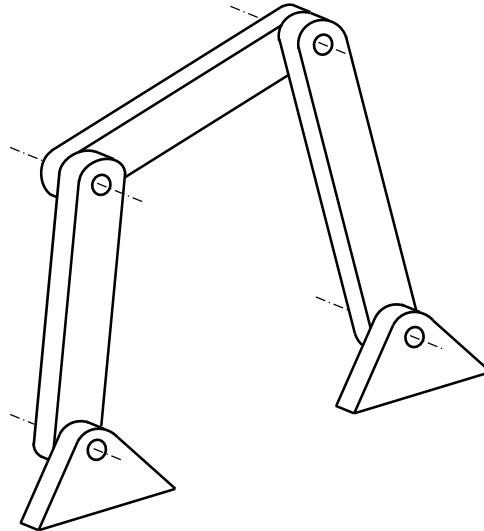


**Figure 2.4** - Four-bar mechanism with redundant constraints.

As it was aforementioned, the number of equations associated with a kinematic joint is equal to the number of degrees of freedom restricted by the same joint. Typically, a constrained multibody system with  $m$  constraint equations, and  $n_b$  bodies, should

have  $6n_b - m$  DoF as it is expressed in Eq. (2.1). However, this hypothesis is not always true due to the possibility of having a system with redundant constraints. This problem appears when some of the constraint equations are not independent, which means there is more than one equation imposing the same constraint. To better understand this issue, it should be considered the example from Fig. 2.4 which shows a planar four-bar linkage with three moving bodies and four revolute joints. Each revolute joint involves five constraint equations. Thus, according to the previous expression to calculate the degrees of freedom, the system should have -2 DoF ( $n_{\text{DoF}} = 6 \times 4 - 4 \times 5 - 6 = -2$ ). Nevertheless, it is well-known that this mechanism has one DoF which denotes the existence of three redundant constraints. It will be shown later on this chapter the consequences of having redundant constraints.

Hereupon, considering a constrained multibody system, the set of kinematic constraint equations can be written in the following form

$$\Phi \equiv \Phi(\mathbf{q}) = \mathbf{0} \quad (2.12)$$

where  $\mathbf{q}$  is the vector of the generalized coordinates of the whole system. These equations can also be a function of time or the generalized velocities of the bodies, although this work will only focus on scleronomic and holonomic constraints.

Yielding the first time derivative of Eq. (2.12), it is possible to obtain the equations of constraints at the velocity level as follows

$$\dot{\Phi} \equiv \mathbf{D}\mathbf{v} = \mathbf{0} \quad (2.13)$$

where  $\mathbf{D}$  denotes the Jacobian matrix of the constraint equations in order to the generalized coordinates, and  $\mathbf{v}$  is the vector of generalized velocities which is described in Eq. (2.6). It must be highlighted that the right-hand side of Eq. (2.13) is only null for scleronomic constraints, due to inexistence of time variable explicitly.

The Jacobian matrix generally has dimensions  $k \times n$  where  $k$  is the total number of constraints, however if the system has no redundant constraints  $k = m$ , and the matrix can be written as

$$\mathbf{D} = \begin{bmatrix} \frac{\partial \Phi_1}{\partial q_1} & \frac{\partial \Phi_1}{\partial q_2} & \dots & \frac{\partial \Phi_1}{\partial q_n} \\ \frac{\partial \Phi_2}{\partial q_1} & \frac{\partial \Phi_2}{\partial q_2} & \dots & \frac{\partial \Phi_2}{\partial q_n} \\ \vdots & \vdots & \ddots & \vdots \\ \frac{\partial \Phi_m}{\partial q_1} & \frac{\partial \Phi_m}{\partial q_2} & \dots & \frac{\partial \Phi_m}{\partial q_n} \end{bmatrix} \quad (2.14)$$



Proceeding with the second time derivative of Eq. (2.12), the acceleration constraints can be written as

$$\ddot{\Phi} \equiv \mathbf{D}\dot{\mathbf{v}} + \dot{\mathbf{D}}\mathbf{v} = \mathbf{0} \quad (2.15)$$

where  $\dot{\mathbf{v}}$  is the vector of generalized accelerations that is defined by Eq. (2.8). The previous expression is commonly rewritten in the following form

$$\mathbf{D}\dot{\mathbf{v}} = \gamma \quad (2.16)$$

in which

$$\gamma = -\dot{\mathbf{D}}\mathbf{v} \quad (2.17)$$

where  $\gamma$  is the right-hand side of the acceleration kinematic equations. Thus, Eq. (2.16) shows that it is possible to write these constraints as a system of linear equations.

A kinematic analysis of a multibody system can be performed recurring to the previous equations. This analysis involves studying the motion of the system without considering the force elements acting on it. For that purpose, it is normally prescribed the time history of position of one or more bodies which are the driving elements, and, in that sense, overcome the existence of degrees of freedom. Then, the time histories of positions, velocities and accelerations of the remaining bodies can be determine by solving Eq. (2.12), Eq. (2.13) and Eq. (2.16), respectively.

When the system experiences a finite displacement caused by the change of position of driving elements, it is necessary to find the new set of generalized coordinates  $\mathbf{q}$  that satisfies the Eq. (2.12). For this case, it is normally implemented a nonlinear solver as the Newton-Raphson method which convergence relies in a good initial approximation (García de Jalón and Bayo, 1994). To find the velocities and accelerations, Eq. (2.13) and Eq. (2.16) can be solved using a standard method to solve linear algebraic equation. For a large multibody system, the Jacobian matrix can have a sparse structure, bearing that in mind, it can be used a method to deal with this type of matrices. When the multibody system contains redundant constraints, the problem becomes more complex, and the user has to implement additional techniques to solve kinematic equations.

In the present work, several types of kinematic constraints will be considered for computational simulation, such as revolute joints, spherical joints, universal joints or translational joints. The derivation of the kinematic constraint equations, as well as the Jacobian matrix and the right-hand side of the acceleration constraint equations is not in the scope of this text. Nevertheless, the formulation for these types of joints can be found in the literature (Nikravesh, 1988).

As it was aforementioned, the formulation used in this work to compute the equations of motion is the Newton-Euler's approach. This formulation is straightforward in term of assembling the equations of motion.

This approach considers the Newton's first law of motion to describe the translational motion of each body as a free particle (Newton, 1687) and can be written as

$$m_b \ddot{\mathbf{r}} = \mathbf{f} \quad (2.18)$$

where  $m_b$  denotes the mass of the body,  $\ddot{\mathbf{r}}$  denotes the acceleration vector of the center of mass, and  $\mathbf{f}$  represents the sum of all forces acting on the body.

The Euler's rotation equations (Euler, 1776) are used to describe the rotational motion of a rigid body as it follows

$$\mathbf{J}\dot{\boldsymbol{\omega}} + \tilde{\boldsymbol{\omega}}\mathbf{J}\boldsymbol{\omega} = \mathbf{n} \quad (2.19)$$

where  $\mathbf{J}$  is the global inertia tensor,  $\boldsymbol{\omega}$  denotes the vector of global angular velocities,  $\mathbf{n}$  is the sum of moments acting on the body, the second term on the left hand-side represents the gyroscopic moments, and  $\tilde{\boldsymbol{\omega}}$  denotes the skew-symmetric matrix associated with the vector  $\boldsymbol{\omega}$  and it is written as

$$\tilde{\boldsymbol{\omega}} = \begin{bmatrix} 0 & -\omega_z & \omega_y \\ \omega_z & 0 & -\omega_x \\ -\omega_y & \omega_x & 0 \end{bmatrix} \quad (2.20)$$

Gathering the Eq. (2.18) and Eq. (2.19), the translational and rotational equations of motion, it results the Newton-Euler equations of motion for an unconstrained rigid body which can be expressed as

$$\begin{bmatrix} m_b \mathbf{I} & \mathbf{0} \\ \mathbf{0} & \mathbf{J} \end{bmatrix} \begin{Bmatrix} \ddot{\mathbf{r}} \\ \dot{\boldsymbol{\omega}} \end{Bmatrix} = \begin{Bmatrix} \mathbf{f} \\ \mathbf{n} - \tilde{\boldsymbol{\omega}}\mathbf{J}\boldsymbol{\omega} \end{Bmatrix} \quad (2.21)$$

or, alternatively, in a compact form,

$$\mathbf{M}_i \dot{\mathbf{v}}_i = \mathbf{g}_i \quad (2.22)$$

where

$$\mathbf{M}_i = \begin{bmatrix} m_{b,i} \mathbf{I} & \mathbf{0} \\ \mathbf{0} & \mathbf{J}_i \end{bmatrix}, \quad \dot{\mathbf{v}}_i = \begin{Bmatrix} \ddot{\mathbf{r}}_i \\ \dot{\boldsymbol{\omega}}_i \end{Bmatrix}, \quad \mathbf{g}_i = \begin{Bmatrix} \mathbf{f}_i \\ \mathbf{n}_i - \tilde{\boldsymbol{\omega}}_i \mathbf{J}_i \boldsymbol{\omega}_i \end{Bmatrix} \quad (2.23)$$

To construct the equations of motion for a multibody system with unconstrained bodies, it should be assembled Eq. (2.22) for each different body, and it can be written in the following form

$$\mathbf{M}\dot{\mathbf{v}} = \mathbf{g} \quad (2.24)$$

where

$$\mathbf{M} = \begin{bmatrix} \mathbf{M}_1 & & & \\ & \mathbf{M}_2 & & \\ & & \ddots & \\ & & & \mathbf{M}_{n_b} \end{bmatrix}, \quad \dot{\mathbf{v}} = \begin{Bmatrix} \dot{\mathbf{v}}_1 \\ \dot{\mathbf{v}}_2 \\ \vdots \\ \dot{\mathbf{v}}_{n_b} \end{Bmatrix}, \quad \mathbf{g} = \begin{Bmatrix} \mathbf{g}_1 \\ \mathbf{g}_2 \\ \vdots \\ \mathbf{g}_{n_b} \end{Bmatrix} \quad (2.25)$$

For constrained multibody systems, it has to be considered the reaction forces between the connected bodies that each kinematic joint introduces. Hence, Eq. (2.24) should be rewritten as

$$\mathbf{M}\dot{\mathbf{v}} = \mathbf{g} + \mathbf{g}^{(c)} \quad (2.26)$$

in which  $\mathbf{g}^{(c)}$  denotes the sum of all reaction forces. Thus, Eq. (2.12) and Eq. (2.26) constitute the equations of motion for a constrained MBS. Moreover,  $\mathbf{g}^{(c)}$  can be written as function of the constraint equations. However, Eq. (2.12) is expressed in terms of the generalized coordinates,  $\mathbf{q}$ , and Eq. (2.26) is expressed in terms of the generalized velocities,  $\mathbf{v}$ . For that purpose, it should be considered a vector of reactions forces which is consistent with the generalized coordinates denoted as  $\mathbf{g}^{(*)}$ .

Considering again  $m$  independent constraint equations which can be expressed as

$$\Phi \equiv \Phi(\mathbf{q}) = \mathbf{0} \quad (2.27)$$

Assuming frictionless joints, there are no dissipative forces acting as reaction forces which guarantees that the work done by the constraint forces in a virtual displacement  $\delta\mathbf{q}$  is always zero as it follows

$$\mathbf{g}^{(*)T} \delta\mathbf{q} = 0 \quad (2.28)$$

The constraints equations for the virtual displacement can be approximated by Taylor series expansion of Eq. (2.27) about  $\mathbf{q}$ ,

$$\Phi(\mathbf{q} + \delta\mathbf{q}) = \Phi(\mathbf{q}) + \mathbf{D}\delta\mathbf{q} + \dots \quad (2.29)$$

Since the constraints should be fulfilled for a system with a virtual displacement, it is considered

$$\Phi(\mathbf{q} + \delta\mathbf{q}) = \mathbf{0} \quad (2.30)$$

Bearing that in mind, and neglecting the higher-order terms, the following equation can be expressed

$$\mathbf{D}\delta\mathbf{q} = \mathbf{0} \quad (2.31)$$

In order to find the relation between the constraint equations and the constrained reaction forces, the vector of  $n$  the generalized coordinates  $\mathbf{q}$  should be divided into a set

of  $m$  dependent coordinates  $\mathbf{u}$ , and a set of  $n-m$  independent coordinates  $\mathbf{w}$ , as it follows

$$\mathbf{q} = \begin{bmatrix} \mathbf{u}^T & \mathbf{w}^T \end{bmatrix}^T \quad (2.32)$$

In the same way, the vector of virtual displacements, the Jacobian matrix, and the vector of reaction forces should be partitioned in the following form

$$\delta \mathbf{q} = \begin{bmatrix} \delta \mathbf{u}^T & \delta \mathbf{w}^T \end{bmatrix}^T, \quad \mathbf{D} = \begin{bmatrix} \mathbf{D}_u & \mathbf{D}_w \end{bmatrix}, \quad \mathbf{g}^{(*)} = \begin{bmatrix} \mathbf{g}_u^{(*)T} & \mathbf{g}_w^{(*)T} \end{bmatrix}^T \quad (2.33)$$

Hence, considering these divisions, Eq. (2.28) can be rewritten as

$$\mathbf{g}_u^{(*)T} \delta \mathbf{u} + \mathbf{g}_w^{(*)T} \delta \mathbf{w} = 0 \quad (2.34)$$

or, alternatively,

$$\mathbf{g}_u^{(*)T} \delta \mathbf{u} = -\mathbf{g}_w^{(*)T} \delta \mathbf{w} \quad (2.35)$$

Equivalently, Eq. (2.31) can also be modified introducing the previous partitions which gives

$$\mathbf{D}_u \delta \mathbf{u} = -\mathbf{D}_w \delta \mathbf{w} \quad (2.36)$$

Gathering Eq. (2.35) and Eq. (2.36), it results the following expression

$$\begin{bmatrix} \mathbf{g}_u^{(*)T} \\ \mathbf{D}_u \end{bmatrix} \delta \mathbf{u} = -\begin{bmatrix} \mathbf{g}_w^{(*)T} \\ \mathbf{D}_w \end{bmatrix} \delta \mathbf{w} \quad (2.37)$$

The matrix of the left hand side of Eq. (2.37) is a  $(m+1) \times m$  matrix. Since the  $m$  constraints are independent,  $\mathbf{D}_u$  is an  $m \times m$  nonsingular matrix. Thus, the first row of the  $(m+1) \times m$  matrix can be rewritten as a linear combination of the others

$$\mathbf{g}_u^{(*)} = \mathbf{D}_u^T \boldsymbol{\lambda} \quad (2.38)$$

where  $\boldsymbol{\lambda}$  is a vector of multipliers mostly called Lagrange multipliers. Eq. (2.38) can be introduced into Eq. (2.35) yielding

$$\boldsymbol{\lambda}^T \mathbf{D}_u \delta \mathbf{u} = -\mathbf{g}_w^{(*)T} \delta \mathbf{w} \quad (2.39)$$

Moreover, Eq. (2.36) is employed into Eq. (2.39) which results in

$$-\boldsymbol{\lambda}^T \mathbf{D}_w \delta \mathbf{w} = -\mathbf{g}_w^{(*)T} \delta \mathbf{w} \quad (2.40)$$

Vector  $\delta \mathbf{w}$  is an arbitrary independent vector, since it contains independent components of virtual displacements. To assure the consistency of the constraints for virtual displacements, Eq. (2.36) should be solved for  $\delta \mathbf{u}$  which is dependent of  $\delta \mathbf{w}$ . Hence,

$$\boldsymbol{\lambda}^T \mathbf{D}_w = \mathbf{g}_w^{(*)T} \quad (2.41)$$

which can be written in the following form

$$\mathbf{g}_w^{(*)} = \mathbf{D}_w^T \boldsymbol{\lambda} \quad (2.42)$$

Assembling Eq. (2.38) and Eq. (2.42) yields

$$\mathbf{g}^{(*)} = \mathbf{D}^T \boldsymbol{\lambda} \quad (2.43)$$

Thus, it was shown the relation between the joint reaction forces and the constraint equations. Finally, the dynamic equations of motion for constrained multibody systems can be written as

$$\mathbf{M}\dot{\mathbf{v}} + \mathbf{D}^T \boldsymbol{\lambda} = \mathbf{g} \quad (2.44)$$

The second term in Eq. (2.44) represents the vector of the sum of joints reaction forces consistent with the global coordinate system. Although, the Lagrange multipliers vector has  $m$  elements wherein each of them represent the reaction force of each different constraint.

In the following section, different methodologies of resolution of the equations of motion will be discussed.

### 2.3 Methods to Solve Equations of Motion

It was seen in the previous section how to use Newton-Euler formulation to obtain the dynamic equations of motion. In this sense, Eq. (2.44) was derived. Although, it is not possible to solve the motion of the system merely with this equation, since it represents  $n$  independent equations and has  $n+m$  unknowns to be determined ( $n$  generalized accelerations and  $m$  Lagrange multipliers). For this purpose, it should be also considered the second derivative of constraint equations which is given as

$$\mathbf{D}\dot{\mathbf{v}} = \boldsymbol{\gamma} \quad (2.45)$$

Thus, Eq. (2.44) and Eq. (2.45) can be gathered and create a system of differential algebraic equations which can be solved for the accelerations vector,  $\dot{\mathbf{v}}$ , and the Lagrange multipliers vector,  $\boldsymbol{\lambda}$ , and can be expressed as it follows

$$\begin{bmatrix} \mathbf{M} & \mathbf{D}^T \\ \mathbf{D} & \mathbf{0} \end{bmatrix} \begin{Bmatrix} \dot{\mathbf{v}} \\ \boldsymbol{\lambda} \end{Bmatrix} = \begin{Bmatrix} \mathbf{g} \\ \boldsymbol{\gamma} \end{Bmatrix} \quad (2.46)$$

The motion of the multibody system is determined recurring to the time integration process. In each step, Eq. (2.46) is solved and, the obtained accelerations vector is integrated together with the velocities vector in order to get the velocities and positions for the new time step. As the resolution of the equations of motion for multibody systems is an initial value problem, it becomes necessary to provide the initial positions and velocities of the system. The quality of the initial conditions has direct influence on

the accuracy of the dynamic simulation.

There are several different methods to solve the equations of motion. The most straightforward approach is to apply a method to solve linear algebraic equations to solve Eq. (2.46). Due to the existence of null elements in the main matrix and the possibility of ill-conditioned matrices, it is preferred methods using partial and full pivoting.

However, the main matrix of Eq. (2.46) can be inverted analytically. To do so, it is assumed that the system does not contain any body with null mass and inertia so that the inverse of mass matrix  $\mathbf{M}$  exists and, Eq. (2.44) can be rearranged to put accelerations vector in evidence as it follows

$$\dot{\mathbf{v}} = \mathbf{M}^{-1}(\mathbf{g} - \mathbf{D}^T \boldsymbol{\lambda}) \quad (2.47)$$

Thus, introducing Eq. (2.47) into Eq. (2.45) and, solving for the Lagrange multipliers, it results in

$$\boldsymbol{\lambda} = (\mathbf{D}\mathbf{M}^{-1}\mathbf{D}^T)^{-1} \mathbf{D}\mathbf{M}^{-1}\mathbf{g} - (\mathbf{D}\mathbf{M}^{-1}\mathbf{D}^T)^{-1} \boldsymbol{\gamma} \quad (2.48)$$

Since Eq. (2.48) represents an explicit expression to calculate the Lagrange multipliers, it can be introduced into Eq. (2.47) and, the accelerations vector is given explicitly by

$$\dot{\mathbf{v}} = \left[ \mathbf{M}^{-1} - \mathbf{M}^{-1}\mathbf{D}^T (\mathbf{D}\mathbf{M}^{-1}\mathbf{D}^T)^{-1} \mathbf{D}\mathbf{M}^{-1} \right] \mathbf{g} + \mathbf{M}^{-1}\mathbf{D}^T (\mathbf{D}\mathbf{M}^{-1}\mathbf{D}^T)^{-1} \boldsymbol{\gamma} \quad (2.49)$$

Hence, Eq. (2.48) and Eq. (2.49) can be gathered and rewritten in a compact form

$$\begin{Bmatrix} \dot{\mathbf{v}} \\ \boldsymbol{\lambda} \end{Bmatrix} = \begin{bmatrix} \mathbf{M}^{-1} - \mathbf{M}^{-1}\mathbf{D}^T (\mathbf{D}\mathbf{M}^{-1}\mathbf{D}^T)^{-1} \mathbf{D}\mathbf{M}^{-1} & \mathbf{M}^{-1}\mathbf{D}^T (\mathbf{D}\mathbf{M}^{-1}\mathbf{D}^T)^{-1} \\ (\mathbf{D}\mathbf{M}^{-1}\mathbf{D}^T)^{-1} \mathbf{D}\mathbf{M}^{-1} & -(\mathbf{D}\mathbf{M}^{-1}\mathbf{D}^T)^{-1} \end{bmatrix} \begin{Bmatrix} \mathbf{g} \\ \boldsymbol{\gamma} \end{Bmatrix} \quad (2.50)$$

As it was aforementioned, the accelerations vector is integrated to obtain the positions and velocities for the next step. This method to solve the equations of motion is frequently called standard Lagrange multipliers method. The flowchart that represents the algorithm of resolution of the equations of motion is presented in Figure 2.5. To start a dynamic analysis of a multibody system, the initial conditions should be properly defined. In order to not start the analysis with constraints violation, the initial positions and velocities vectors,  $\mathbf{q}^0$  and  $\mathbf{v}^0$ , respectively, cannot be defined arbitrarily. Bearing that in mind, the independent coordinates and velocities should be defined in first place and, the remaining coordinates and velocities must fulfill Eq. (2.12) and Eq. (2.13), respectively. After introducing initial conditions, based on the system properties, it must be constructed the global mass matrix  $\mathbf{M}$ , the Jacobian matrix  $\mathbf{D}$ , the right-hand side of

accelerations constraints  $\gamma$ , and the external generalized forces vector  $\mathbf{g}$ . The next step is to solve Eq. (2.46), which can be performed with the methodology previously presented. Before proceeding to the integration process, it is necessary to create an auxiliary vector where the time derivative of Eq. (2.3) and the accelerations vector,  $\dot{\mathbf{q}}$  and  $\dot{\mathbf{v}}$ , respectively, are gathered. To do so, Eq. (2.11) must be used to calculate the time derivative of the Euler parameters. The positions and velocities for the time step  $t+\Delta t$  are obtained through numerical integration of the auxiliary vector. This procedure must be repeated until reaching the final time of simulation.

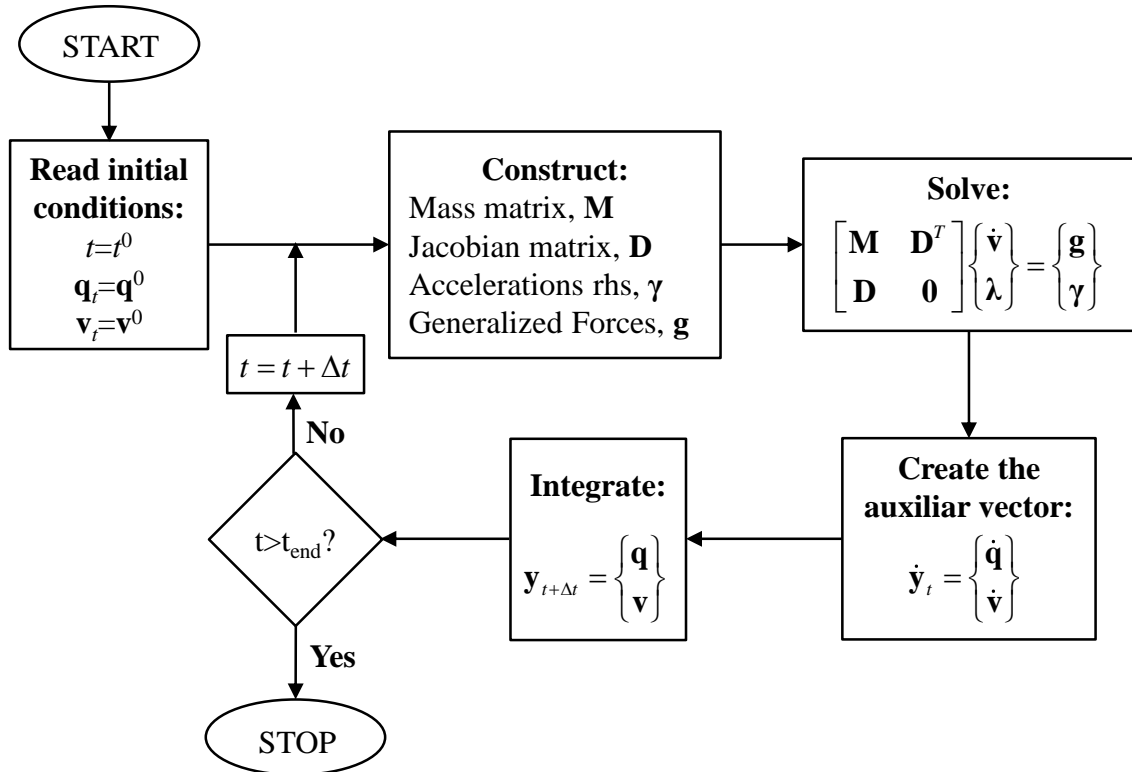


**Figure 2.5** - Flowchart of dynamic analysis of multibody systems (Flores, 2012).

The standard Lagrange multipliers method is the most simple and straightforward approach, however, it does not include explicitly in its formulation the equations for the positions and velocities kinematic constraints which are given by Eq. (2.12) and Eq. (2.13), respectively. Thus, for long simulations, the constraint equations tend to be violated due to the errors introduced by the integration process and by the inaccuracy of the initial conditions.

In order to solve this problem, several techniques have been proposed to stabilize or even eliminate the constraints violation. Some of the most relevant methods will be presented throughout this section.

Baumgarte (1972) introduced a method in which the errors in the positions and

velocities equations are kept under control. For that purpose, this approach suggests that Eq. (2.45) should be replaced by the following expression

$$\ddot{\Phi} + 2\alpha\dot{\Phi} + \beta^2\Phi = \mathbf{0} \quad (2.51)$$

This approach allows the violation of the constraints before their correction. Contrary to the standard Langrange multipliers method, Baumgarte method is a closed-loop system which use the terms  $2\alpha\dot{\Phi}$  and  $\beta^2\Phi$  as control terms to damp the accelerations constraints. In an open-loop system, if any perturbation occurs,  $\Phi$  and  $\dot{\Phi}$  do not converge to zero which makes the system unstable. Thus, with this technique the equations of motion can be replaced for the following system

$$\begin{bmatrix} \mathbf{M} & \mathbf{D}^T \\ \mathbf{D} & \mathbf{0} \end{bmatrix} \begin{Bmatrix} \dot{\mathbf{v}} \\ \lambda \end{Bmatrix} = \begin{Bmatrix} \mathbf{g} \\ \gamma - 2\alpha\dot{\Phi} - \beta^2\Phi \end{Bmatrix} \quad (2.52)$$

The choice of the parameters  $\alpha$  and  $\beta$  are of paramount importance for the stability of the method. The selection of positive constants normally ensures stability, however, depending on the parameters, the convergence of the constraints violation can be achieved with or without oscillations, and faster or slower. In order to choose correctly the parameters, it should be performed several numerical experiments, since this is an empirical process that most of times involves a trial and error procedure. Some techniques for the selection of the parameters  $\alpha$  and  $\beta$  have been studied and parametric analyses of their influence in the stability of constraints violation were presented (Flores et al., 2011b).

Bayo, García de Jalón and Serna (1988) proposed the penalty method in which the accelerations, velocities and positions are used in the equations of motion as a penalty spring-damper-mass system. This approach considers that constraints reaction forces are replaced by forces proportional to violations at accelerations, velocities and positions as

$$\lambda = m_c \ddot{\Phi} + d_c \dot{\Phi} + k_c \Phi \quad (2.53)$$

where  $m_c$ ,  $d_c$  and  $k_c$  are the mass, damping and stiffness coefficients. The previous equation can be rewritten as

$$\lambda = \alpha (\ddot{\Phi} + 2\mu\omega\dot{\Phi} + \omega^2\Phi) \quad (2.54)$$

where

$$\alpha = m_c, \quad \frac{d_c}{m_c} = 2\mu\omega \quad \text{and} \quad \frac{k_c}{m_c} = \omega^2 \quad (2.55)$$

For a system of constrained bodies the equations of motion are given by Eq.



(2.44), which is represented by the following equality

$$\mathbf{M}\dot{\mathbf{v}} + \mathbf{D}^T \boldsymbol{\lambda} = \mathbf{g} \quad (2.56)$$

Introducing Eq. (2.54) into Eq. (2.56) yields

$$\mathbf{M}\dot{\mathbf{v}} + \mathbf{D}^T \alpha (\ddot{\Phi} + 2\mu\omega\dot{\Phi} + \omega^2\Phi) = \mathbf{g} \quad (2.57)$$

Considering Eq. (2.15) and Eq. (2.17), and performing some algebraic manipulation, Eq. (2.57) turns into

$$(\mathbf{M} + \alpha \mathbf{D}^T \mathbf{D}) \dot{\mathbf{v}} = \mathbf{g} - \alpha \mathbf{D}^T (-\gamma + 2\mu\omega\dot{\Phi} + \omega^2\Phi) \quad (2.58)$$

This equation should be solved in order to the generalized accelerations. Contrary to the previous presented approaches, the penalty method needs to solve a small number of equation, and can easily solve problems with redundant constraints and kinematic singularities. In order to use this method, three parameters should be defined, the penalty factor,  $\alpha$ , the damping ratio,  $\mu$ , and the natural frequency of the penalty system,  $\omega$ . For high penalty factors, this technique returns good results, it was seen that a factor  $10^7$  times the largest term of the mass matrix is a suitable choice (García de Jalón and Bayo, 1994). The coefficients  $\mu$  and  $\omega$  have a similar stabilization behavior to the coefficients  $\alpha$  and  $\beta$  of the Baumgarte method presented above.

In the same work, Bayo, García de Jalón and Serna (1988) presented the augmented Lagrangian formulation whose main objective is overcome some drawbacks of the penalty method. The penalty formulation presents convergence for large penalty values, although that may lead to ill conditioning problems. It also needs a certain level of violation of constraints to ensure sufficiently large reaction forces to stabilize the constraints which indicates that the violation of the constraints is not completely vanished.

The augmented Lagrangian formulation consists in a combination of the penalty formulation and the Lagrange multipliers technique which results in a iterative procedure of solving the equations of motion. In this approach the penalty terms of Eq. (2.54) should be added to the Eq. (2.44) instead of replacing the original reaction forces. Thus, the equations of motion can be written in the following form

$$\mathbf{M}\dot{\mathbf{v}} + \mathbf{D}^T \boldsymbol{\lambda}^* + \mathbf{D}^T \alpha (\ddot{\Phi} + 2\mu\omega\dot{\Phi} + \omega^2\Phi) = \mathbf{g} \quad (2.59)$$

where  $\boldsymbol{\lambda}^*$  is a vector of Lagrange multipliers which plays a role of corrective term. In order to make Eq. (2.59) having a similar configuration to Eq. (2.44), it can be written

$$\boldsymbol{\lambda}_{i+1} = \boldsymbol{\lambda}_i + \alpha (\ddot{\Phi} + 2\mu\omega\dot{\Phi} + \omega^2\Phi) \quad (2.60)$$

in which  $i$  represents the iteration number. Thus, Eq. (2.59) results in

$$\mathbf{M}\dot{\mathbf{v}}_i + \mathbf{D}^T \boldsymbol{\lambda}_i = \mathbf{g} \quad (2.61)$$

For the first step ( $i=0$ ), it is considered an unconstrained multibody system, i.e.,  $\boldsymbol{\lambda}_0=0$ , in the forward steps, Eq. (2.60) should be used and the result may be introduced into Eq. (2.61) to solve for the generalized accelerations. For a given iteration step, if  $\boldsymbol{\lambda}_{i+1}=\boldsymbol{\lambda}_i$ , the constraint conditions are satisfied. However, the Eq. (2.60) cannot be solved directly, since the acceleration constraints depend on the generalized accelerations of the iteration  $i+1$ . Introducing Eq. (2.15) and Eq. (2.17) into Eq. (2.60) and replacing that into Eq. (2.61) is obtained the final expression for the iterative procedure

$$(\mathbf{M} + \alpha \mathbf{D}^T \mathbf{D}) \dot{\mathbf{v}}_{i+1} = \mathbf{M}\dot{\mathbf{v}}_i - \alpha \mathbf{D}^T (-\boldsymbol{\gamma} + 2\mu\omega\dot{\boldsymbol{\Phi}} + \omega^2 \boldsymbol{\Phi}) \quad (2.62)$$

For the first iteration, the unconstrained system can be considered and the accelerations are given by solving this equation

$$\mathbf{M}\dot{\mathbf{v}}_0 = \mathbf{g} \quad (2.63)$$

To stop the iterative procedure, the following criterion is widely used

$$\|\dot{\mathbf{v}}_{i+1} - \dot{\mathbf{v}}_i\| \leq \varepsilon \quad (2.64)$$

where  $\varepsilon$  is a specified tolerance. This method also allows dealing with redundant constraints and singular configurations. If the parameters for each method are equal, it is possible to conclude from the analysis of the presented equations that the penalty method will return the same results as the augmented Lagrangian formulation when just one iteration is performed.

The coordinate partitioning method (Wehage and Haug, 1982) eliminates the errors from the violation of the constraints at position and velocity levels. This approach consists in dividing the coordinates of the multibody system into two sets, independent and dependent coordinates. The equations of motion should be solved in order to determine the generalized accelerations of the system, for that it can be applied the standard Lagrange multipliers method presented earlier. Then, the independent accelerations and velocities are integrated in order to obtain the independent velocities and positions for the new step. The dependent quantities are obtained from the resolution of constraint equations as it will be shown.

The division of the coordinates can be performed manually by the user, or automatically with a matrix factorization technique, such as Gaussian elimination with full pivoting. Although, the automatic selection presents the inconvenient of changing the

independent coordinates over the time due to motion of the mechanism. Considering a multibody system with  $k$  constraints and  $n$  coordinates, the Jacobian matrix will have  $k \times n$  dimension, and it can be factorized in the following form

$$\mathbf{D} = \begin{bmatrix} & m & n-m \\ \mathbf{A} & \mathbf{B} \\ \mathbf{S} & \mathbf{T} \end{bmatrix} \begin{matrix} m \\ k-m \end{matrix} \quad (2.65)$$

where  $m$  is the number of independent constraints which means the Jacobian matrix has  $k-m$  redundant rows that remain in the bottom of the factorized matrix. In the top rows, the independent constraints are partitioned into the matrix  $\mathbf{A}$  which is a non-singular  $m \times m$  matrix related with the dependent coordinates, and matrix  $\mathbf{B}$  which is a submatrix  $m \times (n-m)$  associated with the independent coordinates.

Considering that the multibody system has no redundant constraints, the Jacobian matrix will only include submatrices  $\mathbf{A}$  and  $\mathbf{B}$ , and it can be represented in the same form of Eq. (2.33), as

$$\mathbf{D} = [\mathbf{D}_u \quad \mathbf{D}_w] \quad (2.66)$$

Similarly to the Jacobian matrix, the positions vector can be also divided as it follows

$$\mathbf{q} = [\mathbf{u}^T \quad \mathbf{w}^T]^T \quad (2.67)$$

The generalized velocities and accelerations have to be partitioned, yielding the following vectors

$$\mathbf{v} = [\mathbf{v}_u^T \quad \mathbf{v}_w^T]^T \quad \text{and} \quad \dot{\mathbf{v}} = [\dot{\mathbf{v}}_u^T \quad \dot{\mathbf{v}}_w^T]^T \quad (2.68)$$

After dividing the coordinates, Eq. (2.46) should be solved in order to find the accelerations vector,  $\dot{\mathbf{v}}$ . Resembling to the standard method, this technique needs to use an auxiliary vector for the integration process. However in this case the vector only contains independent quantities, and it can be expressed as

$$\dot{\mathbf{y}} = [\mathbf{v}_w^T \quad \dot{\mathbf{v}}_w^T]^T \quad (2.69)$$

which is integrated and returns the following vector

$$\mathbf{y} = [\mathbf{w}^T \quad \mathbf{v}_w^T]^T \quad (2.70)$$

The dependent positions and velocities are determined using the respective constraints equations. The positions constraint equations are solved in order to calculate the dependent positions, Eq. (2.12) can be rewritten as

$$\Phi(\mathbf{u}, \mathbf{w}) = \mathbf{0} \quad (2.71)$$

Since Eq. (2.71) is generally a nonlinear set of equations, it must be applied a nonlinear solver, such as Newton-Raphson method. To ensure the convergence of the method, a suitable approximation for the dependent positions is needed to start the iterative procedure. It was found a reliable estimation using information of the previous step, which is

$$\mathbf{u}^i = \mathbf{u}^{i-1} + \dot{\mathbf{v}}_{\mathbf{u}}^{i-1} \Delta t + 0.5 \ddot{\mathbf{v}}_{\mathbf{u}}^{i-1} \Delta t^2 \quad (2.72)$$

The dependent velocities are obtained introducing Eq. (2.66) and Eq. (2.68) into the velocities constraint equations, Eq. (2.13), which results in

$$\mathbf{D}_{\mathbf{u}} \mathbf{v}_{\mathbf{u}} + \mathbf{D}_{\mathbf{w}} \mathbf{v}_{\mathbf{w}} = \mathbf{0} \quad (2.73)$$

Thus, Eq. (2.73) can be rewritten as

$$\mathbf{D}_{\mathbf{u}} \mathbf{v}_{\mathbf{u}} = -\mathbf{D}_{\mathbf{w}} \mathbf{v}_{\mathbf{w}} \quad (2.74)$$

Since  $\mathbf{D}_{\mathbf{u}}$  is a nonsingular matrix, the dependent velocities are determined solving the previous equation using a method to solve linear algebraic equations.

A method based on the projection matrix  $\mathbf{R}$  (García de Jalón and Bayo, 1994) is an alternative approach to solve the equations of motion of a constrained multibody system. From the analysis of Eq. (2.13), it can be concluded that the vector of the generalized velocities  $\mathbf{v}$  belongs to the nullspace<sup>3</sup> of the Jacobian matrix  $\mathbf{D}$ . Since Eq. (2.13) is a linear system, the nullspace of Jacobian matrix is the subspace of allowable motions (García de Jalón and Bayo, 1994). This subspace considers every velocity vectors that are compatible to the constraint equations. The dimension of the subspace is equal to the number of DoF of the multibody system.

The generalized velocities of the system are generally described by the vector  $\mathbf{v}$  with  $n$  components. The objective of this approach is to define the velocities with a lower number of variables, in that sense they can be represented by the vector  $\mathbf{v}_{\mathbf{w}}$  which contains only the independent velocities.

Since the nullspace of  $\mathbf{D}$  has dimension equal to the number of DoF, there are  $n-m$  independent vectors  $\mathbf{r}^i$  ( $i=1,2,\dots,n-m$ ) that constitute the nullspace basis. Any arbitrary vector of generalized velocities that fulfill the constraints equations is a linear combination of  $\mathbf{r}^i$  as follows

---

<sup>3</sup> The nullspace of matrix  $\mathbf{A}$  is the set of all vectors  $\mathbf{x}$  that satisfy the equation  $\mathbf{Ax}=\mathbf{0}$ .

$$\mathbf{v} = \mathbf{r}^1 v_{w,1} + \mathbf{r}^2 v_{w,2} + \dots + \mathbf{r}^{n-m} v_{w,n-m} \quad (2.75)$$

Gathering the vectors  $\mathbf{r}^i$  in a matrix  $\mathbf{R}$   $n \times (n-m)$ , the Eq. (2.75) can be rewritten in the following form

$$\mathbf{v} = \mathbf{R} \mathbf{v}_w \quad (2.76)$$

Matrix  $\mathbf{R}$  is responsible for the transformation from independent velocities to the vector of generalized velocities of the multibody system. Since vectors  $\mathbf{r}^i$  are the components of the nullspace of the Jacobian matrix, it can be written

$$\mathbf{D} \mathbf{r}^i = \mathbf{0} \quad (i = 1, 2, \dots, n-m) \quad (2.77)$$

hence,

$$\mathbf{D} \mathbf{R} = \mathbf{0} \quad (2.78)$$

Bearing in mind that the Jacobian matrix is position dependent, it can be concluded that in order to have Eq. (2.78) verified, matrix  $\mathbf{R}$  must also depend on the positions of system.

So far, this technique only affects the kinematics of the system. In order to be used to solve the equations of motion, Eq. (2.44) should be pre-multiplied by the transposed of matrix  $\mathbf{R}$ , as it follows

$$\mathbf{R}^T \mathbf{M} \dot{\mathbf{v}} + \mathbf{R}^T \mathbf{D}^T \boldsymbol{\lambda} = \mathbf{R}^T \mathbf{g} \quad (2.79)$$

Thus, introducing Eq. (2.78) into Eq. (2.79), it can be reduced to

$$\mathbf{R}^T \mathbf{M} \dot{\mathbf{v}} = \mathbf{R}^T \mathbf{g} \quad (2.80)$$

Gathering Eq. (2.16) and Eq. (2.80), the following system is obtained

$$\begin{bmatrix} \mathbf{D} \\ \mathbf{R}^T \mathbf{M} \end{bmatrix} \dot{\mathbf{v}} = \begin{bmatrix} \boldsymbol{\gamma} \\ \mathbf{R}^T \mathbf{g} \end{bmatrix} \quad (2.80)$$

This system of equations can be easily solved for the generalized accelerations, since the leading matrix is nonsingular  $n \times n$ . Then, the process is similar to the standard Lagrange multipliers method, as it is constructed an auxiliary vector to the integration process. This approach also does not include explicitly the constraint equations for positions and velocities. In that sense, for long simulations, it is necessary to apply a method for stabilization or elimination of the constraints violation.

Arabyan and Wu (1998) improved a method to solve equations of motion which was originally used for systems of constrained particles (Kalaba and Udwadia, 1993). This method is based on the construction of a generalized inverse, and it is suitable to handle multibody systems with redundant constraints.

The equations of motion of an unconstrained multibody system are given by Eq. (2.24), which can be solved for the generalized accelerations, yielding

$$\dot{\mathbf{v}}_{\text{unc}} = \mathbf{M}^{-1} \mathbf{g} \quad (2.81)$$

Considering Eq. (2.81), and performing some algebraic manipulation, Eq. (2.49) can be rewritten as

$$\dot{\mathbf{v}} = \dot{\mathbf{v}}_{\text{unc}} + \mathbf{M}^{-1} \mathbf{D}^T (\mathbf{D} \mathbf{M}^{-1} \mathbf{D}^T)^{-1} (\boldsymbol{\gamma} - \mathbf{D} \dot{\mathbf{v}}_{\text{unc}}) \quad (2.82)$$

Since  $\mathbf{M}$  is a diagonal matrix, its inverse can be decomposed in the following form  $\mathbf{M}^{-1} = \mathbf{M}^{-1/2} \mathbf{M}^{-1/2}$ , where  $\mathbf{M}^{-1/2}$  is also a diagonal matrix in which the coefficients are the square root of the coefficients of the mass matrix  $\mathbf{M}$ . Thus, Eq. (2.82) is expressed as

$$\dot{\mathbf{v}} = \dot{\mathbf{v}}_{\text{unc}} + \mathbf{M}^{-1/2} (\mathbf{M}^{-1/2} \mathbf{D}^T) (\mathbf{D} \mathbf{M}^{-1/2} \mathbf{M}^{-1/2} \mathbf{D}^T)^{-1} (\boldsymbol{\gamma} - \mathbf{D} \dot{\mathbf{v}}_{\text{unc}}) \quad (2.83)$$

It is defined an auxiliary matrix  $\mathbf{C} = \mathbf{D} \mathbf{M}^{-1/2}$  which is introduced into Eq. (2.83), yielding

$$\dot{\mathbf{v}} = \dot{\mathbf{v}}_{\text{unc}} + \mathbf{M}^{-1/2} \mathbf{C}^T (\mathbf{C} \mathbf{C}^T)^{-1} (\boldsymbol{\gamma} - \mathbf{D} \dot{\mathbf{v}}_{\text{unc}}) \quad (2.84)$$

The key point of this method is using the properties of Moore-Penrose generalized inverse for matrix  $\mathbf{C}$ . Thus, it will be denoted by  $\mathbf{C}^+$ , and holds the following properties

$$\mathbf{C} \mathbf{C}^+ \mathbf{C} = \mathbf{C} \text{ and } \mathbf{C}^+ \mathbf{C} \mathbf{C}^+ = \mathbf{C}^+ \quad (2.85)$$

where  $\mathbf{C}^+ \mathbf{C}$  and  $\mathbf{C} \mathbf{C}^+$  are symmetric matrices. Hence, the following equality can be derived

$$\mathbf{C}^T (\mathbf{C} \mathbf{C}^T)^{-1} = \mathbf{C}^T (\mathbf{C}^+)^T \mathbf{C}^+ = (\mathbf{C}^+ \mathbf{C})^T \mathbf{C}^+ = \mathbf{C}^+ \mathbf{C} \mathbf{C}^+ = \mathbf{C}^+ \quad (2.86)$$

Thus, Eq. (2.86) should be used to simplify Eq. (2.84) which results in

$$\dot{\mathbf{v}} = \dot{\mathbf{v}}_{\text{unc}} + \mathbf{M}^{-1/2} \mathbf{C}^+ (\boldsymbol{\gamma} - \mathbf{D} \dot{\mathbf{v}}_{\text{unc}}) \quad (2.87)$$

This approach consists in solving Eq. (2.87) in order to obtain the generalized accelerations. Since all the bodies of the system have non-null masses and inertias, the solution of this equation always exists even when the leading matrix of Eq. (2.46) is not invertible. This means that Eq. (2.87) can be solved in the presence of redundant constraints or constraints that vanish instantaneously. There are different methods to compute the generalized inverse, such as singular value decomposition and Gram-Schmidt Orthogonalization (Neto and Ambrósio, 2003). Similarly to other methods, this formulation also presents some problems related to constraints violation, bearing that in mind it must be used along a method to prevent violation of the constraints.

A methodology for the direct correction of the constraints violations at positions and velocities levels was presented by Flores (2013). This approach does not consider the correction of the positions and velocities during the process of solving the equations of motion. Instead, the following technique corrects those quantities after the integration procedure which introduces numerical errors in the system. Bearing that in mind, this approach is applied after solving Eq. (2.16) and it starts by the correction of the positions vector as follows

$$\mathbf{q}^c = \mathbf{q}'' + \delta\mathbf{q} \quad (2.88)$$

where  $\mathbf{q}^c$  and  $\mathbf{q}''$  represent the vectors of corrected and uncorrected coordinates, respectively, and  $\delta\mathbf{q}$  is the vector of corrections to eliminate the constraints violation. Thus,  $\mathbf{q}^c$  satisfies Eq. (2.12), and a corrective term must be added to  $\mathbf{q}''$  in order to equally fulfill the constraints. Hence, Eq. (2.88) can be written in terms of constraints as

$$\Phi(\mathbf{q}^c) = \Phi(\mathbf{q}'') + \delta\Phi = \mathbf{0} \quad (2.89)$$

in which  $\delta\Phi$  represents the variation of the constraint equations, and it can be expanded to first-order derivatives in the following form

$$\delta\Phi = \frac{\partial\Phi}{\partial q_1} \delta q_1 + \frac{\partial\Phi}{\partial q_2} \delta q_2 + \dots + \frac{\partial\Phi}{\partial q_n} \delta q_n = \mathbf{D}\delta\mathbf{q} \quad (2.90)$$

Introducing Eq. (2.90) into Eq. (2.89), results in

$$\Phi(\mathbf{q}'') + \mathbf{D}\delta\mathbf{q} = \mathbf{0} \quad (2.91)$$

Thus, Eq. (2.91) can be rewritten to calculate the corrections of coordinates

$$\delta\mathbf{q} = -\mathbf{D}^{-1}\Phi(\mathbf{q}'') \quad (2.92)$$

In order to solve the previous equation, the inverse of the Jacobian matrix must be provided. Although, in the general case, the Jacobian matrix is not square, this means that it is not invertible. Thus, to provide a solution for Eq. (2.92), the properties of Moore-Penrose generalized inverse must be employed to the Jacobian matrix  $\mathbf{D}$ . For this case, Eq. (2.85) and Eq. (2.86) remain valid. Hence, Eq. (2.92) is given by

$$\delta\mathbf{q} = -\mathbf{D}^T (\mathbf{D}\mathbf{D}^T)^{-1} \Phi(\mathbf{q}'') \quad (2.93)$$

The corrected coordinates can be calculated by introducing Eq. (2.93) into Eq. (2.88) which yields

$$\mathbf{q}^c = \mathbf{q}'' - \mathbf{D}^T (\mathbf{D}\mathbf{D}^T)^{-1} \Phi(\mathbf{q}'') \quad (2.94)$$

This equation must be used in each time step to correct the coordinates. Neverthe-

less, the kinematic constraints equations are generally nonlinear which means that Eq. (2.94) should be solved iteratively. A tolerance value should be specified in order to define the stopping criterion for the iterative procedure as

$$\sqrt{\Phi^T \Phi} \leq \varepsilon \quad (2.95)$$

Similarly to Eq. (2.88), the generalized velocities must be correct as

$$\mathbf{v}^c = \mathbf{v}^u + \delta \mathbf{v} \quad (2.96)$$

where  $\mathbf{v}^c$  and  $\mathbf{v}^u$  denote the vectors of corrected and uncorrected generalized velocities, and  $\delta \mathbf{v}$  expresses the vector of correction of velocities. Analogously to Eq. (2.89), the corrected velocities satisfy Eq. (2.13), and a corrective term must be summed to the uncorrected velocities to ensure that the velocities constraints are satisfied, i.e.,

$$\dot{\Phi}(\mathbf{q}^c, \mathbf{v}^c) = \dot{\Phi}(\mathbf{q}^c, \mathbf{v}^u) + \delta \dot{\Phi} = \mathbf{0} \quad (2.97)$$

The velocity constraints depend on both generalized positions and velocities of the system. Thus, the term of variation of velocity constraints is expanded in the following form

$$\delta \dot{\Phi} = \frac{\partial \dot{\Phi}}{\partial \mathbf{q}} \delta \mathbf{q} + \frac{\partial \dot{\Phi}}{\partial \dot{\mathbf{q}}} \delta \dot{\mathbf{q}} \quad (2.98)$$

The correction of the generalized velocities implies that the generalized coordinates are previously corrected. In that case, the vector of positions is already corrected which means that  $\delta \mathbf{q} = \mathbf{0}$ . It should be noted that the derivative of the velocity constraints with respect to the velocity vector is the Jacobian matrix. Hence, Eq. (2.98) results in

$$\delta \dot{\Phi} = \mathbf{D} \delta \mathbf{v} \quad (2.99)$$

Substituting Eq. (2.99) into Eq. (2.97) yields

$$\dot{\Phi}(\mathbf{q}^c, \mathbf{v}^u) + \mathbf{D} \delta \mathbf{v} = \mathbf{0} \quad (2.100)$$

Applying once more the definition of Moore-Penrose generalized inverse, Eq. (2.100) can be used to calculate the velocity variations as follows

$$\delta \mathbf{v} = -\mathbf{D}^T (\mathbf{D} \mathbf{D}^T)^{-1} \dot{\Phi}(\mathbf{q}^c, \mathbf{v}^u) \quad (2.101)$$

Thus, replacing Eq. (2.101) into Eq. (2.96), the corrected velocities can be expressed as

$$\mathbf{v}^c = \mathbf{v}^u - \mathbf{D}^T (\mathbf{D} \mathbf{D}^T)^{-1} \dot{\Phi}(\mathbf{q}^c, \mathbf{v}^u) \quad (2.102)$$

Since the velocity constraints own a linear dependence to the generalized velocities, Eq. (102) must be solved once in each time step.



A brief overview about several methodologies to solve equations of motions was presented. Each of them shows different capabilities in what concerns to implementation complexity, constraints stabilization or handling redundant constraints. A brief comparison will be displayed in the following section.

## 2.4 Example of Application

After providing a brief explanation on the multibody system formulation and on the several methods to solve the equations of motion, it is presented a simple example of application. Bearing that in mind, it will be considered a spatial slider-crank mechanism, as it shown in Figure 2.6. The general purpose of this section is to give a generic comprehension of the influence of using different methods to solve the equations of motion on the accuracy of the simulation and on the computational effort.

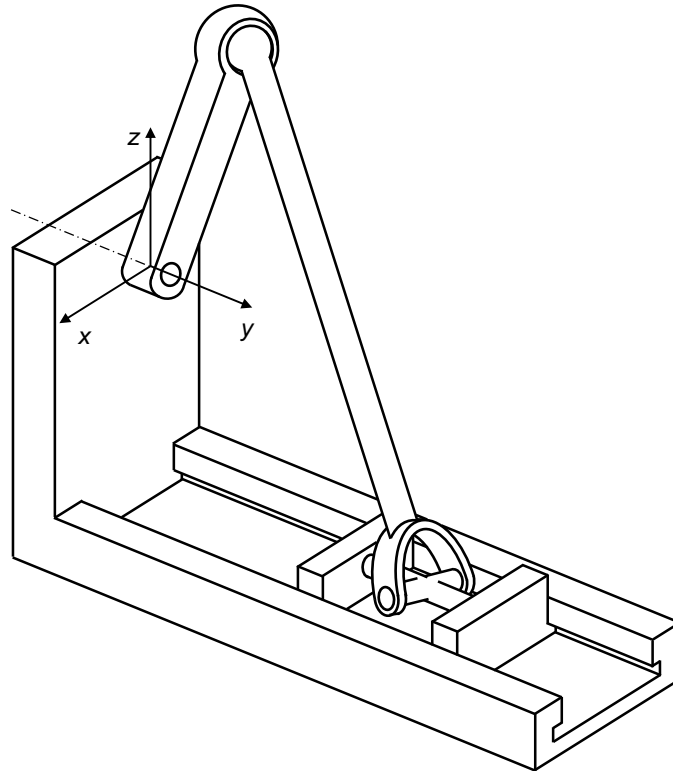


**Figure 2.6** - Spatial slider-crank mechanism.

The spatial slider-crank mechanism is constituted by three different bodies, namely the crank, the connecting rod and the slider. It has four different kinematic joints: one revolute joint connecting the ground and the crank (5 constraints), one spherical joint between the crank and the connecting rod (3 constraints), one universal joint gathering the connecting rod and the slider (4 constraints), and one translational joint between the slider and the ground (5 constraints). From the analysis of the configuration of the

mechanism, it can be concluded that every constraints are independent. Thus, the number of degrees of freedom can be determined recurring to Eq. (2.1) which results in 1 DoF ( $n_{\text{DoF}}=6 \times 3 - (5+3+4+5)=1$ )

In order to correctly describe the mechanism, the length and the inertial properties of each body are presented in Table 2.1. Moreover, to perform a multibody system simulation is of paramount importance to properly define the initial conditions, namely positions and velocities. The initial conditions should fulfill the constraint equations to minimize the constraints violation during the simulation. In this sense, the initial conditions for this spatial slider-crank mechanism are displayed in Table 2.2.

**Table 2.1** - Dimensional and inertia properties of each body.

Body	Length [m]	Mass [kg]	Principal Moments of Inertia [kg m <sup>2</sup> ]		
			$I_{\xi\xi}$	$I_{\eta\eta}$	$I_{\zeta\zeta}$
Crank	0.10	0.12	0.0001	0.0001	0.00001
Rod	0.29	0.5	0.004	0.0004	0.004
Slider	-	0.5	0.0001	0.0001	0.0001

**Table 2.2** - Initial conditions for the dynamic analysis.

Body	Initial Positions						
	$x$	$y$	$z$	$e_0$	$e_1$	$e_2$	$e_3$
Crank	0.0000	0.0000	0.0500	1.0000	0.0000	0.0000	0.0000
Rod	0.0000	0.0735	-0.0250	0.8680	-0.4966	0.0000	0.0000
Slider	0.0000	0.1470	-0.1500	1.0000	0.0000	0.0000	0.0000
	Initial Velocities						
	$v_x$	$v_y$	$v_z$	$\omega_x$	$\omega_y$	$\omega_z$	
Crank	-0.3142	0.0000	0.0000	0.0000	-6.2832	0.0000	
Rod	-0.3142	0.0000	0.0000	0.0000	-1.5661	-1.6112	
Slider	0.0000	0.0000	0.0000	0.0000	0.0000	0.0000	

For these dynamic simulations, beyond the inertia and reaction forces, the weight of each body is the only external force considered, and it is applied in the negative direction of  $z$  axis ( $g=9.81 \text{ m/s}^2$ ).

The integration process is carried out with the fourth-order Runge-Kutta method with fixed time step. The choice of the integration scheme is directly connected to the error of the process and, the local error for this method is of order  $(\Delta t)^5$ . Long time sim-

ulations were performed to compare the accuracy and efficiency of different methods to solve the equations of motion. For this comparison, several approaches were considered, namely the standard multipliers technique, the Baumgarte stabilization method, the penalty method, the augmented Lagrangian formulation and the direct correction approach. The efficiency of these methods is analyzed through the evaluation of the constraints violation at position and velocity levels, additionally the computational time is also considered. The set of parameters necessary to apply each methodology to calculate the motion of the system is shown in Table 2.3.

**Table 2.3** - Parameters used for the dynamic simulation.

Parameter	Value	Parameter	Value
Time step	0.001 s	Penalty/Augmented - $\omega$	10
Baumgarte - $\alpha$	5	Penalty/Augmented - $\mu$	1
Baumgarte - $\beta$	5	Augmented - $\varepsilon$	$1 \times 10^{-10}$
Penalty/Augmented - $\alpha$	$1 \times 10^{-7}$	Direct Correction - $\varepsilon$	$1 \times 10^{-10}$

The evolution of the constraints violation at position ( $\Phi^T \Phi$ ) and velocity ( $\dot{\Phi}^T \dot{\Phi}$ ) levels for the different methods are presented in Figures 2.7 and 2.8, respectively. The simulation time was 20 s, although the results are presented only for the first 5 s due to an easier interpretation.

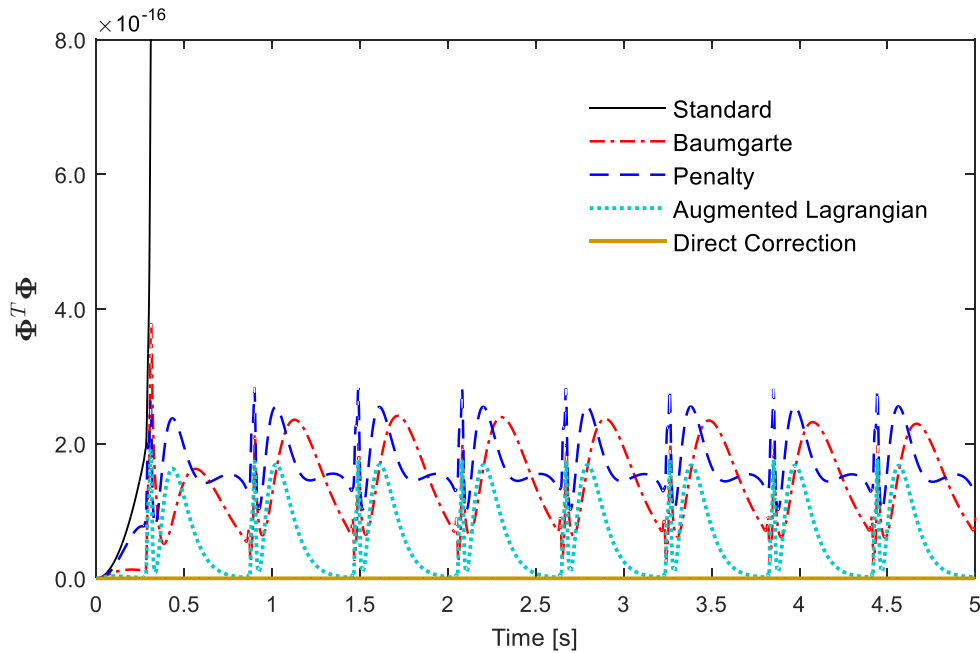


**Figure 2.7** - Positions constraints violation ( $\Phi^T \Phi$ ).

Through the analysis of Figures 2.7 and 2.8, it can be deduced that the standard method let the violation of the constraints grow open-endedly with time, either for positions or velocities. This behavior makes this approach inadequate for long time simulation. However, the constraints violation can be kept under control with the utilization of stabilization methods, such as Baumgarte method, penalty method or augmented Lagrangian. These approaches allow a certain oscillation of the violation of the constraint equations as it is represented in Figures 2.7 and 2.8, the magnitude and frequency of this oscillation vary according the selected penalty factors. In turn, the direct correction approach completely eliminates the errors of the constraints, since the values of violation presented for that technique are not significant.

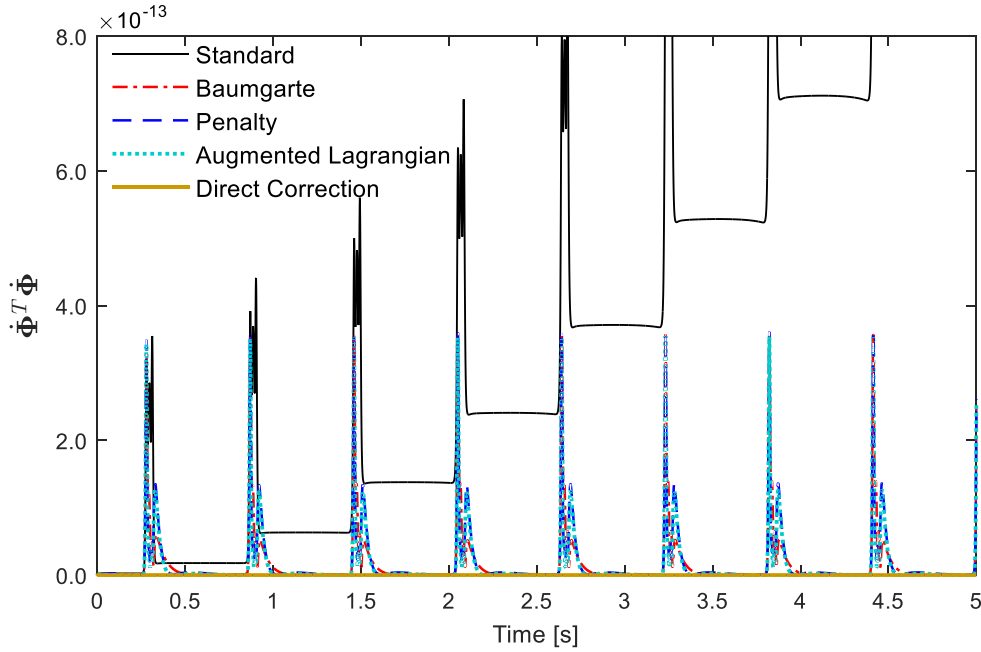


**Figure 2.8** - Velocities constraints violation ( $\dot{\Phi}^T \dot{\Phi}$ ).

Another manner to measure the accuracy of each method consists on the evaluation of the mechanical energy. Since the only external force acting on the system is the weight of the bodies, the mechanical energy must remain constant. However, due to integration errors the energy of the system may suffer alterations. In Figure 2.9, it is represented the variation of the mechanical energy given as

$$\Delta E_M = E_M - E_M^0 \quad (2.103)$$

where  $E_M$  is the sum of kinetic and potential energy ( $E_M = T + V$ ), and  $E_M^0$  is the initial mechanical energy of the system. From the analysis of Figure 2.9, it can be concluded that the standard approach, the Baumgarte method and the augmented Lagrangian for-

mulation make the energy increase. In turn, the penalty method and the direct correction approach cause a reduction of energy, wherein the latter is the method that provokes the largest energy variation.

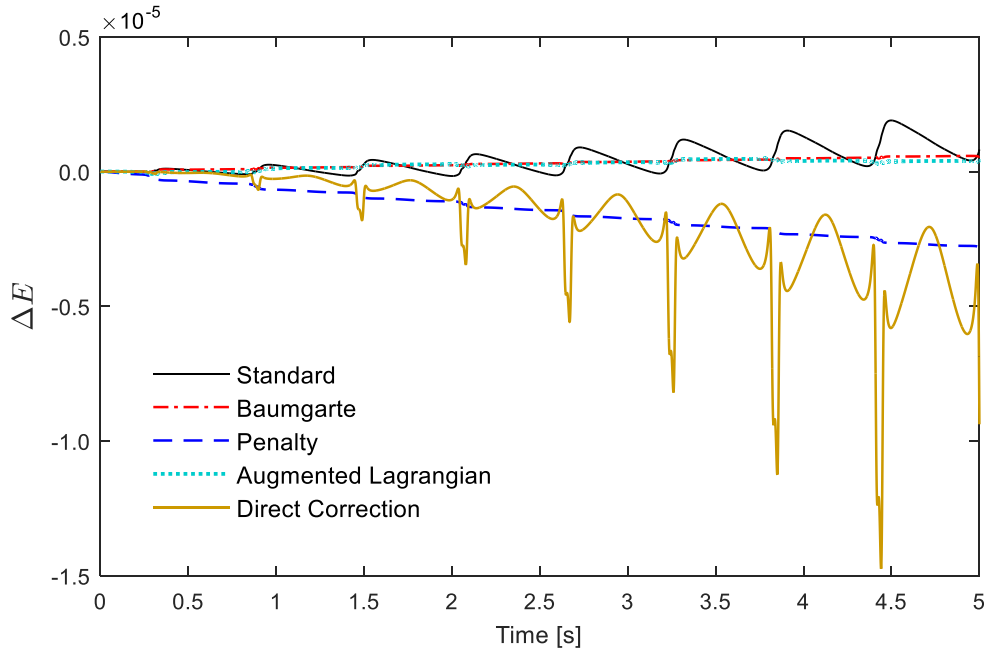


**Figure 2.9** - Variation of mechanical energy.

The computation time ratio for the five approaches considered is presented in Figure 2.10. As it was expected, the standard Lagrange multipliers method is the most efficient, although it does not handle the constraints violation. The Baumgarte method, the penalty method and the augmented Lagrangian formulation present similar computation time, nevertheless the Baumgarte method is not able to handle redundant constraints. For this case, the direct correction approach showed to be the least efficient method.

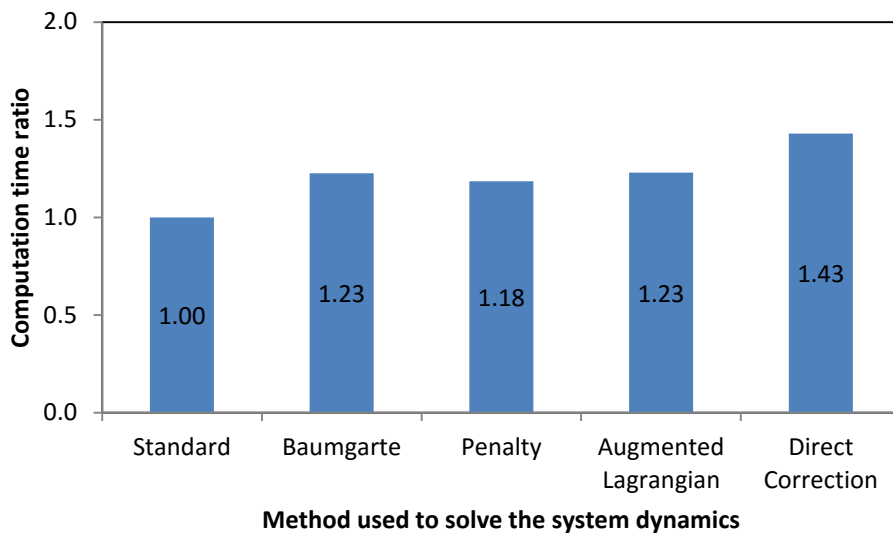


**Figure 2.10** - Comparison of computation time for different methods.

## 2.5 Summary and Conclusions

In this chapter, the basic concepts on multibody dynamics were introduced. A brief study of the available formulations to analyze multibody systems was presented. In the scope of this work, it was chosen to use a body coordinate formulation, and the Newton-Euler approach to construct the equations of motion. This selection concerns to its simplicity and easiness, and since the multibody systems here studied have a small number of bodies, this formulation appears more suitable.

In order to build the equations of motion for spatial multibody systems, it was necessary to introduce the Euler parameters for the representation of rotational coordinates. The kinematic constraint equations were characterized, although any particular case of a kinematic joint is presented in this text. In the wake of the study of the constraints equations it was presented procedure to perform a kinematic analysis of a multibody system.

Then, the Newton-Euler equations for constrained multibody systems were derived. The equations of motion of a free particle were the starting point, they were followed by the rigid body and unconstrained multibody system formulations. The constraints were considered recurring to the Lagrange multipliers technique. Hence, the dynamic equations of a constrained multibody system were presented through Eq. (2.46).

However, the process of solving the equations of motion can present some difficulties, namely the system can hold redundant constraints or singular configurations. Moreover, the equations of motion do not consider the positions and velocities constraints explicitly which leads to the constraints violation. Several methods to solve the equations of motion were described. They have different characteristics and can handle different issues. Some of them were compared with respect to the constraints violation and computational efficiency.

For the comparison of the different methods, it was used a simple example of a spatial slider-crank mechanism. The results showed that the Standard Lagrange multipliers method is more efficient, although it allows the growth of the constraints violation indefinitely. It was verified that other approaches are capable of stabilize or eliminate the errors of the constraints with just a small increase in computational effort.

*“If you can't explain it simply, you don't understand it well enough.”*

Albert Einstein

### **3. FRICTION MODELS FOR MULTIBODY DYNAMICS**

The dynamic simulation of multibody systems is increasingly requiring the accuracy of the results. Bearing that in mind, it is of paramount importance to use reliable techniques to evaluate the friction force in the contacts.

The Coulomb friction law was the major precursor of the evolution of the friction force models. This model however shows a huge inability to capture different friction phenomena. These phenomena have a direct influence on the dynamic response of the system. To mitigate the differences between the reality and friction modelling, robust models have been proposed.

This chapter aims to provide a comprehensive analysis of different friction models for multibody dynamics. In this context, a brief explanation of the main phenomena related to friction will be delivered. Then, the most relevant static and dynamic friction models are summarily described. In the sequel of this process, the main limitations and implications of each approach are highlighted. Finally, the dynamic response of a one degree of freedom mass-spring model is utilized to analyze and compare the various friction models.

#### **3.1 General Issues on Friction**

Friction is a very complex phenomenon. The attempts to describe correctly its behavior have distinct approaches. Their differences are close-banded to their ability to model different characteristics of friction. Preceding the description of the several fric-

tion models, it is of paramount importance to detail the diverse phenomena associated therewith.

Friction consists in the tangential force which opposes to the relative motion of two contacting surfaces. This force can have different outcomes depending on the relative velocity and displacement of the bodies. Moreover, contact geometry and topology, properties of the surface materials and presence of lubrication are also relevant factors.

Thus, friction's properties have been intensively studied (Olsson, 1998; Berger, 2002) and several conclusions were made about its main characteristics and dependences. Throughout this section, there will be discussed some issues that must be considered when modelling friction, namely, stick-slip, viscous friction, frictional lag, pre-sliding displacement and break-away force.

### 3.1.1 Stick-Slip

When the relative velocity of two contacting surfaces is null, the friction force is known as stiction<sup>4</sup>. Several experiments proved that the friction force at rest is higher than the kinetic friction (Rabinowicz, 1951; Scieszka and Jankowski, 1996). Thus, it is usual to consider two different friction coefficients (Borsotto et al., 2009), one for zero velocity (static) and another when relative motion occurs (kinetic).

Bearing that in mind, in case that the relative velocity between two surfaces drops, the friction force will increase which leads to the sticking thereof. This phenomenon is the so called stick-slip (Rabinowicz, 1956; Dieterich, 1978), and it is overcome since the external tangential force is larger than the static friction force, so the bodies start sliding.

The stick-slip is a major problem during the modelling and simulation of mechanical systems since is an unstable phenomenon which is not easy to predict. In this sense, it is important to choose a friction model capable of capturing its behavior. To do so, the model has to consider a different coefficient of friction for the static and kinetic cases, but most of all it should describe a correct transition between them.

This transition was studied by Stribeck (1902) who showed experimentally that, for low velocities, friction decreases with the increase of the relative velocity. This effect implies a continuous drop of friction force which contradicts the discontinuous behavior of considering just two different coefficients of friction. This behavior is de-

---

<sup>4</sup> The term "stiction" results from the contraction of the expression "static friction".



scribed by the Stribeck curve, which was named after him, and represents the steady-state friction as a function of velocity.

Rabinowicz (1951) studied the essence of the static and the kinetic coefficients of friction and their transition. The experimental results showed that the coefficient of friction is not only a function of the relative velocity, but also of the displacement. It was demonstrated that the maximum friction force is reached for low displacements. This behavior along with the Stribeck effect should be carefully implemented to lead to stick-slip motion.

### 3.1.2 Viscous Friction

The existence of a fluid lubricant layer between two rubbing surfaces has a significant influence in the resultant friction force. Thus, there is the necessity to take that into account when using a friction model (Fréne and Cicone, 2001).

To do so, it is generally employed a linear relation between the relative velocity and the viscous friction force, because most of fluid lubricants can be considered Newtonian fluids<sup>5</sup>. However, sometimes nonlinear models can be also applied to describe this phenomenon. Normally, the component of friction force related with viscosity is simply summed to the regular friction model.

### 3.1.3 Frictional Lag

Frictional lag is the delay in change of friction force as a function of velocity. This characteristic behaves as the inertia to the change of friction state. As a consequence there is a hysteresis loop in the relationship between friction force and velocity.

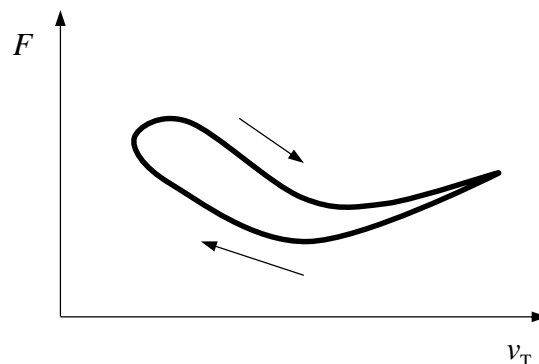


**Figure 3.1** - The friction-velocity relation for a hysteresis loop.

---

<sup>5</sup> A Newtonian fluid presents a linear relation between the applied shear stress and the resulting strain rate. Air, water and thin motor oil are some examples of Newtonian fluids.

Hess and Soom (1990) verified empirically that the friction force does not respond instantaneously to the variation of velocity. Thus, friction lag is a dynamical behavior which results in lower friction forces when velocity is decreasing and larger forces for increasing velocities (Dupont and Dunlap, 1993), as it is shown in Figure 3.1. This phenomenon becomes more evident with larger accelerations and enhances the need to use dynamic friction models.

### 3.1.4 Pre-sliding Displacement

Some researches (Courtney-Pratt and Eisner, 1957; Hsieh and Pan, 2000) have been made in order to study the influence of displacement in friction forces. It was shown experimentally that when any external tangential force is applied between two contacting bodies, always occurs a displacement, which is given by an elastic spring behavior, as it is shown in Figure 3.2.

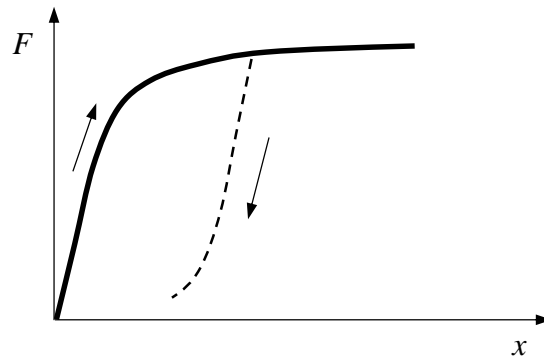


**Figure 3.2-** Pre-sliding displacement behavior.

This phenomenon of a small motion in elastic range when the applied force is less than the break-away force is often called pre-sliding displacement. The explanation for this small displacement relies on the elastic deformation of the asperities of the contacting surfaces (Bowden and Leben, 1939). The adhesion theory states that in the presence of a normal load the asperities tend to adhere. So, when a tangential load is applied the bond tends to break. Before that happening, the asperities should have elastic and, then, plastic deformation which provokes the relative displacement of the contacting surfaces. Since the junctions of asperities are broken, the sticking regime ends and the bodies start sliding.

Although the magnitude of the pre-sliding displacement is small, it should not be neglected. Firstly, it has a relevant impact in the friction force during velocity reversal. Secondly, this displacement can have a narrow importance locally, but if the analyzed

mechanical system has substantial dimensions, it may result in meaningful displacements on the global system.

Furthermore, when the applied external force is diminished, the contacting surfaces will present the same behavior and it will result in a hysteresis loop, as it is represented in Figure 3.2

### 3.1.5 Break-Away Force

The necessary force to initiate the motion and surmount the static friction is called the break-away force which is also the maximum friction force (Rabinowicz, 1951). Normally, the overcoming of this force defines the boundary between the sticking and sliding regimes. Before reaching the break-away force, there is only the aforementioned pre-sliding displacement.

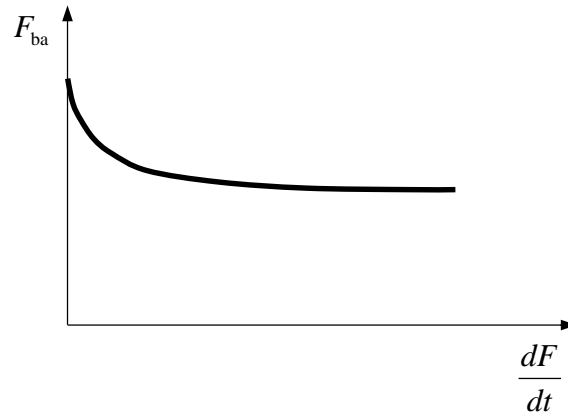


**Figure 3.3** - Relation between rate of force and break-away force.

Johannes et al. (1973) demonstrated that the break-away force depends on the rate of the external applied force. In Figure 3.3, it is shown that the increase of force rate leads to the reduction of the break-away force.

## 3.2 Static Friction Models

This section includes several “static” friction force models frequently used in the simulations of multibody mechanical systems. It must be stated that most of these models present a discontinuity of friction force when the relative velocity is zero, which can cause difficulties in describing friction realistically. In general, these models have some limitations as regards to reproducing the previously mentioned frictional phenomena.

### 3.2.1 Coulomb Friction

Coulomb (1785) presented the first friction model which states that the friction always opposes relative motion between contacting bodies and its magnitude is proportional to the normal contact force. This model depends on the relative velocity direction, except for zero velocity where the friction force is a multivalued function of the external tangential force. This model can be described as

$$\mathbf{F} = \begin{cases} F_C \operatorname{sgn}(\mathbf{v}_T) & \text{if } \|\mathbf{v}_T\| \neq 0 \\ \min(\|\mathbf{F}_e\|, F_C) \operatorname{sgn}(\mathbf{F}_e) & \text{if } \|\mathbf{v}_T\| = 0 \end{cases} \quad (3.1)$$

where

$$F_C = \mu_k \|\mathbf{F}_N\| \quad (3.2)$$

in which  $\mathbf{F}_N$  is the normal force,  $F_C$  is the magnitude of Coulomb friction,  $\mu_k$  is the kinetic coefficient of friction,  $\mathbf{F}_e$  is the external tangential force, and  $\mathbf{v}_T$  is the relative velocity of the contacting bodies. This model presents a dependence on the velocity by the *signum* function,

$$\operatorname{sgn}(\mathbf{v}_T) = \begin{cases} \frac{\mathbf{v}_T}{\|\mathbf{v}_T\|} & \text{if } \|\mathbf{v}_T\| \neq 0 \\ \mathbf{0} & \text{if } \|\mathbf{v}_T\| = 0 \end{cases} \quad (3.3)$$

where  $\mathbf{0}$  is a null vector with the same dimensions as  $\mathbf{v}$ . In Figure 3.4, it is represented the friction force as a function of the relative velocity for the 1D case.

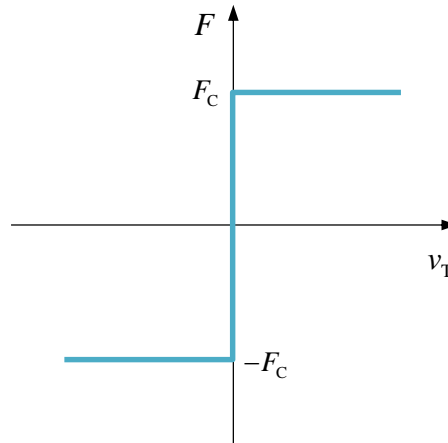


**Figure 3.4** - Representation of Coulomb friction for 1D case.

Although this model is straightforward, it presents some difficulties since it does not specify a friction force at zero velocity. Thus, this velocity dependence can originate perturbations in the dynamic simulations system's response. Nevertheless, the Coulomb friction law is used quite often to simulate friction behavior for the sake of simplicity,

and since it only requires one input parameter; i.e. the coefficient of friction.

### 3.2.2 Coulomb Model with Stiction

Since the friction force at zero velocity is higher than the kinetic friction, several studies have presented the necessity of introducing a friction model which includes two different friction coefficients. This modified Coulomb approach has a similar behavior to Coulomb's except in the vicinity of zero velocity. It is also a multivalued function, but can reach a higher friction force, and can be described as follows

$$\mathbf{F} = \begin{cases} F_C \operatorname{sgn}(\mathbf{v}_T) & \text{if } \|\mathbf{v}_T\| \neq 0 \\ \min(\|\mathbf{F}_e\|, F_S) \operatorname{sgn}(\mathbf{F}_e) & \text{if } \|\mathbf{v}_T\| = 0 \end{cases} \quad (3.4)$$

where

$$F_S = \mu_s \|\mathbf{F}_N\| \quad (3.5)$$

in which  $F_S$  is the magnitude of static friction, and  $\mu_s$  is the static coefficient of friction which is higher than the kinetic,  $\mu_k$ . The variation of the friction force with the relative velocity is shown in Figure 3.5.

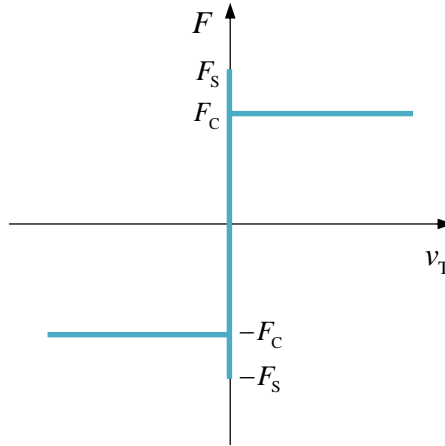


**Figure 3.5** - Representation of the Coulomb model with stiction for 1D case.

Although this model considers stiction, since it hardly reach exact null velocity during a simulation. In practice, it provides similar behavior compared to Coulomb's law, with an oscillatory force for low velocities.

### 3.2.3 Coulomb Model with Viscous Friction

One of most common modification of Coulomb's friction law deals with is the introduction of viscous friction component. Considering a linear relationship between the relative velocity and the friction force related to the lubricants viscosity, the friction

model can be written as

$$\mathbf{F} = \begin{cases} F_C \operatorname{sgn}(\mathbf{v}_T) + F_v \mathbf{v}_T & \text{if } \|\mathbf{v}_T\| \neq 0 \\ \min(\|\mathbf{F}_e\|, F_C) \operatorname{sgn}(\mathbf{F}_e) & \text{if } \|\mathbf{v}_T\| = 0 \end{cases} \quad (3.6)$$

where  $F_v$  is the viscous friction coefficient which is deeply related to the viscosity of the fluid. The behavior of this model is presented in Figure 3.6.

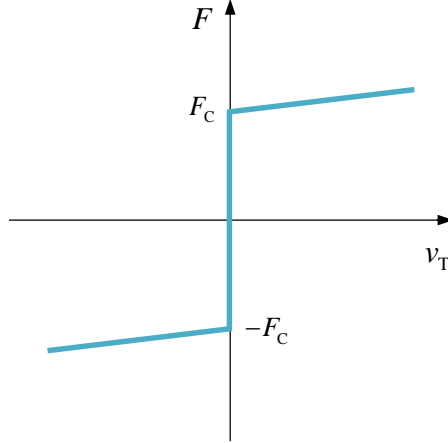


**Figure 3.6** - Representation of Coulomb model with linear viscous friction for 1D case.

Although, sometimes it can be adopted a nonlinear relation with the velocity, because it could be a better fit with the experimental data,

$$\mathbf{F} = \begin{cases} F_C \operatorname{sgn}(\mathbf{v}_T) + F_v \|\mathbf{v}_T\|^{\delta_v} \operatorname{sgn}(\mathbf{v}_T) & \text{if } \|\mathbf{v}_T\| \neq 0 \\ \min(\|\mathbf{F}_e\|, F_C) \operatorname{sgn}(\mathbf{F}_e) & \text{if } \|\mathbf{v}_T\| = 0 \end{cases} \quad (3.7)$$

where  $\delta_v$  depends on the geometry of the contact. Notwithstanding, this type of approximation is not commonly employed, since it requires an extra parameter.

### 3.2.4 Model with Stribeck Effect

In contrast with Coulomb model with stiction, the Stribeck effect (Stribeck, 1902) ensures that the decrease from static to kinetic friction is a continuous process. Thus, the friction force during relative motion is expressed as a continuous function of velocity as

$$\mathbf{F} = \begin{cases} \mathbf{F}(\mathbf{v}_T) & \text{if } \|\mathbf{v}_T\| \neq 0 \\ \min(\|\mathbf{F}_e\|, F_S) \operatorname{sgn}(\mathbf{F}_e) & \text{if } \|\mathbf{v}_T\| = 0 \end{cases} \quad (3.8)$$

where  $\mathbf{F}(\mathbf{v}_T)$  is an arbitrary function that depends on the relative velocity. With this model the friction force diminishes when the relative motion is initiated, as it is represented in Figure 3.7.

Several mathematical expressions have been proposed to describe that curve. Hess and Soom (1990) suggested

$$\mathbf{F}(\mathbf{v}_T) = \left( F_C + \frac{F_S - F_C}{1 + \left( \frac{\|\mathbf{v}_T\|}{v_s} \right)^2} \right) \text{sgn}(\mathbf{v}_T) + F_v \mathbf{v}_T \quad (3.9)$$

where  $v_s$  is the Stribeck velocity. However, the most popular was introduced by Bo and Pavelescu (1982) which considers an exponential function as follows

$$\mathbf{F}(\mathbf{v}_T) = \left( F_C + (F_S - F_C) e^{-\left( \frac{\|\mathbf{v}_T\|}{v_s} \right)^{\delta_\sigma}} \right) \text{sgn}(\mathbf{v}_T) + F_v \mathbf{v}_T \quad (3.10)$$

in which  $\delta_\sigma$  is a factor that relies on the geometry of the contacting surfaces, which is often considered 2 as suggested by Armstrong-Hélouvry (1991).

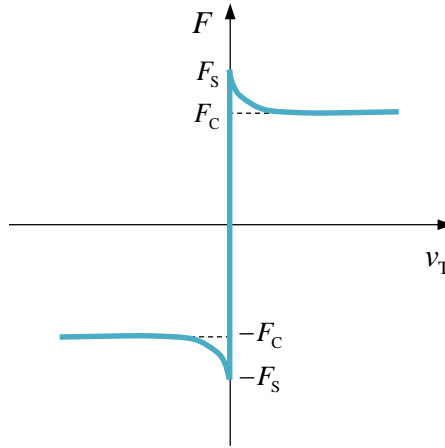


**Figure 3.7** - Representation of the Stribeck curve without viscous friction.

This friction model takes into account the Coulomb, viscous, stiction and Stribeck friction effects. However, it presents the same problem as the previous approaches at zero velocity.

### 3.2.5 Karnopp Model

Since the aforementioned models are multivalued functions for zero velocity, their static behavior cannot be captured during a simulation. To overcome this difficulty, Karnopp (1985) proposed a model where the velocity is considered zero, for a specified range, as it is shown in Figure 3.8. Thus, when the velocities are within the interval, the system's state can change and the model's response will be the same as when the relative velocity is zero.

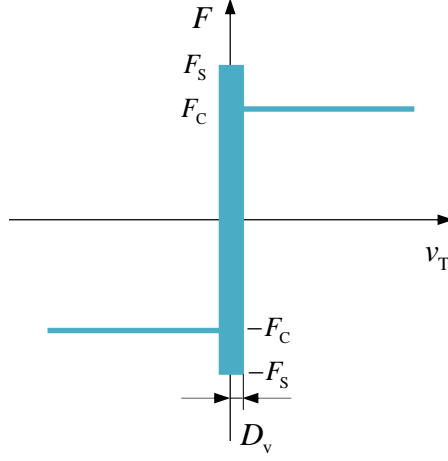


**Figure 3.8** - Representation of Karnopp model with Coulomb friction for 1D case.

Karnopp model is usually used along the Coulomb model and can be expressed as

$$\mathbf{F} = \begin{cases} \mathbf{F}(\mathbf{v}_T) & \text{if } \|\mathbf{v}_T\| > D_v \\ \min(\|\mathbf{F}_e\|, F_s) \text{sgn}(\mathbf{F}_e) & \text{if } \|\mathbf{v}_T\| \leq D_v \end{cases} \quad (3.11)$$

where  $D_v$  is the tolerance for zero velocity and  $\mathbf{F}(\mathbf{v}_T)$  is an arbitrary function for the friction force outside of the tolerance velocity. It is important to select a suitable range of the null velocity (Liu et al., 2009; Bicakci et al., 2014). Nevertheless, this zero velocity interval does not comply with the real behavior of the contact.

### 3.2.6 Switch Model

In order to reduce the numerical instability for the sticking phase, Leine et al. (1998) proposed a modification of Karnopp friction model. The main difference between both models occurs during the sticking phase when the external tangential force is lower than the maximum static friction force. In that case, for Karnopp model, the friction force equalizes the external tangential force, which means there is null acceleration in the tangential direction.

However, this sudden change of the acceleration will result in numerical instability. To solve that problem Leine et al. suggested the direct determination of the acceleration instead of calculating the friction force, as it follows

$$\mathbf{a} = -\mathbf{v}_T \sqrt{\frac{k}{m}} \quad (3.12)$$

where  $k$  is the stiffness of the external force, and  $m$  is the mass of the body. Thus, the acceleration is exactly zero only for null relative velocity.



### 3.2.7 Models with Finite Slope at Zero-Velocity

In most of the static models described above, the friction force at zero velocity is multivalued, being evaluated as a function of the external tangential force. In order to simplify and ensure computational efficiency, several researchers have proposed alternative methods, which replace the discontinuity at zero velocity by a finite slope model. This strategy normally avoids computational instability due to the change of the direction of the velocity.

In order to smooth the discontinuity of the Coulomb friction model at zero velocity, several modifications were proposed (Andersson et al., 2007). One approach consists in using linear friction velocity dependence for low velocities, which can be expressed by the following equation

$$\mathbf{F} = F_C \min(k \|\mathbf{v}_T\|, 1) \text{sgn}(\mathbf{v}_T) \quad (3.13)$$

where  $k$  is a coefficient that gives the slope for null velocity. In Figure 3.9, it is displayed this model for the 1D case.

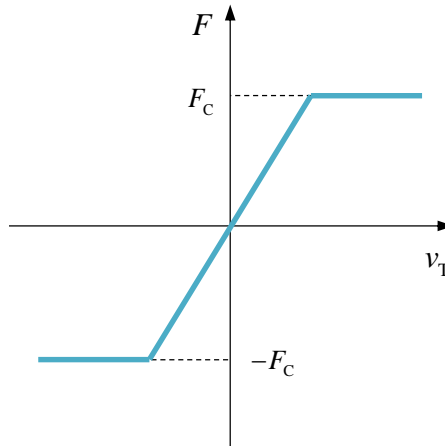


**Figure 3.9** - Representation of Coulomb model with linear friction modification for 1D case.

Another possibility resides in utilizing a hyperbolic tangent approximation, which is a more numerically stable model since it has a continuous derivative. The friction force is given by

$$\mathbf{F} = F_C \tanh(k \|\mathbf{v}_T\|) \text{sgn}(\mathbf{v}_T) \quad (3.14)$$

Threlfall (1978) also presented a model which softens the existing discontinuity in the Coulomb law. The curve that represents this model is displayed in Figure 3.10. This approach also does not pay attention to most of friction characteristics, and can be described by the following expression

$$\mathbf{F} = \begin{cases} F_C \left( 1 - e^{-\frac{3\|\mathbf{v}_T\|}{v_0}} \right) \text{sgn}(\mathbf{v}_T) & \text{if } \|\mathbf{v}_T\| \leq v_0 \\ F_C \text{sgn}(\mathbf{v}_T) & \text{if } \|\mathbf{v}_T\| > v_0 \end{cases} \quad (3.15)$$

where  $v_0$  is a tolerance velocity. The resemblance with Coulomb friction law increases with the decreasing of this tolerance velocity.

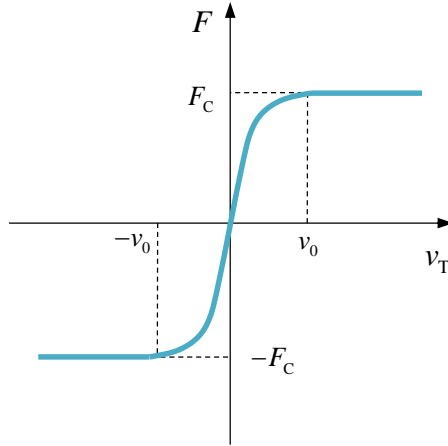


**Figure 3.10** - Representation of Threlfall model for 1D case.

The use of a finite slope at zero velocity has been also extended to models which take into account stiction. One of the most popular approaches consists in considering a peak of friction force for a given velocity, and performing a linear interpolation, as it is shown in Figure 3.11. The model can be expressed as

$$\mathbf{F} = \begin{cases} \left( \frac{\|\mathbf{v}_T\|}{v_0} F_S \right) \text{sgn}(\mathbf{v}_T) & \text{if } \|\mathbf{v}_T\| \leq v_0 \\ \left( F_S - \frac{\|\mathbf{v}_T\| - v_0}{v_1 - v_0} (F_S - F_C) \right) \text{sgn}(\mathbf{v}_T) & \text{if } v_0 < \|\mathbf{v}_T\| < v_1 \\ F_C \text{sgn}(\mathbf{v}_T) & \text{if } \|\mathbf{v}_T\| \geq v_1 \end{cases} \quad (3.16)$$

where  $v_0$  and  $v_1$  are the tolerances for the tangential velocity.

Bengisu and Akay (1994) proposed a model capable of modelling the Stribeck effect, as it is represented in Figure 3.12. The model is constituted by two equations (one for the slope and another to describe the Stribeck effect) which are given as

$$\mathbf{F} = \begin{cases} \left( -\frac{F_S}{v_0^2} (\|\mathbf{v}_T\| - v_0)^2 + F_S \right) \text{sgn}(\mathbf{v}_T) & \text{if } \|\mathbf{v}_T\| < v_0 \\ \left( F_C + (F_S - F_C) e^{-\xi(\|\mathbf{v}_T\| - v_0)} \right) \text{sgn}(\mathbf{v}_T) & \text{if } \|\mathbf{v}_T\| \geq v_0 \end{cases} \quad (3.17)$$

in which  $\zeta$  should be a positive parameter which represents the negative slope of the sliding state.

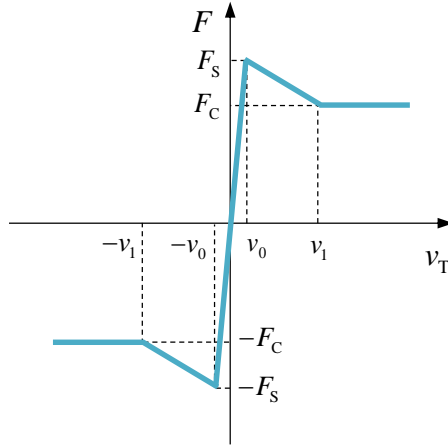


**Figure 3.11** - Representation of the linear model with stiction for 1D case.

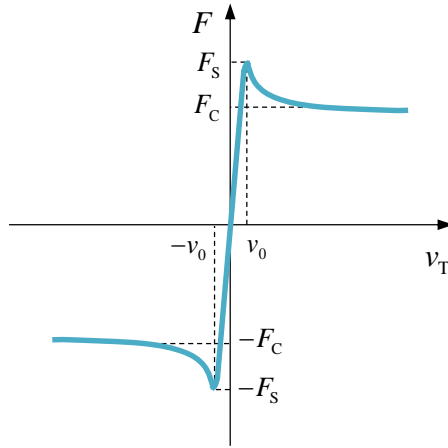


**Figure 3.12** - Representation of the Bengisu and Akay model for 1D case.

However, these models have some particularities. When the slope at zero velocity is too large, a small step size is needed to correctly capture friction for low velocities, which will slow down the simulation. In addition, for velocities close to zero, the friction force will always be low irrelevant of the displacement.

### 3.2.8 Ambrósio Model

The above mentioned limitations associated with friction force's discontinuity led Ambrósio (2003) to propose a modified Coulomb's friction law in which the friction force can be defined as

$$\mathbf{F} = \begin{cases} \mathbf{0} & \text{if } \|\mathbf{v}_T\| \leq v_0 \\ \frac{\|\mathbf{v}_T\| - v_0}{v_1 - v_0} F_C \operatorname{sgn}(\mathbf{v}_T) & \text{if } v_0 < \|\mathbf{v}_T\| < v_1 \\ F_C \operatorname{sgn}(\mathbf{v}_T) & \text{if } \|\mathbf{v}_T\| \geq v_1 \end{cases} \quad (3.18)$$

where  $v_0$  and  $v_1$  are the tolerances for the velocity. The main difference of this model is the null friction force for low velocities, as it is shown in Figure 3.13.

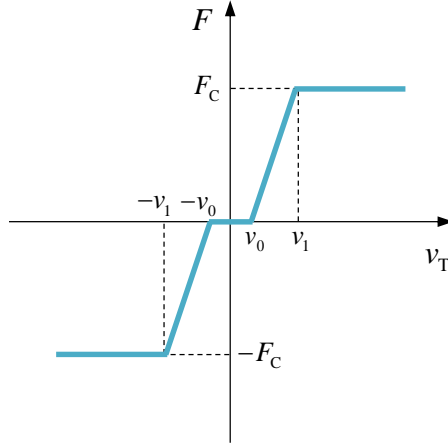


**Figure 3.13** - Representation of Ambrósio friction model for 1D case.

This approach prevents the friction force from changing direction when the relative velocity is close to zero. However, it does not describe the stick-slip motion.

### 3.2.9 The Seven Parameter Model

This model is also known as Armstrong model (Armstrong-Hélouvry et al., 1994), and it includes several frictional effects as the pre-sliding displacement, Coulomb and viscous friction, Stribeck effect and frictional lag. It consists of two separate equations, one for sticking

$$\mathbf{F} = \sigma_0 \mathbf{x} \quad (3.19)$$

and another for the sliding regime

$$\mathbf{F} = \left( F_C + \frac{F_S(\gamma, t_d) - F_C}{1 + \left( \frac{\|\mathbf{v}_T(t - \tau_L)\|}{v_S} \right)^2} \right) \operatorname{sgn}(\mathbf{v}_T) + F_v \mathbf{v}_T \quad (3.20)$$

with

$$F_S(\gamma, t_2) = F_{S,a} + (F_{S,\infty} - F_{S,a}) \frac{t_d}{t_d + \gamma} \quad (3.21)$$

where  $F_C$  is the Coulomb friction force,  $F_v$  denotes the viscous friction coefficient,  $F_S$  is the magnitude of static friction,  $F_{S,a}$  represents the magnitude of static friction at the end of the previous sliding period,  $F_{S,\infty}$  is the magnitude of static friction after a long time at rest,  $\sigma_0$  expresses the tangential stiffness of the contact,  $v_S$  is the Stribeck velocity,  $\tau_L$  denotes the time constant of frictional memory,  $\gamma$  is the temporal parameter of the rising static friction and  $t_d$  is the dwell time, *i.e.*, the time at zero velocity.

Although this approach seems to describe most of the characteristics of friction behaviour, it also presents some drawback. Firstly, to implement this model is necessary to define seven parameters, which is not an easy task since most of them have to be determined experimentally. Secondly, the Armstrong model is constituted by two separate states, one for sticking and another for sliding, and there is no criterion defined to determine when the switch must occur. Since it is not easy to predict when the transition has to happen, it must be defined an eighth parameter to evaluate if the model should switch between states. Moreover, every time the switch occurs, the model state variables must be properly initialized.

### 3.2.10 Awrejcewicz et al. Model

Awrejcewicz et al. (2008) proposed a static friction model for dry contact which is dependent of both tangential force and relative velocity. This model is governed by four different equations, one for sliding, two for the transition from stick to slip, and one for sticking, as follows

$$\mathbf{F} = \begin{cases} \mathbf{F}(\mathbf{v}_T) & \text{if } \|\mathbf{v}_T\| > v_0 \\ F_S \operatorname{sgn}(\mathbf{F}_e) & \text{if } \|\mathbf{v}_T\| \leq v_0 \wedge \|\mathbf{F}_e\| > F_S \wedge \mathbf{F}_e \cdot \mathbf{v}_T \geq 0 \\ (2A-1)F_S \operatorname{sgn}(\mathbf{v}_T) & \text{if } \|\mathbf{v}_T\| \leq v_0 \wedge \|\mathbf{F}_e\| > F_S \wedge \mathbf{F}_e \cdot \mathbf{v}_T < 0 \\ A(-\mathbf{F}_e + F_S \operatorname{sgn}(\mathbf{v}_T)) + \mathbf{F}_e & \text{if } \|\mathbf{v}_T\| \leq v_0 \wedge \|\mathbf{F}_e\| \leq F_S \end{cases} \quad (3.22)$$

in which

$$A = \frac{\|\mathbf{v}\|^2}{v_0^2} \left( 3 - 2 \frac{\|\mathbf{v}_T\|}{v_0} \right)$$

where  $v_0$  is a velocity tolerance, and  $\mathbf{F}(\mathbf{v}_T)$  is an arbitrary friction function for sliding which depends on the velocity. The tolerance velocity defines the limit for sliding state. Below this tolerance, the friction force is also calculated as a function of the external tangential force.

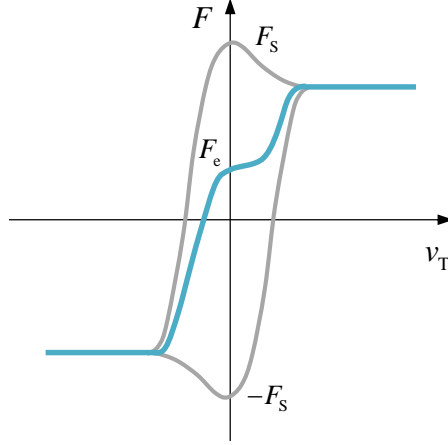


**Figure 3.14** - Representation of the Awrejcewicz et al. model for 1D case.

In Figure 3.14, it is displayed a curve of friction force for a given external tangential force ( $F_e$ ). There are also represented the curves for the minimum and maximum friction force.

### 3.2.11 Wojewoda et al. Model

In order to capture most of friction features, Wojewoda et al (2008) proposed a static friction model for dry contact of hysteretic type with a stochastic component. This model is divided into three different states, one for sticking, and two for sliding (acceleration and deceleration), and it can be expressed as

$$\mathbf{F}(\mathbf{v}_T, \dot{\mathbf{v}}_T) = \begin{cases} F_{st} \operatorname{sgn}(\mathbf{v}_T) & \text{if } F_{st} \leq F_{d+} \wedge \operatorname{sgn}(\mathbf{v}_T \cdot \dot{\mathbf{v}}_T) \geq 0 \\ F_{d+} \operatorname{sgn}(\mathbf{v}_T) & \text{if } F_{st} > F_{d+} \wedge \operatorname{sgn}(\mathbf{v}_T \cdot \dot{\mathbf{v}}_T) \geq 0 \\ F_{d-} \operatorname{sgn}(\mathbf{v}_T) & \text{if } \operatorname{sgn}(\mathbf{v}_T \cdot \dot{\mathbf{v}}_T) < 0 \end{cases} \quad (3.23)$$

with

$$F_{st} = \frac{1}{2} k_s \frac{\|\mathbf{v}_T\|^2}{\|\dot{\mathbf{v}}_T\|} - F_0 \quad (3.24)$$

$$F_{d+} = F_C + (F_S(\mathbf{v}_T) - F_C)(g(\mathbf{v}_T, \dot{\mathbf{v}}_T) + f_R(\mathbf{x}, \mathbf{v}_T)) \quad (3.25)$$

$$F_{d-} = F_C - (F_S - F_C)(g(\mathbf{v}_T, \dot{\mathbf{v}}_T) + f_R(\mathbf{x}, \mathbf{v}_T)) \quad (3.26)$$

where  $F_{st}$  is the friction for the sticking phase,  $F_{d+}$  and  $F_{d-}$  represent the friction force in acceleration and deceleration, respectively,  $k_s$  is the contact stiffness,  $F_0$  denotes the initial value for sticking force,  $f_R(\mathbf{x}, \mathbf{v}_T)$  is a stochastic function, and  $g(\mathbf{v}_T, \dot{\mathbf{v}}_T)$  expresses a function to model the Stribeck curve. The stochastic function intends to simulate random features as variations of normal pressure force or inhomogeneous asperity of con-

tacting surfaces.

The researchers considered a variable static friction force during the acceleration phase, as it is shown in Eq. (3.25). They suggested the following expression

$$F_s(\mathbf{v}_T) = F_s + \Delta F_s \frac{1}{1 + \frac{\|\mathbf{v}_T\|}{v_s}} \quad (3.27)$$

where  $\Delta F_s$  represents the range of break-away force variation, and  $v_s$  is the Stribeck velocity.

### 3.3 Dynamic Friction Models

This section includes some of the most relevant dynamic friction models. As described earlier, in general, the static friction approaches have limitations in capturing some friction phenomena, such as pre-sliding displacement or frictional lag. Thus, better alternatives should be discussed, namely the available dynamic friction models, also named state variable models. In a simple manner, the dynamic models introduce an extra state variable which is used together with the velocity to calculate the friction force.

#### 3.3.1 Dahl Model

The Dahl friction model (Dahl, 1968, 1976) was developed with the aim of describing the friction behavior of ball bearings. The basis of this solution is an analogy with the classical stress-strain curve of materials. Dahl observed that in brittle materials, the difference between the stiction and Coulomb friction is difficult to capture. Ductile materials, however, are more probable of having the stiction behavior and then decrease the stress until Coulomb friction is reached. Moreover, it was shown that, the friction force is dependent on relative velocity and displacement. Dahl model states that when the contacting surfaces are subjected to stress, the friction force increases until rupture occurs. In this context, the stress-strain curve can be described by a differential equation as

$$\frac{dF}{dx} = \sigma_0 \left| 1 - \frac{F}{F_C} \operatorname{sgn}(v_T) \right|^\alpha \operatorname{sgn} \left( 1 - \frac{F}{F_C} \operatorname{sgn}(v_T) \right) \quad (3.28)$$

where  $F$  denotes the friction force,  $x$  is the displacement,  $F_C$  is the Coulomb friction,  $\sigma$  represents the stiffness coefficient and  $\alpha$  is a parameter that defines the shape of the material curve. This parameter depends on the material, and usually varies between 0 and 1

for brittle materials, and is higher than 1 for ductile materials. From the analysis of Eq. (3.28), when  $F$  tends to  $F_C$ , the derivative tends to zero, so it can be concluded that the magnitude of the friction force does not exceed  $F_C$ .

Equation (3.28) can be modified to a time derivative, yielding

$$\frac{dF}{dt} = \frac{dF}{dx} \frac{dx}{dt} = \frac{dF}{dx} v_T = \sigma_0 \left| 1 - \frac{F}{F_C} \operatorname{sgn}(v_T) \right|^\alpha \operatorname{sgn} \left( 1 - \frac{F}{F_C} \operatorname{sgn}(v_T) \right) v_T \quad (3.29)$$

This formulation can be generalized for the 3D case. The most common value for  $\alpha$  is 1, yielding the Dankowicz model (Dankowicz, 1999) as,

$$\frac{d\mathbf{F}}{dt} = \sigma_0 \left( 1 - \frac{\mathbf{F} \cdot \operatorname{sgn}(\mathbf{v}_T)}{F_C} \right) \mathbf{v}_T \quad (3.30)$$

Introducing the state variable  $\mathbf{z}$ , and assuming that  $\mathbf{F} = \sigma_0 \mathbf{z}$ , Eq. (3.30) can be rewritten as

$$\frac{d\mathbf{z}}{dt} = \left( 1 - \frac{\sigma_0}{F_C} \mathbf{z} \cdot \operatorname{sgn}(\mathbf{v}_T) \right) \mathbf{v}_T \quad (3.31)$$

It can be observed from Eq. (3.31) that when the system reaches the steady state, the friction force can be simplified as

$$\mathbf{F} = F_C \operatorname{sgn}(\mathbf{v}_T) \quad (3.32)$$

which is in fact the Coulomb friction model.

It must be highlighted that the Dahl model is not capable of capturing the Stribeck effect and stiction, since it is based on the dry Coulomb friction model with the introduction of pre-sliding displacement through a new state variable, eliminating the discontinuity at zero velocity.

### 3.3.2 The Bristle Model

One type of friction models is the so called physics-motivated friction models. They can describe friction in one of three levels: atomic-molecular, asperity-scale and tectonic-plate level. The most common is the asperity-scale level and its most recognized example is the bristle model.

Haessig and Friedland (1991) presented a model which intends to simulate the randomness associated with frictional behavior of the contact between two surfaces with irregularities.

This model considers that the friction force is originated by the deformation of the asperities. Each contact is modelled as a bond between a rigid bristle and a massless



bristle. The contact behaves as a spring, when relative motion happens, the strain in the bristle increases as well as the friction force. The total friction force is given by the summation of each spring force,

$$\mathbf{F} = \sum_{i=1}^N \sigma_i (\mathbf{x}_i - \mathbf{b}_i) \quad (3.33)$$

where  $N$  denotes the number of bristles,  $\sigma_i$  represents the stiffness of the bristles,  $\mathbf{x}_i$  is the relative position of the bristles, and  $\mathbf{b}_i$  is the location where the connection was formed. When the strain at a certain bristle exceeds its limit ( $\|\mathbf{x}_i - \mathbf{b}_i\| > \delta_i$ ), the rupture of that bond occurs and a new bond is formed in a random location which is calculated from the previous one.

The capacity of the bristle model to capture the random behavior highly depends on the number of bristles chosen. Instead of considering the real number of bonds, this approach only regards a much smaller number. The authors suggest less than 50. The higher the number of used bristles, the more complex the model becomes. This makes the model inefficient for computational simulation and, therefore, it is not usually employed.

### 3.3.3 The Reset Integrator Model

The same authors of the bristle model (Haessig and Friedland, 1991) proposed also a more efficient and workable model, which is an evolution of the Dahl model. In this approach, the friction force is originated by the elastic and plastic deformations of the surface asperities. Each contact is modeled as a bond between two bristles. The reset integrator model does not allow for the bond to break, which means that when the strain of a connection increases until reaching the rupture point, the model ensures that it is kept constant. This model uses an extra state variable ( $\mathbf{z}$ ) to determine the strain in the bond and to account the stiction, as

$$\frac{d\mathbf{z}}{dt} = \begin{cases} \mathbf{0} & \text{if } \|\mathbf{z}\| \geq z_0 \wedge \mathbf{z} \cdot \mathbf{v}_T > 0 \\ \mathbf{v}_T & \text{otherwise} \end{cases} \quad (3.34)$$

Similar to other friction models, the reset integrator model is also composed of two state equations, one for sticking and another for sliding. The transition between those two phases occurs when the deflection reaches its maximum value  $z_0$ . This friction force can then be defined as follows

$$\mathbf{F} = \begin{cases} \sigma_0(\mathbf{v}_T)(1+a)\mathbf{z} + \sigma_1 \frac{d\mathbf{z}}{dt} & \text{if } \|\mathbf{z}\| < z_0 \\ \sigma_0(\mathbf{v}_T) z_0 \text{sgn}(\mathbf{z}) & \text{if } \|\mathbf{z}\| \geq z_0 \end{cases} \quad (3.35)$$

where  $\sigma_1 d\mathbf{z}/dt$  is the damping term that introduces some physical meaning by having damping oscillations and viscous friction effects,  $a$  denotes the coefficient pertaining to the stiction, and  $\sigma_0(\mathbf{v}_T)$  is the contact stiffness. This friction force model has a discontinuity when the analysis changes between sticking and sliding situations.

### 3.3.4 Bliman-Sorine Model

Bliman and Sorine (1991, 1993, 1995) developed a family of dynamic friction models based on the approach proposed by Dahl (1968). In this model, the magnitude of friction force only depends on the sign of relative velocity and the space variable  $s$ , which produces a variable transformation,

$$ds = |v_T(t)| dt \quad (3.36)$$

or in the integral form

$$s = \int_0^t |v_T(\tau)| d\tau \quad (3.37)$$

This space variable can be defined as the absolute relative displacement of the contacting bodies since the last velocity's change. Hence, these models can be expressed as linear system,

$$\frac{dx_s}{ds} = Ax_s + Bv_s \quad (3.38)$$

$$F = Cx_s \quad (3.39)$$

where  $v_s = \text{sgn}(v_T)$ .

Bliman and Sorine introduced a family of models which have variable complexity. For the first-order model, the constants are given by

$$A = -\frac{1}{\epsilon_f}, B = \frac{f_1}{\epsilon_f} \text{ and } C = 1 \quad (3.40)$$

Considering these values, the differential equation for the friction force can be written as

$$\frac{dF}{dt} = \frac{dF}{ds} \frac{ds}{dt} = \frac{dF}{ds} |v_T| = \frac{f_1}{\epsilon_f} \left( v_T - |v_T| \frac{F}{f_1} \right) \quad (3.41)$$

Thus, Eq. (3.41) is similar to Eq. (3.29) and consequently, to the Dahl model, if  $F_C = f_1$ ,  $\sigma = f_1/\epsilon_f$ , and  $\alpha = 1$ . Bearing that in mind, this model is not capable of capturing

stiction or the Stribeck effect. Although the second-order model allows including that phenomena, considering the following constants

$$A = \begin{pmatrix} -\frac{1}{\eta\epsilon_f} & 0 \\ 0 & -\frac{1}{\epsilon_f} \end{pmatrix}, B = \begin{pmatrix} \frac{f_1}{\eta\epsilon_f} \\ -\frac{f_2}{\epsilon_f} \end{pmatrix} \text{ and } C = (1 \quad 1) \quad (3.42)$$

This model works as a parallel connection of a fast and a slow Dahl model. The force generated by the slow model should be subtracted from the fast model, which results in a stiction peak.

### 3.3.5 Models for Lubricated Contact

In the presence of very large normal load and relative velocity, it is not possible to design a system with a dry friction mechanism. In those cases, it is convenient to use a fluid lubricant, which is widely employed in several engineering applications. The lubricants normally lead to the diminishing of the friction force and the temperature in the interface.

Regardless the existence of some mechanisms of calculating the friction forces due to the presence of lubricants, it appeared the need of developing new friction models based on hydrodynamics. In that sense, Harnoy and Friedland (1994) proposed a new approach based on the hydrodynamics of a lubricated journal bearing. In this model, the friction force can be determined by Eq. (3.43) and the most relevant state variable is the eccentricity of the bearing  $\epsilon$ ,

$$F = K_1 (\epsilon - \epsilon_{tr})^2 \Delta + \frac{K_2}{\sqrt{1 - \epsilon^2}} v \quad (3.43)$$

in which

$$\Delta = \begin{cases} 1 & \text{if } \epsilon > \epsilon_{tr} \\ 0 & \text{otherwise} \end{cases} \quad (3.44)$$

The first term of Eq. (3.43) is related to the shearing of the contacts between asperities, and the second term concerns to the viscosity of lubricants.  $K_1$  and  $K_2$  are constant coefficients for each type of force,  $\epsilon_{tr}$  is the threshold eccentricity and  $\Delta$  is a function which imposes that, for small eccentricities, there is no friction force due to asperities contacts. The eccentricity can be calculated by a fourth-order differential equation, which determines the pressure distribution in the lubricant.

### 3.3.6 LuGre Model

The LuGre<sup>6</sup> model was proposed by Canudas de Wit et al. (1995) and can be considered as a derivation from the Dahl model (Dahl, 1968). This model is capable of capturing the Stribeck and stiction effects. In a simple way, this model considers friction as the result of the interactions of the surfaces bristles, it only regards to the average of the bristle deflection. When a force is applied, the bristles start to deform with spring behavior during the sticking phase. Then if the force is sufficiently large, the bodies start to slip.

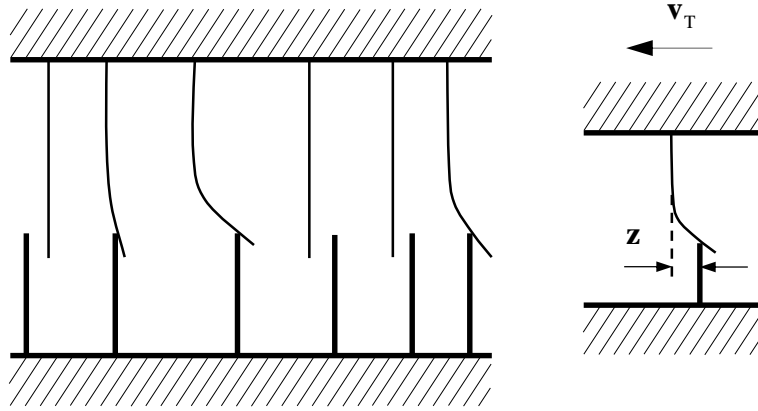


**Figure 3.15** - Physical interpretation of LuGre model.

To quantify the average bristle deflection, it is necessary to introduce an internal state variable  $\mathbf{z}$ , as it is represented in Figure 3.15. Thus, the model follows as

$$\frac{d\mathbf{z}}{dt} = \left( 1 - \frac{\sigma_0}{g(\mathbf{v}_T)} \mathbf{z} \cdot \text{sgn}(\mathbf{v}_T) \right) \mathbf{v}_T \quad (3.45)$$

$$\mathbf{F} = \sigma_0 \mathbf{z} + \sigma_1(\mathbf{v}_T) \frac{d\mathbf{z}}{dt} + f(\mathbf{v}_T) \quad (3.46)$$

where  $\sigma_0$  is the stiffness of the bristles,  $\sigma_1(\mathbf{v}_T)$  is the damping of the bristles which can be set at constant, or can be a function of velocity,  $f(\mathbf{v}_T)$  is an arbitrary function that describes the viscous effect and  $g(\mathbf{v}_T)$  is an arbitrary function that accounts for the Stribeck effect as

$$g(\mathbf{v}_T) = F_C + (F_S - F_C) e^{-\left( \frac{\|\mathbf{v}_T\|}{v_s} \right)^2} \quad (3.47)$$

where  $F_C$  is the Coulomb friction,  $F_S$  is the static friction and  $v_s$  is the characteristic velocity of the Stribeck friction (Armstrong-Hélouvry, 1991).

---

<sup>6</sup> The name “LuGre” arose from the cooperation between the universities of Lund and Grenoble.

For  $f(\mathbf{v}_T)$ , typically a linear viscous friction is considered, that is

$$f(\mathbf{v}_T) = \sigma_2 \mathbf{v}_T \quad (3.48)$$

The effect of this term is quite important when there is a fluid lubricant or when the relative velocity is high.

The bristles damping is given as a function of relative velocity. In most cases, this parameter is set constant, however it is reasonable to let the damping decrease with the increasing of velocity. This happens due to the more amount of lubricant that is forced into the interface for high velocities. Thus, one possible approach to express the bristle damping is

$$\sigma_1(\mathbf{v}_T) = \sigma_1 e^{-\left(\frac{\|\mathbf{v}_T\|}{v_d}\right)^2} \quad (3.49)$$

where  $v_d$  is a characteristic damping velocity.

For a constant velocity, that is, when the system reaches the steady state ( $d\mathbf{z}/dt=0$ ), the expression to the friction force can be reduced to

$$\mathbf{F} = g(\mathbf{v}_T) \text{sgn}(\mathbf{v}_T) + f(\mathbf{v}_T) \quad (3.50)$$

Thus, considering the Eq. (3.47) and Eq. (3.48), it is possible to conclude that the steady-state values of the LuGre model agrees with the static model defined by Eq. (3.10).

### 3.3.7 Elasto-Plastic Model

The elasto-plastic model was developed by Dupont et al (2000, 2002), and it is based on the division of the body displacement  $\mathbf{x}$  into two different components, the elastic and plastic displacement,  $\mathbf{z}$  and  $\mathbf{w}$ . When the bodies are sticking, the plastic displacement remains constant, while during the sliding phase, the elastic displacement is constant. Figure 3.16 shows the physical meaning of each of these two types of displacement, the elastic displacement represents the bristle deflection.

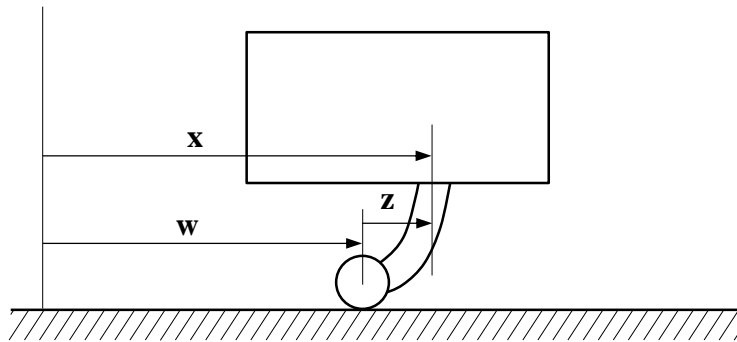


**Figure 3.16** - Physical interpretation of the elastic and plastic displacements.

The friction force can be calculated in a similar way as compared to the case of LuGre model (Canudas de Wit et al., 1995),

$$\mathbf{F} = \sigma_0 \mathbf{z} + \sigma_1 \frac{d\mathbf{z}}{dt} + \sigma_2 \mathbf{v}_T \quad (3.51)$$

where  $\sigma_0$  is the contact stiffness,  $\sigma_1$  is the contact damping, and  $\sigma_2$  is viscosity coefficient. The velocity of bristle deflection is given by

$$\frac{d\mathbf{z}}{dt} = \mathbf{v}_T \left( 1 - \alpha(\mathbf{z}, \mathbf{v}_T) \frac{\sigma_0}{g(\mathbf{v}_T)} \mathbf{z} \cdot \text{sgn}(\mathbf{v}_T) \right) \quad (3.52)$$

in which the function  $\alpha(\mathbf{z}, \mathbf{v}_T)$  is used to capture stiction, since it just allows elastic displacement until the system reaches the break-away force. This function is described as

$$\alpha(\mathbf{z}, \mathbf{v}_T) = \begin{cases} \alpha(\mathbf{z}) & \text{if } \mathbf{v}_T \cdot \mathbf{z} \geq 0 \\ 0 & \text{if } \mathbf{v}_T \cdot \mathbf{z} < 0 \end{cases} \quad (3.53)$$

with

$$\alpha(\mathbf{z}) = \begin{cases} 0 & \text{if } \|\mathbf{z}\| < z_{ba} \\ \frac{1}{2} \left( \sin \left( \pi \frac{\|\mathbf{z}\| - z_{\max} + z_{ba}}{z_{\max} - z_{ba}} \right) + 1 \right) & \text{if } z_{ba} < \|\mathbf{z}\| < z_{\max} \\ 1 & \text{if } z_{\max} < \|\mathbf{z}\| \end{cases} \quad (3.54)$$

where  $z_{\max}$  is the maximum bristle deflection and  $z_{ba}$  is the break-away bristle deflection. The value of  $z_{\max}$  can be determined based on the steady state friction, and the relation  $z_{ba}/z_{\max} \approx 0.7$  can be used to calculate  $z_{ba}$  (Dupont et al., 2000). The function  $g(\mathbf{v})$  describe the Stribeck curve and, similarly to LuGre is given by Eq. (3.47).

### 3.3.8 Leuven Model

This model was proposed by Swevers et al. (2000) as being an improvement of the LuGre model (Canudas de Wit et al., 1995). The Leuven model can capture the Stribeck effect, frictional lag, break-away force variation, stick-slip behavior and pre-sliding hysteresis with nonlocal memory. The latter property is not modelled by the LuGre model.

Leuven model considers also the average deflection of the asperities  $z$ , and it can be defined by

$$\frac{dz}{dt} = v_T \left( 1 - \operatorname{sgn} \left( \frac{F_d(z)}{g(v_T) - F_b} \right) \left| \frac{F_d(z)}{g(v_T) - F_b} \right|^n \right) \quad (3.55)$$

$$F = F_h(z) + \sigma_1 \frac{dz}{dt} + \sigma_2 v_T \quad (3.56)$$

where  $n$  represents the coefficient that defines the shape of the transition curve, and  $g(v_T)$  is an arbitrary function that models the steady state behavior of friction force, which is commonly described in a similar way to Eq. (3.47) by

$$g(v_T) = \left( F_C + (F_S - F_C) e^{\left| \frac{v_T}{v_s} \right|^\sigma} \right) \operatorname{sgn}(v_T) \quad (3.57)$$

The hysteresis friction force is represented by  $F_h(z)$ , and it is constituted by two components as follows

$$F_h(z) = F_b + F_d(z) \quad (3.58)$$

where  $F_b$  is the hysteresis friction force at the beginning of a transition curve when there is a velocity reversal and  $F_d(z)$  represents the transition curve active at a certain time.

The Leuven model presents a good characterization of friction phenomena, nevertheless it has also several implementation problems and a discontinuity in the friction force for some circumstances.

Few years later, the same authors (Lampaert et al., 2002) proposed some modifications to the model. The discontinuity issue was overcome by changing the state equation to the following form

$$\frac{dz}{dt} = v_T \left( 1 - \operatorname{sgn} \left( \frac{F_h(z)}{g(v_T)} \right) \left| \frac{F_h(z)}{g(v_T)} \right|^n \right) \quad (3.59)$$

### 3.3.9 Generalized Maxwell Slip Model

The generalized Maxwell slip model (Lampaert et al., 2003; Al-Bender et al., 2005) is a development of Leuven model (Lampaert et al., 2002), and it considers a parallel connection of  $N$  single state friction models, as it shown in Figure 3.17. They are described by the same dynamical model, and have the same input displacement and velocity, but with different sets of parameter values. Each single state friction model is evaluated separately to check whether it is sticking or sliding.

Thus, if the element  $i$  is sticking, it is governed by the following equation

$$\frac{dz_i}{dt} = v_T \quad (3.60)$$

which happens until  $z_i = g_i(v_T)$ , then, for sliding, the state equation is written as

$$\frac{dz_i}{dt} = \text{sgn}(v_T) C_i \left( 1 - \frac{z_i}{g_i(v_T)} \right) \quad (3.61)$$

and it is valid until the relative velocity passes through zero. From the previous equations,  $z_i$  denotes the spring deflection,  $g_i(v_T)$  is the Stribeck curve for the deformation of element  $i$ , and  $C_i$  is the attraction parameter which determines how fast  $z_i$  converges to  $g_i(v_T)$ .

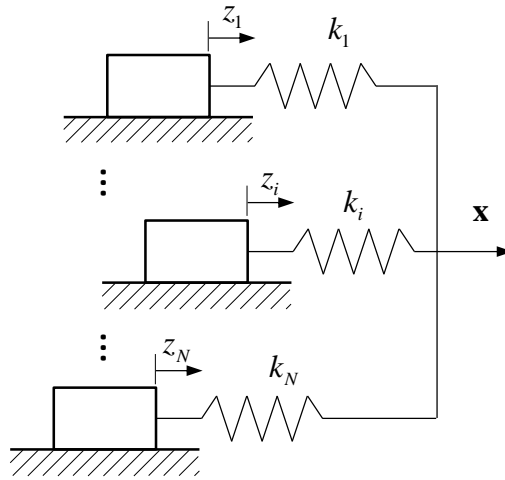


**Figure 3.17** - Representation of the generalized Maxwell slip model.

To calculate the total friction force, it should be summed the contribution of each single state model, plus the viscous friction component, as it follows

$$F_f(t) = \sum_{i=1}^N \left( k_i z_i + \sigma_i \frac{dz_i}{dt} \right) + f(v_T) \quad (3.62)$$

where  $k_i$  is the spring stiffness and  $\sigma_i$  is damping coefficient, and  $f(v_T)$  is the viscous component which is normally set with a linear dependence of velocity as in Eq. (3.48).

Hence, to implement this model, it is necessary to define three parameters per element beyond the Stribeck function which normally uses three more parameters. However, it can be introduced scale parameters,  $\alpha_i$ , which can be used to calculate the attraction parameter for each element based on a global value, i.e.,  $C_i = \alpha_i C$ . The scaling parameters can also be applied for the Stribeck functions and the damping coefficients. Though, these parameters should guarantee the following relation

$$\sum_{i=1}^N \alpha_i = 1 \quad (3.63)$$



Thus, the model is reduced to two parameters per element, and six for the whole system. It was shown by Piatkowski (2014b) that using only four elements could provide good results.

### 3.3.10 Gonthier et al. Model

Gonthier et al. (2004) introduced a two-dimensional friction model based on LuGre approach (Canudas de Wit et al., 1995). The authors considered a force from the bending of the bristles, given by

$$\mathbf{F}_{br} = \sigma_0 \mathbf{z} + \sigma_1 \frac{d\mathbf{z}}{dt} \quad (3.64)$$

where  $\sigma_0$  is the stiffness and  $\sigma_1$  is the damping coefficient. To ensure a smooth transition between the stick-slip friction regimes, an auxiliary parameter is defined as,

$$s = e^{-\left(\frac{\|\mathbf{v}_T\|}{v_s}\right)^2} \quad (3.65)$$

where  $v_s$  is the Stribeck velocity. When the bodies are sticking, the deformation rate will be equal to the relative velocity, while for sliding, the resultant friction force will approach the Coulomb friction force,  $\mathbf{F}_C$ .

$$\frac{d\mathbf{z}}{dt} = s\mathbf{v}_T + (1-s)\left(\frac{1}{\sigma_1}\mathbf{F}_C - \frac{\sigma_0}{\sigma_1}\mathbf{z}\right) \quad (3.66)$$

Coulomb friction has always the velocity direction and can be approximated by

$$\mathbf{F}_C = F_C \text{dir}_\epsilon(\mathbf{v}_T, v_\epsilon) \quad (3.67)$$

where  $\text{dir}_\epsilon(\mathbf{v}_T, v_\epsilon)$  returns the unit vector with velocity direction, and it smooths the vector oscillations for velocities under a certain tolerance,  $v_\epsilon$ , to diminish the discontinuities in velocity direction. This tolerance velocity is considered  $v_\epsilon = 0.01 v_s$ .

$$\text{dir}_\epsilon(\mathbf{v}_T, v_\epsilon) = \begin{cases} \frac{\mathbf{v}_T}{\|\mathbf{v}_T\|} & \text{if } \|\mathbf{v}_T\| \geq v_\epsilon \\ \frac{\mathbf{v}_T}{v_\epsilon} \left( \frac{3}{2} \frac{\|\mathbf{v}_T\|}{v_\epsilon} - \frac{1}{2} \left( \frac{\|\mathbf{v}_T\|}{v_\epsilon} \right)^3 \right) & \text{if } \|\mathbf{v}_T\| < v_\epsilon \end{cases} \quad (3.68)$$

This approach includes a temporal lag associated with the dwell-time dependence. To capture that phenomenon, a new state variable is defined as

$$\dot{s}_{dw} = \begin{cases} \frac{1}{\tau_{dw}}(s - s_{dw}) & \text{if } s - s_{dw} \geq 0 \\ \frac{1}{\tau_{br}}(s - s_{dw}) & \text{if } s - s_{dw} < 0 \end{cases} \quad (3.69)$$

where  $\tau_{dw}$  is the dwell-time dynamics time constant, and  $\tau_{br}=\sigma_1/\sigma_0$  is the bristle dynamics time constant. The time constants should be set according to the desired time delay, a large one for sticking, and a small time delay for sliding. Thus, the maximum friction force can be defined as

$$F_{\max} = F_C + (F_S - F_C) s_{dw} \quad (3.70)$$

where  $F_C$  and  $F_S$  are the magnitude of Coulomb and static friction, respectively. Thus, the friction force can be expressed as

$$\mathbf{F} = \begin{cases} \mathbf{F}_{br} + \sigma_2 \mathbf{v}_T & \text{if } \|\mathbf{F}_{br}\| \leq F_{\max} \\ F_{\max} \text{sgn}(\mathbf{F}_{br}) + \sigma_2 \mathbf{v}_T & \text{if } \|\mathbf{F}_{br}\| > F_{\max} \end{cases} \quad (3.71)$$

where  $\sigma_2$  is the viscous damping coefficient. The use of this model results in a set of ordinary differential equations that are very stiff at low relative velocities and cannot be solved using explicit ODE solvers.

### 3.3.11 Liang et al. Bristle Model

This bristle friction model (Liang et al., 2012) is an extension of the model presented by Heissig and Friedland (1991) to the 3D space. The average deflection of the bristles is represented by a linear spring, which can stretch and rotate, and it is constrained to the tangential plane of the contact.

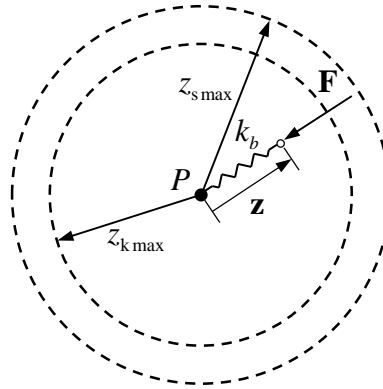


**Figure 3.18** - Representation of the Liang et al. bristle model.

An illustration of the tangential plane for a single contact is represented in Figure 3.18. The central point P represents the contact point, where the normal and friction forces are applied. Thus, for each individual contact, the friction force can be calculated as

$$\mathbf{F} = k_b \mathbf{z} \quad (3.72)$$

where  $k_b$  is the bristle stiffness and  $\mathbf{z}$  is the average bristle deflection and can be ex-

pressed as

$$\mathbf{z}(t) = \begin{cases} \mathbf{z}(t_0) + \int_{t_0}^t \mathbf{v}_T(t) dt & \text{if } \|\mathbf{z}\| < z_{\max} \\ z_{\max} \text{sgn}(\mathbf{v}_T) & \text{if } \|\mathbf{z}\| \geq z_{\max} \end{cases} \quad (3.73)$$

where  $t_0$  is the starting time of the contact,  $t$  is the current time and  $z_{\max}$  is the maximum bristle deflection that can be defined as

$$z_{\max} = \begin{cases} z_{k\max} = \frac{F_C}{k_b} & \text{if } \|\mathbf{v}_T\| > v_d \\ z_{s\max} = \frac{F_S}{k_b} & \text{if } \|\mathbf{v}_T\| \leq v_d \end{cases} \quad (3.74)$$

where  $v_d$  is a threshold velocity, which represents the numerical boundary between the sticking and sliding regimes. Thus, there is a maximum value for bristle deflection for sticking ( $z_{s\max}$ ) and another for sliding ( $z_{k\max}$ ), both parameters are represented in Figure 3.18.

The major drawback of this model is related to the transition of the sticking regime to the sliding regime. This is because it corresponds a sudden decrease of the maximum value of the average bristle deflection, which can result in an abrupt change of the friction force. To stabilize the friction force, the Eq. (3.72) can be modified through the introduction of a damping term; i.e.,

$$\mathbf{F} = k_b \mathbf{z} + c_b \dot{\mathbf{z}} \quad (3.75)$$

where  $c_b$  is the bristle damping coefficient. When the model reaches the steady-state in the sliding mode, the friction force will be equal to Coulomb friction force. In the sticking mode, the friction force will be higher, and equal to the static friction.

### 3.4 Example of Application

In this section, the classic 1-DOF spring-mass system is utilized as a numerical example of application, which allows the analysis and comparison of some of the previously presented friction models (see Figure 3.19). This system is widely used as benchmark for the validation of friction models (Rabinowicz, 1956; Heissig and Friedland, 1991; Leine et al., 1998; Gonthier et al., 2004; Andersson et al., 2007; Do et al., 2007; Marques et al., 2015), and it consists of a block with mass  $m$ , which is positioned on a conveyor belt. The belt is moving with a constant velocity. The block is connected by a spring element with stiffness  $k_s$ . The system dynamics is governed by the following dif-

ferential equation

$$F = k_s x + m\ddot{x} \quad (3.76)$$

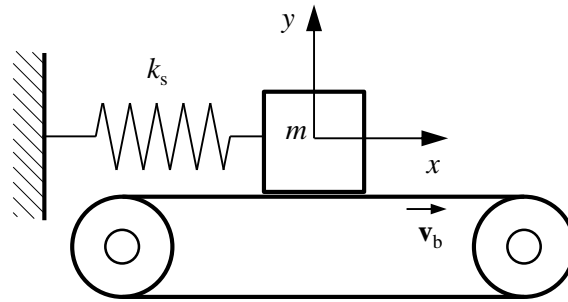


**Figure 3.19** - Representation of the 1DoF spring-mass model.

The simulation parameters for the spring-mass system are presented in Table 3.1. The specific parameters associated with each friction model were extracted from the literature and listed in Table 3.2. Initially, the block is located at the origin of the  $xy$  coordinate system, and its velocity being the same as the belt.

**Table 3.1** - Simulation parameters for the spring-mass model.

Parameter	Symbol	Value	Parameter	Value
Mass of the block	$m$	1 kg	Time step	0.00005 s
Velocity of the belt	$v_b$	0.1 m/s	Simulation time	20 s
Spring stiffness	$k_s$	2 N/m	Integrator scheme	Runge-Kutta 4 <sup>th</sup> order

**Table 3.2** - Parameters considered for the different friction models.

Parameter	S	Value	Parameter	S	Value
Static coefficient of friction	$\mu_s$	0.15	Factor for curve shape	$\zeta$	50 s/m
Kinetic coefficient of friction	$\mu_k$	0.1	Stiction coefficient	$a$	0.5
Coefficient of viscosity	$F_v$	0.1 Ns/m	Stiffness coefficient	$\sigma_0$	$10^5$ N/m
Stribeck velocity	$v_s$	0.001 m/s	Damping coefficient	$\sigma_1$	$\sqrt{10^5}$ Ns/m
Geometry factor	$\delta_\sigma$	2	Coefficient of viscosity	$\sigma_2$	0.1 Ns/m
Tolerance velocity (Karnopp)	$D_v$	0.001 m/s	Dwell-time constant	$\tau_{dw}$	2 s
Tolerance velocity (Threlfall, Bengisu and Akay, Awrejcewicz)	$v_0$	0.001 m/s	Bristle stiffness	$k_b$	50000 N/m
Tolerance velocity (Ambrósio)	$v_0$	0.0001 m/s	Threshold velocity	$v_d$	0.001 m/s
Tolerance velocity (Ambrósio)	$v_1$	0.001 m/s	Bristle damping	$c_b$	80 Ns/m

Figures 3.20 to 3.22 show the main results produced from simulations with different friction models. In order to keep the analysis simple, the friction approaches are grouped into three classes, namely static models without stiction, static models with stiction, and dynamic models. The behavior of the system is quantified by the plots of position, relative velocity and friction force values. The results are relative to 20 s of simulation.

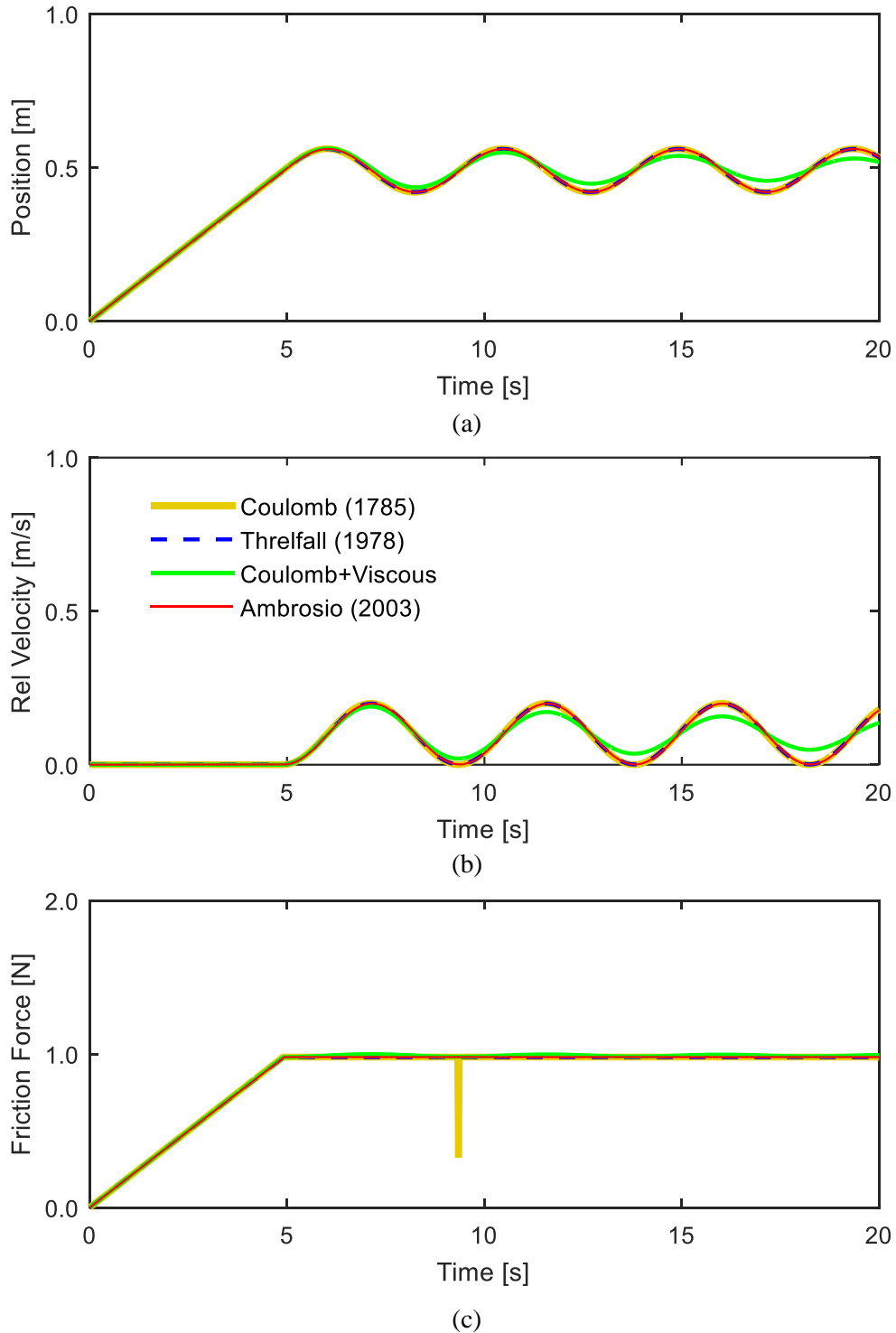


**Figure 3.20** - Results for static models without stiction.

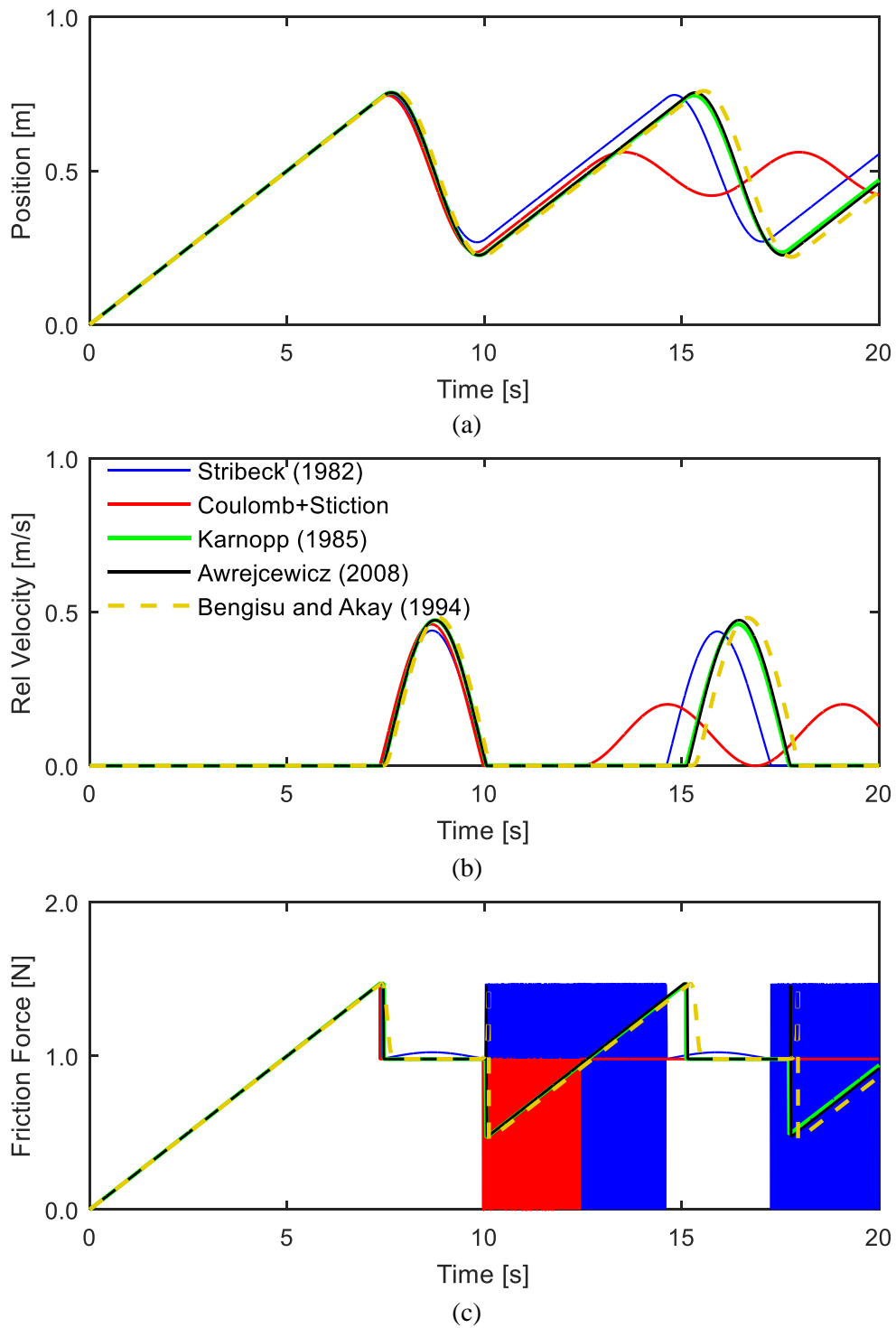


**Figure 3.21** - Results for static models with stiction.

Regarding the static models without stiction, they present a sticking phase related to the initial conditions, since the spring force magnitude is lower than the Coulomb friction force. The fact of having an exact zero relative velocity at the beginning of the simulation avoids any numerical instability for the models with a discontinuity at null velocity, as in the case of the Coulomb model and the Coulomb with viscous approach. Since these models have a constant Coulomb friction force or lower for velocities close

to zero, the block exhibits a spring-like behavior with a frequency equal to  $1/2\pi\sqrt{k_s/m}$ . From the analysis of Figure 3.20, it can be observed that the results corresponding to Coulomb with viscous friction show a distinct behavior since the viscosity introduces a damping effect in the block oscillations.

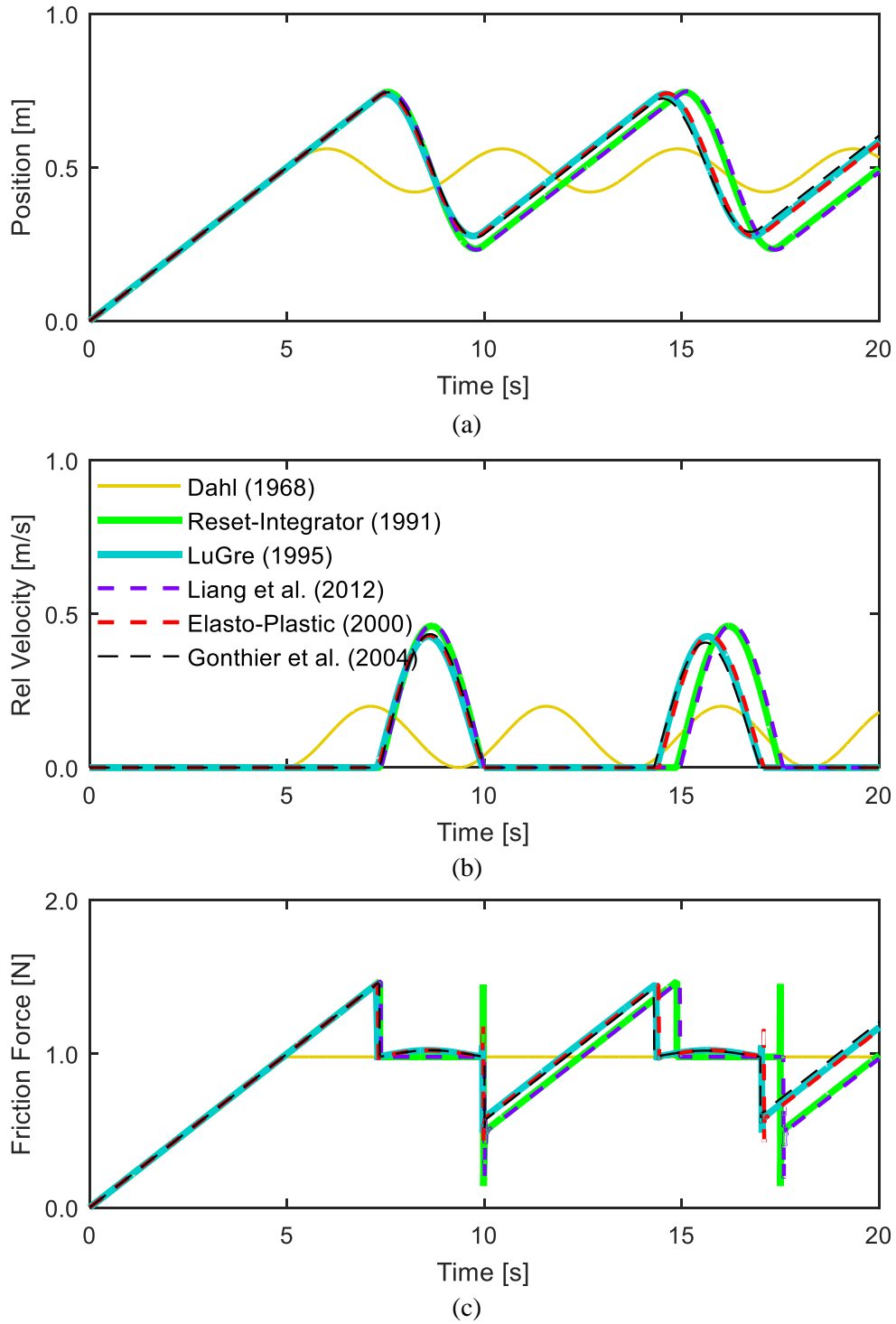


**Figure 3.22** - Results for dynamic models.

For the static models with stiction, the differences are more evident. Both simula-

tions with Coulomb with stiction and Stribeck friction present numerical instability can be observed in the friction force plot on Figure 3.21. This occurs due to the changes in the velocity direction. The Coulomb model with stiction is capable of reaching the static friction only at the first peak, and because of the initial velocity, it does not stick again. Karnopp and Awrejcewicz models have similar responses and present well-defined stick and slip phases. As the model with Stribeck friction is the only one with viscous friction component, it has faster cycles comparing with the other approaches.

Analyzing the dynamic models, it is possible to observe that Dahl's model is the only one that does not capture the stick-slip phenomenon. From Figure 3.22, the remaining models can be divided into two groups, the first includes LuGre, Elasto-Plastic and Gonthier, and the second one includes Reset Integrator and Liang. The difference in the dynamic corresponding to these models behavior is caused by presence of a viscous component in the first set of models.

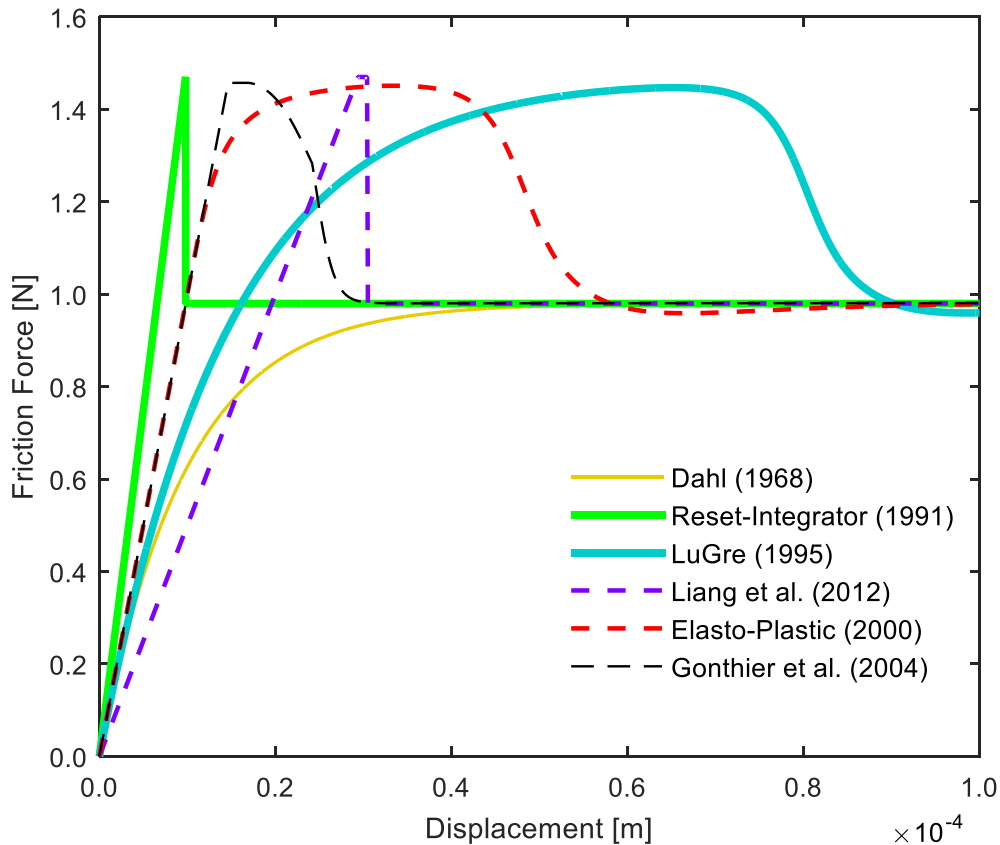


**Figure 3.23-** Dynamic models behavior: friction force versus displacement.

Figures 3.23 and 3.24 show the plots of the friction force versus displacement and friction force versus relative velocity for the dynamic friction approaches. Comparing



these models with Rabinowicz's work (1951), it can be stated that LuGre, Elasto-Plastic and Gonthier's present the friction force as a function of displacement with a similar shape. During the pre-sliding displacement phase, the slope of the friction force is directly related to the stiffness coefficient of each model (see Figure 3.23). In contrast with the static models, the dynamic approaches do not change the force direction with the change of velocity direction, as can be observed in Figure 3.24. The Gonthier, Elasto-Plastic, and LuGre (to some extent) seem increase the friction force before sticking. In turn, the Liang's model shows more instability in velocity, before reaching the sticking phase. From the analysis of Figure 3.24, it is also possible to state that LuGre and Elasto-Plastic can describe the frictional lag phenomenon, since both models present a higher friction force when the relative velocity is increasing.

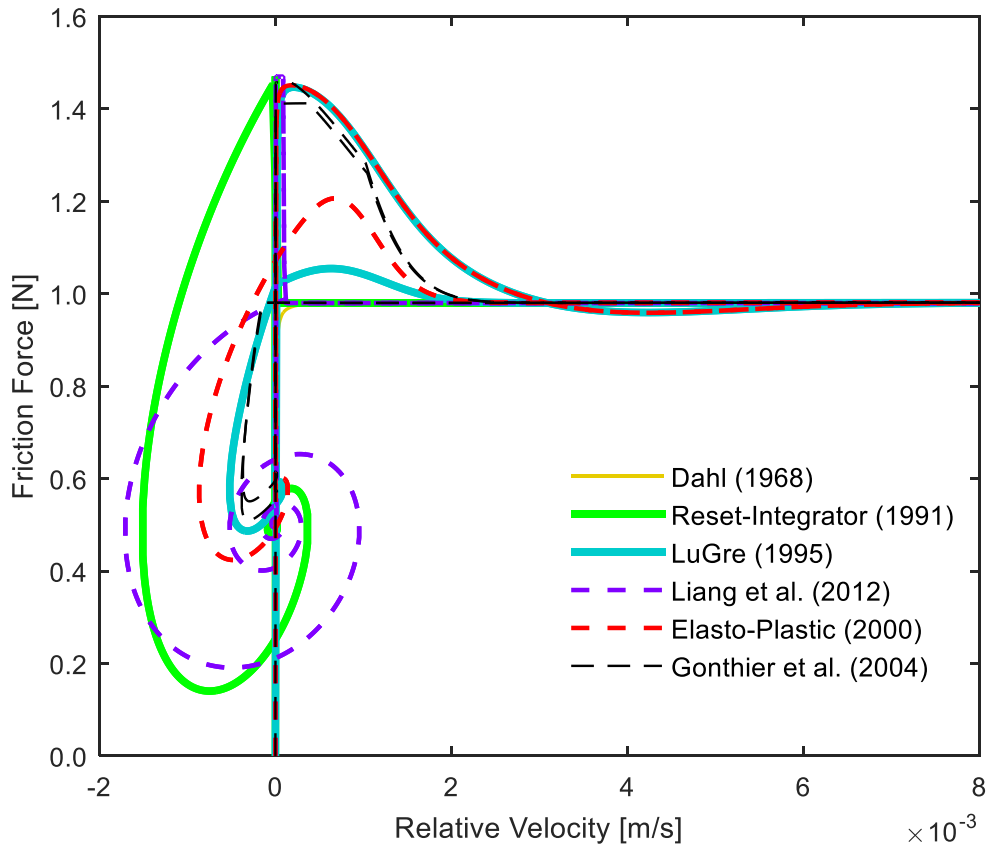


**Figure 3.24** - Dynamic models behavior: friction force versus relative velocity.

### 3.5 Summary and Conclusions

In this chapter, the main considerations about friction modelling in multibody systems were covered. The most relevant issues about friction were addressed in order to understand the characteristics that the friction models should capture. Stick-slip motion,

viscous friction, frictional lag, pre-sliding displacement and break-away force are the discussed topics.

A comparative study of some of the most relevant friction force models for multi-body systems dynamics has been presented in this work. In the sequel of this process, the main characteristics, advantages and limitations of the static and dynamic friction force models were also analyzed. On the one hand, the static friction models are, in general, simpler and describe the steady-state behavior of the friction force. Most of them show incapacity to correctly capture the frictional effects. Several static models present a discontinuity of friction force at zero velocity, this difficulty provokes numerical instability during a dynamic simulation. On the other hand, the dynamic models use extra state variables to be able to take into account more phenomena. These approaches tend to be more complex and require, generally, the determination of more parameters.

To perform a comparative study of the dynamic response of the discussed models, a 1-DOF spring-mass model was utilized as example of application. This example showed that the most significant difference between friction models is the ability to capture the stick-slip motion. However, the viscous friction, the frictional lag or the pre-sliding displacement also have a relevant impact in the system dynamics.

The choice of a friction model to implement in a dynamic simulation is not an easy assignment. Nevertheless, in order to have more complex friction models, it is, in general, necessary to introduce larger number of parameters to fully define the physics of the friction phenomena. These parameters are usually determined experimentally which can become a weakness for those models. This study illustrates that in order to correctly model, analyze and simulate frictional behavior in multibody systems, an appropriate friction model must be adopted.

*“Do not go where the path may lead,  
go instead where there is no path and leave a trail.”*  
Ralph Waldo Emerson

## **4. DEMONSTRATIVE EXAMPLES OF APPLICATION**

The modelling of the frictional contacts in multibody systems dynamics can be used in different contexts. The main aspects about spatial multibody systems formulation and friction modelling approaches were considered in Chapters Two and Three, respectively. Thus, the requirements to conduct a more complex analysis of the impact of friction implementation are gathered. The example presented in Chapter Three was a quite simple mechanical system, mainly friction dependent, which was subjected to a one-dimensional analysis. In that sense, this chapter provide a more sophisticated study of frictional effects in the motion of mechanical systems.

Two main examples will be presented in the following sections, a smooth and a non-smooth cases are modelled. The first consists in the inclusion of friction modelling in a kinematic translational joint. This example represents a smooth motion, since the contact of between the slider and the guide is a continuous phenomenon. The second example involves modelling the behavior of a spatial revolute joint with clearance, which introduces impacts in the system and, therefore, chaotic motion. For these examples, some of the previously presented friction models are employed, and their influence on the response of the system is studied.

### **4.1 Translational Joints with Friction**

In this section, it is presented a study of the influence of friction modelling in a kinematic translational joint. For this approach, it is not considered any clearance and

the generated forces result from continuous contact.

The modelling of friction in mechanism joints has been studied during the past years. Kale and Rampalli (2011) investigated the application of LuGre friction model to revolute, cylindrical and spherical joints. For the specific case of translational joints, Qi et al. (2011) and Zhuang and Wang (2013; 2014) presented methodologies based on nonsmooth mechanics. These approaches considers a very small clearance size, and they use LCP formulation to detect and evaluate the nonsmooth events.

Since the kinematic constraints associated to the translational joint continue to be included in the equations of motion, the reaction forces are only calculated during the process of solving the problem dynamics. Bearing in mind that the friction force is a function of the joints reactions, there are two alternatives of introducing friction modelling in a multibody dynamics simulation with Lagrange multipliers technique.

The first technique consists in applying the friction forces as external generalized forces using an iterative procedure. For this methodology, the equations of motion, given by Eq. (2.46), can be rewritten as

$$\begin{bmatrix} \mathbf{M} & \mathbf{D}^T \\ \mathbf{D} & \mathbf{0} \end{bmatrix} \begin{Bmatrix} \dot{\mathbf{v}} \\ \boldsymbol{\lambda}_{i+1} \end{Bmatrix} = \begin{Bmatrix} \mathbf{g} + \mathbf{f}_F(\boldsymbol{\lambda}_i) \\ \boldsymbol{\gamma} \end{Bmatrix} \quad (4.1)$$

where  $\mathbf{f}_F$  is the vector with the generalized friction forces which is calculate recurring to the reaction forces obtained in the previous iteration. For the initial approximation, it can be considered a null vector. This process ends when the difference between two consecutive vectors of reaction forces are lower than a defined tolerance,  $\varepsilon$ , i.e., the following condition should be fulfilled

$$\varepsilon \leq \|\boldsymbol{\lambda}_{i+1} - \boldsymbol{\lambda}_i\| \quad (4.2)$$

This methodology requires to solve Eq. (4.1) several times in each time step of the integration process which can become computationally inefficient. Therefore, it is not adopted for this work.

The second approach is to include the calculation of the friction forces implicitly in the equations of motion. Most of the friction models considers that friction force is proportional to the magnitude of the normal load, therefore, Eq. (2.44) can be adapted as

$$\mathbf{M}\dot{\mathbf{v}} + \mathbf{D}^T\boldsymbol{\lambda} + \mathbf{F}|\boldsymbol{\lambda}| = \mathbf{g} \quad (4.3)$$

where  $\mathbf{F}$  is a matrix that establishes the relation of proportionality between the reaction and friction forces. However, Eq. (4.3) cannot be employed, so it can should be rewritten in the following form

$$\mathbf{M}\dot{\mathbf{v}} + \mathbf{D}^T \boldsymbol{\lambda} + \mathbf{F} \text{diag}(\text{sgn}(\boldsymbol{\lambda})) \boldsymbol{\lambda} = \mathbf{g} \quad (4.4)$$

where  $\text{diag}(\mathbf{v})$  returns a square diagonal matrix with the elements of vector  $\mathbf{v}$  on the main diagonal.

In order to solve the system dynamics with Eq. (4.4), it is necessary to evaluate the sign of the reaction forces which is unknown. To work around this problem, it is usual to consider the sign of the reaction forces equal to the previous time step. This technique has the inconvenient of using incorrect values in the steps that the reaction forces change their sign. However, in these situations, the reaction forces are close to zero and, since the friction forces are proportional to them, these erroneous friction forces do not have influence on the system due their low magnitude.

Thus, the matrix  $\mathbf{F}$  can be rectified as

$$\mathbf{F}' = \mathbf{F} \text{diag}(\text{sgn}(\boldsymbol{\lambda}_{i-1})) \quad (4.5)$$

Considering Eq. (4.4) and Eq. (4.5), the equations of motion for constrained multibody systems with frictional constraints can be stated as

$$\begin{bmatrix} \mathbf{M} & \mathbf{D}^T + \mathbf{F}' \\ \mathbf{D} & \mathbf{0} \end{bmatrix} \begin{Bmatrix} \dot{\mathbf{v}} \\ \boldsymbol{\lambda} \end{Bmatrix} = \begin{Bmatrix} \mathbf{g} \\ \boldsymbol{\gamma} \end{Bmatrix} \quad (4.6)$$

It should be noticed that, for the modelling of viscous friction forces, those components must be introduced in the equations of motion as external generalized forces, since they do not depend of the normal contact forces.

In order to correctly model the forces acting on the slider, it is necessary to know about its geometry. For an ideal joint, the dimensions of the slider are expendable, while, for this case, they must be defined since the friction force can create moment over the slider.

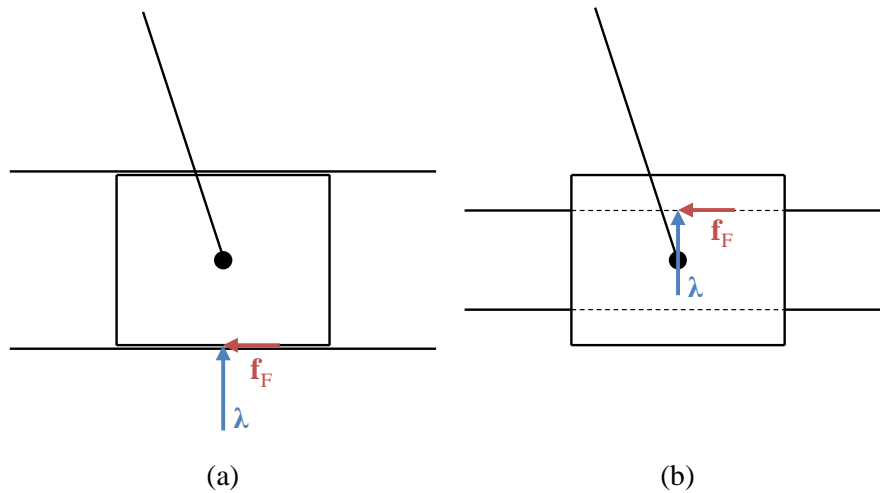


**Figure 4.1** - Distinction of friction force acting on (a) an inner slider and (b) an outer slider.

Another important aspect consists in taking into account the type of the slider, it can be an inner or outer slider. That will influence the direction of the moment generated by the friction force. Figure 4.1 represents two planar sliders in which the reaction force acts in the upward direction. In the figure, it is demonstrated that, although the friction force has the same magnitude, its line of action is different and, therefore, the generated moment acts in the opposite direction.

A spatial slider-crank mechanism is employed to demonstrate the effects of friction modelling in a translational joint, the system is represented in Figure 4.2. This mechanism was also considered in Chapter 2, and its dimensional and inertial properties, as well as the initial conditions can be found in Table 2.1 and Table 2.2, respectively. For these simulations, it was considered an inner slider with a shape of a cube with side length of 0.01 m.

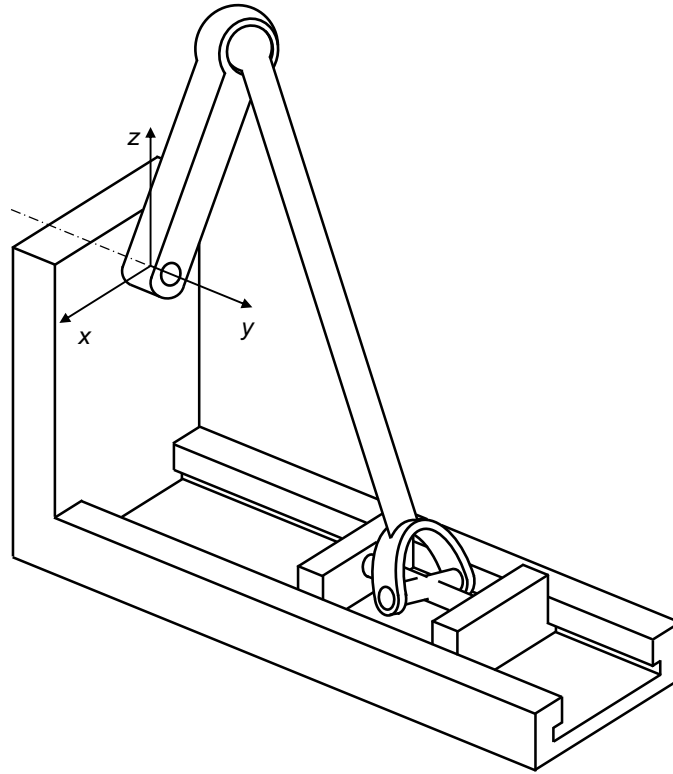


**Figure 4.2** - Spatial slider-crank mechanism.

The dynamic simulation of this mechanical system was carried for the frictionless case, and with four of the most utilized friction models. Two static and two dynamic models were considered, namely Coulomb (1785), Stribeck (Bo and Pavelescu, 1982), Dahl (1968), and LuGre (Canudas de Wit et al., 1995) approaches. The parameters for the friction force models are displayed in Table 4.1. The final time of the simulations is 5 s, the integration process was held with a fourth-order Runge-Kutta integrator with a

time step equal to  $5 \times 10^{-5}$  s.

**Table 4.1** - Parameters considered for the different friction models.

Parameter	Symbol	Value
Static coefficient of friction	$\mu_s$	0.2
Kinetic coefficient of friction	$\mu_k$	0.1
Stribeck velocity	$v_s$	0.001 m/s
Geometry factor	$\delta_\sigma$	2
Stiffness coefficient	$\sigma_0$	$10^5$ N/m
Damping coefficient	$\sigma_1$	$\sqrt{10^5}$ Ns/m
Coefficient of viscosity	$\sigma_2$	0 Ns/m

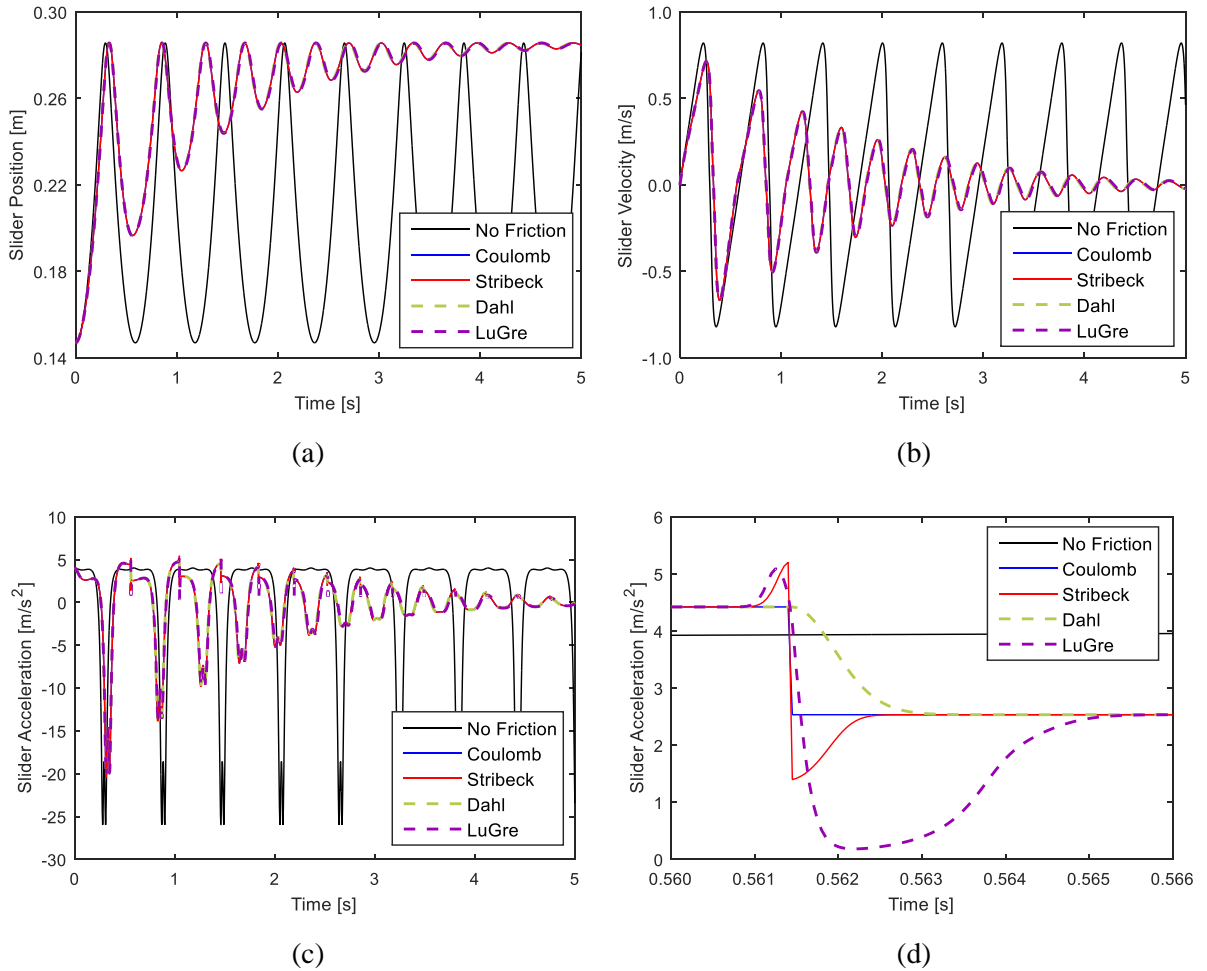


**Figure 4.3** - Comparison of the motion of the slider for different friction models: (a) position; (b) velocity; (c) acceleration; (d) detail of the acceleration.

In Figure 4.3, it is presented the motion of the slider for the different friction models, namely the plots for the position, velocity and acceleration are displayed. From the analysis of position and velocity, it can be stated that the inclusion of friction model-

ling introduces an important dissipative effect, regardless of the friction approach. Figure 4.3c shows the acceleration of the slider which demonstrates more significant differences between the friction models, especially when the velocity changes direction. For that reason, Figure 4.3d shows in detail the slider acceleration during the first time that the velocity changes its direction. In this plot, the static models exhibit a discontinuous behavior, while the dynamic models clearly have a more smooth transition. When compared with Stribeck approach, the LuGre model also presents the advantage of describing the frictional lag behavior, since it has a much higher friction force when the velocity is increasing than for its decreasing.

This example allows to identify the impact of friction modelling in the dynamic analysis of a multibody systems, as well as the main differences between some of the most common friction force models.

## 4.2 Spatial Revolute Joint with Axial and Radial Clearance

A revolute joint is constituted essentially by two elements, a cylindrical case, the bearing, and a cylindrical pin, the journal, as it is illustrated in Figure 4.4. A real joint does not behave smoothly as the kinematic constraints evidence. In contrast, due to manufacturing tolerances, wear or surface deformations, the presence of clearance leads to the occurrence of impacts which highly change the dynamics of the system.

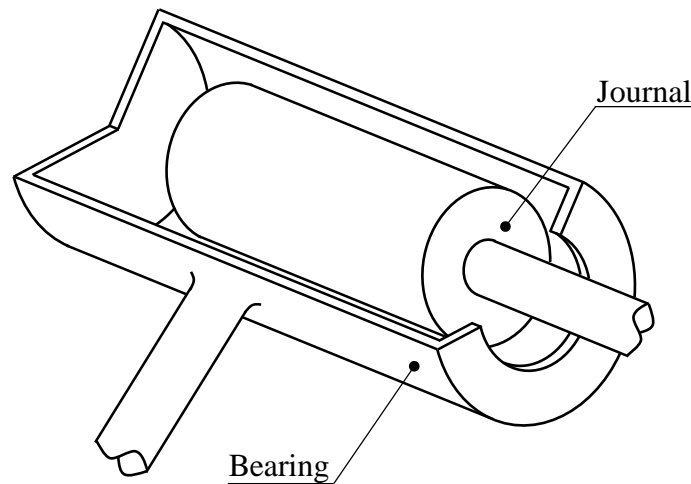


**Figure 4.4** - Typical configuration of a spatial revolute joint with clearance.

In chapter two, it was introduced the basic concepts and formulation for spatial multibody dynamics, and the equations of motion were derived for constrained multibody systems. Before introducing the kinematics and the dynamics of a revolute joint with clearance, the kinematic constraint equations for a perfect joint should be high-



lighted (Nikravesh, 1988). Bearing that in mind, Figure 4.5 must be considered. From now on, the subscripts  $i$  and  $j$  refer to the bearing and the journal, respectively.

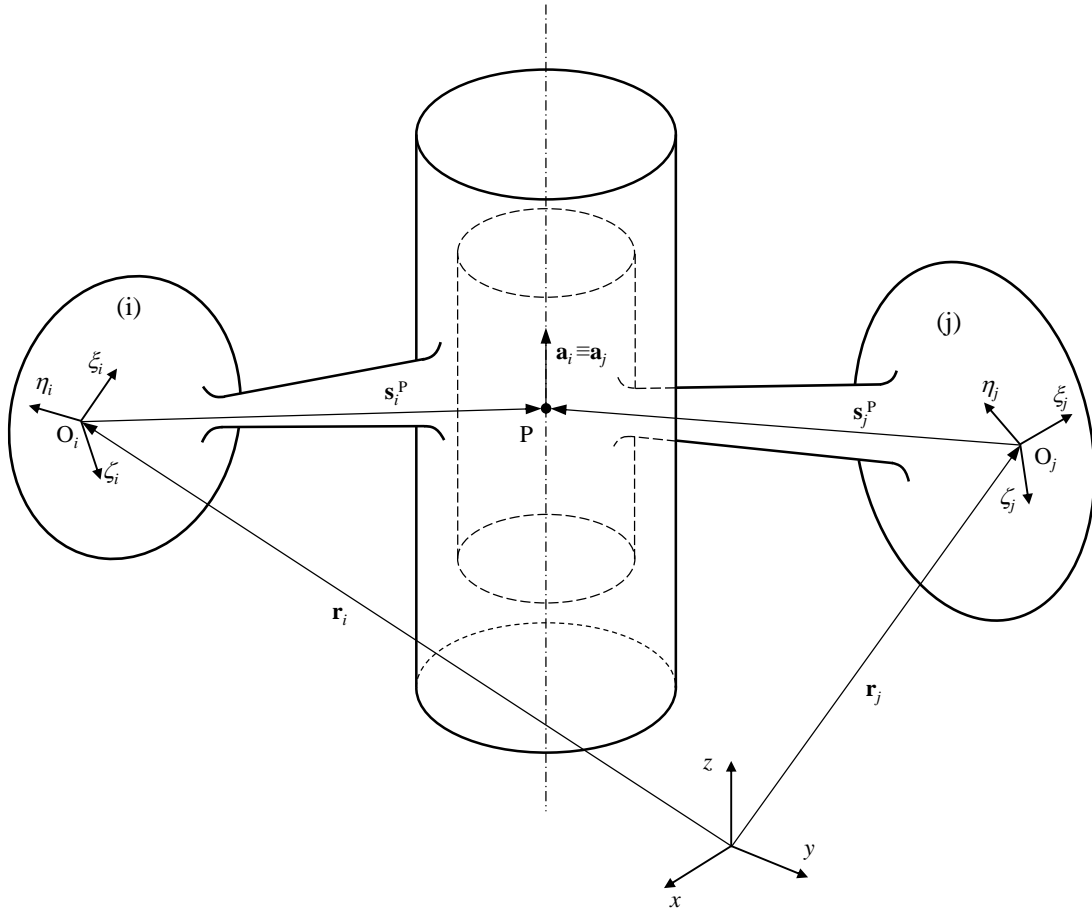


**Figure 4.5** - General configuration of a spatial revolute joint.

In order to impose the constraints of a revolute joint between bodies  $i$  and  $j$ , an arbitrary point  $P$  belonging to the joint axis must have constant coordinates in the local coordinate systems. This restriction is given by a vector loop, and holds three constraint equations which are expressed by Eq. (4.7). In Figure 4.5, there are also represented two unit vector which define the joint axis for the bearing and the journal, respectively,  $\mathbf{a}_i$  and  $\mathbf{a}_j$ . Those two vectors must remain parallel for a perfect revolute joint. Thus, two additional constraints must be considered which are given by Eq. (4.8), resulting in five kinematic constraints.

$$\Phi^{(3)} \equiv \mathbf{r}_i + \mathbf{s}_i^P - \mathbf{s}_j^P - \mathbf{r}_j = \mathbf{0} \quad (4.7)$$

$$\Phi^{(2)} \equiv \tilde{\mathbf{a}}_i \mathbf{a}_j = \mathbf{0} \quad (4.8)$$

The modelling of imperfect joints is a widely studied field in which the revolute joints have paramount importance (Dubowsky and Freudenstein, 1971; Rhee and Akay, 1996; Flores, 2004). Most of the approaches consist in considering the joints as collid-

ing bodies, and they use different force models to evaluate the contact forces. Thus, in order to compare the validity of several force models and their effect in the dynamic response of a multibody system, a few studies were conducted by Schwab et al. (2002), Flores and Ambrósio (2004), Flores et al. (2006a) and Koshy et al. (2013). Other methodologies can be implemented, Brutti et al. (2011) modelled the contact using finite element analysis. The researchers can formulate the clearance joint for planar or spatial multibody systems. The majority of the papers are on the modelling of planar revolute joints (Tian et al., 2010; Flores, 2010; Flores et al., 2011c; Muvengi et al, 2012), this type of joints present more simplicity in the implementation due to the fewer contact scenarios, and easier contact detection. Although, most of mechanical system have spatial behavior which led to the implementation of several models for three-dimensional joints (Flores et al., 2006b; Tian et al.; 2011; Brutti et al., 2011; Yang et al., 2015).

This work aims to present a comprehensive model of spatial revolute joint, and use it for the study of the influence of friction force models in the dynamic response of a mechanical system.

Most of the referred bibliography only takes into account the radial clearance of the joint. This assumption is valid for planar motion since there is no movement in the axial direction. However, a real joint also presents axial clearance (see Figure 4.6) which becomes more important for three dimensional joints. These two types of clearance results from the differences between the dimensions of the bearing and the journal, and they can be calculated as follows

$$c_r = R_i - R_j \quad (4.9)$$

$$c_a = L_i - L_j \quad (4.10)$$

where  $c_r$  and  $c_a$  denote the radial and axial clearance, respectively,  $R_i$  and  $R_j$  are the radii, and  $L_i$  and  $L_j$  are the lengths of the bodies.

This methodology consists in replacing the kinematic constraints of Eq. (4.7) and Eq. (4.8) by forces constraints. These force elements are introduced as external generalized forces, and they are evaluated as a function of the contact cases. When there is no contact, the joint does not establish any force element. If any contact scenario occurs, the contact points and the local deformations should be identified in pursuance of the determination of the generated loads. Thus, to solve the contact dynamics, two main phases have to be considered, (i) the contact detection, and (ii) the determination of the produced forces.

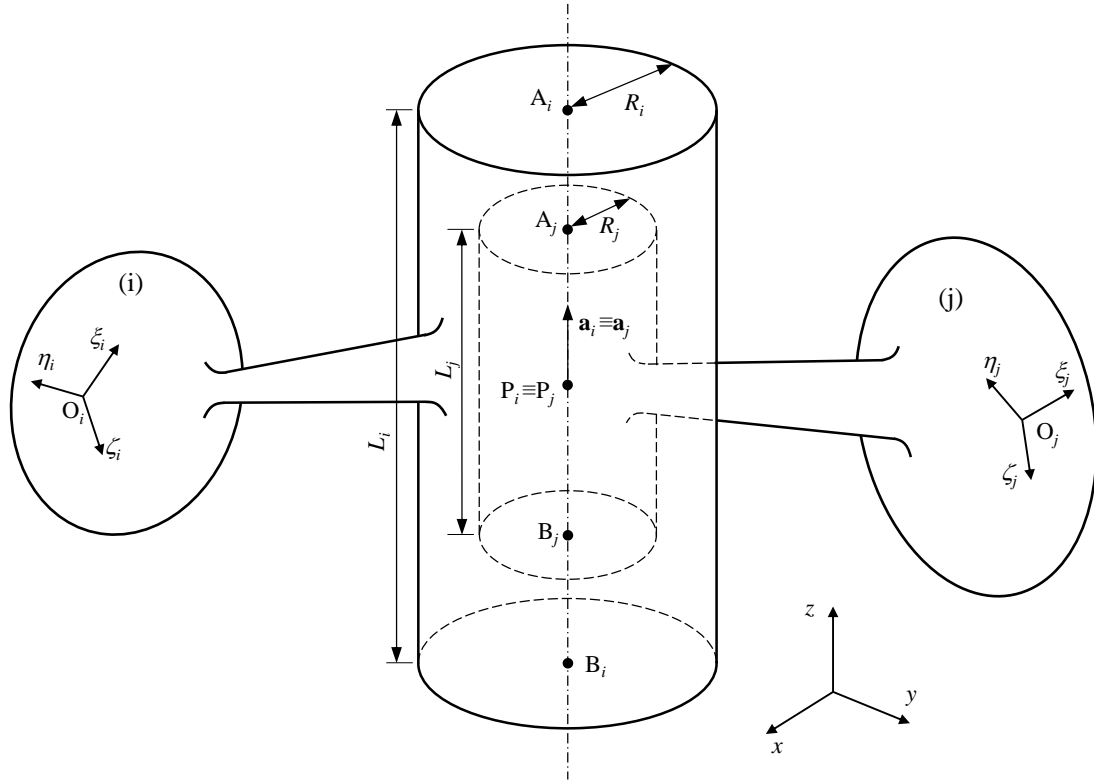


**Figure 4.6** - General configuration of a spatial revolute joint with clearance.

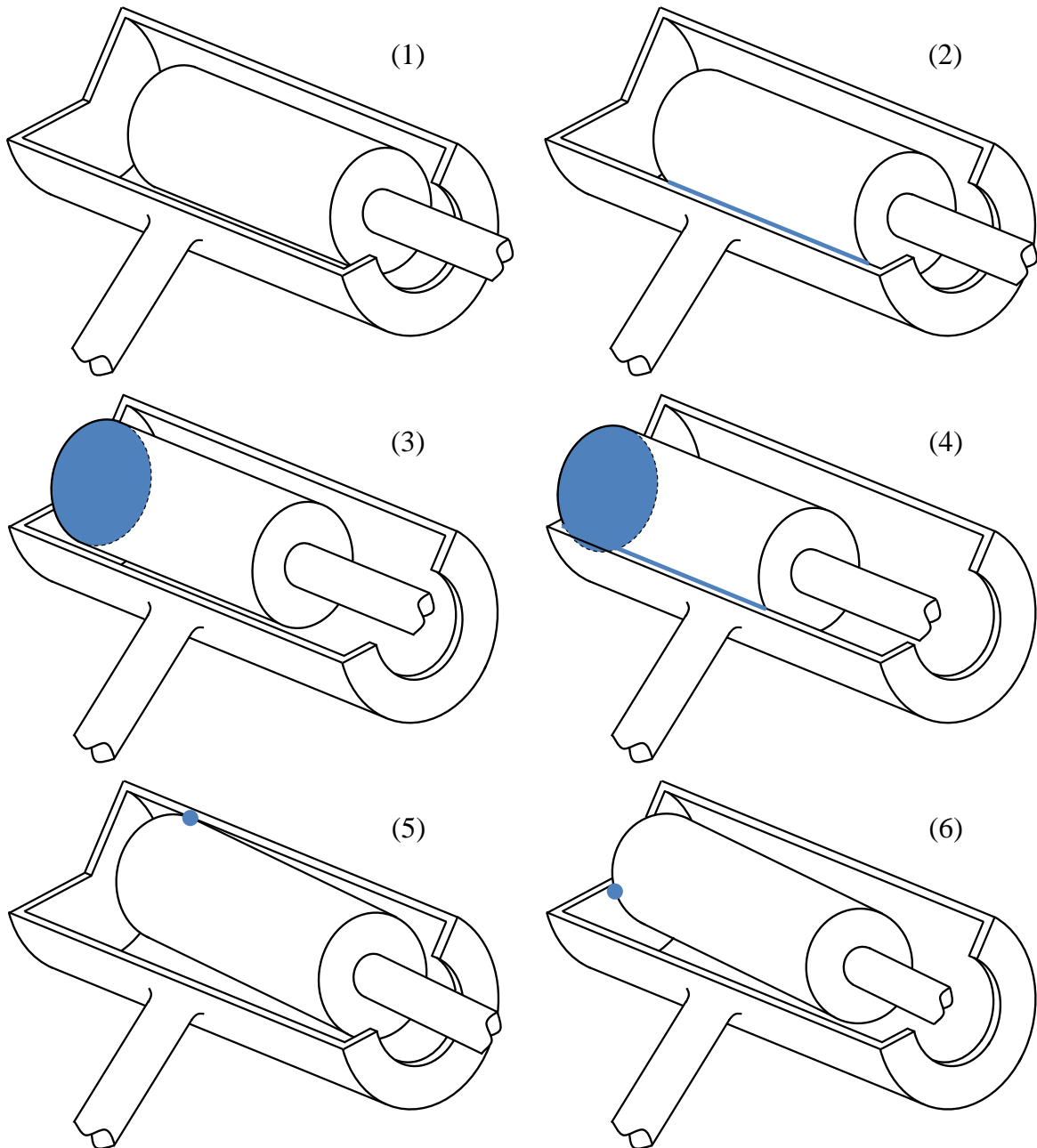
### 4.2.1 Contact Detection

The modelling of spatial revolute joint with radial and axial clearances involves the awareness for several contact scenarios. Hence, there were identified thirteen different types of motion which are represented in Figure 4.7, and can be following enumerated:

1. No contact;
2. Contact in radial line (aligned joint);
3. Contact in axial surface (aligned joint);
4. Contact in radial line and axial surface (aligned joint);
5. Contact in one point in the lateral wall;
6. Contact in one point in the top wall;
7. Contact in two points in the lateral wall;
8. Contact in two points in the two top walls;
9. Contact in two points in the lateral wall and in the top wall (same end);
10. Contact in two points in the lateral wall and in the top wall (different end);
11. Contact in three points, two in the lateral wall, and one in the top wall;
12. Contact in three points, two in the top walls, and one in the lateral wall;

13. Contact in four points, two in the lateral wall and two in the top walls.

It should be stated that some of the presented contact cases can be impractical, since the possibility of some contact scenarios are directly related to the dimensions of the journal and bearing. The proportions of the bodies introduce some restrictions which do not allow the joint to have some particular configurations.



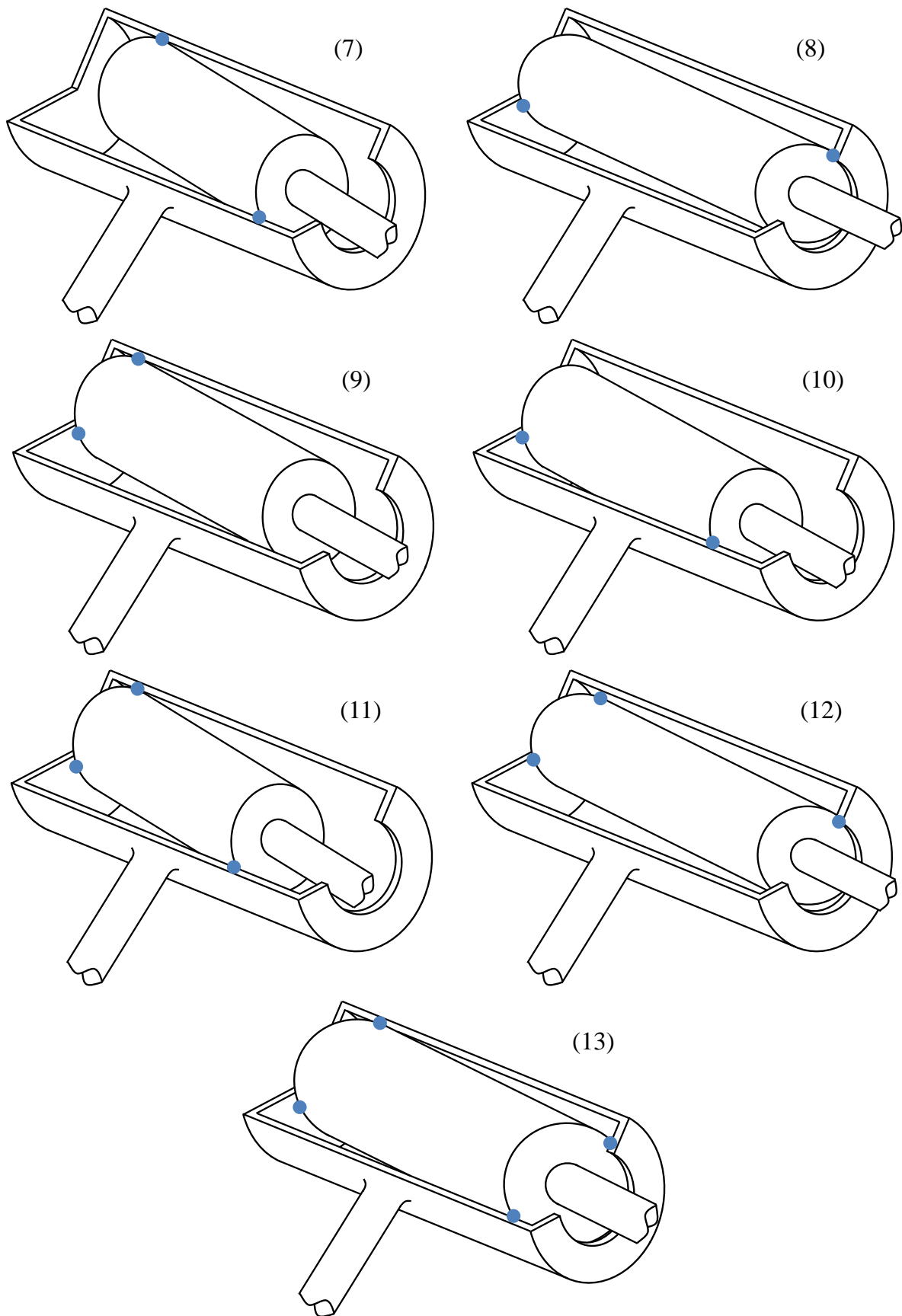


**Figure 4.7** - Representation of the different contact scenarios.

In order to promote an easier contact detection, there are considered two auxiliary

points in each element which are located at the centers of both ends, as it shown in Figure 4.6. The two extremities must be differentiated, therefore, they will be named end A and end B. The position of those points can be determined by the following expressions

$$\mathbf{r}^{A_k} = \mathbf{r}^{P_k} + \frac{L_k}{2} \mathbf{a}_k, \quad (k=i,j) \quad (4.11)$$

$$\mathbf{r}^{B_k} = \mathbf{r}^{P_k} - \frac{L_k}{2} \mathbf{a}_k, \quad (k=i,j) \quad (4.12)$$

The previously presented contact scenarios can be divided in two main groups, the cases where the journal and the bearing are aligned (ii-iv) and misaligned (v-xiii). In order to verify the alignment, the parallelism of the unit vectors of each element should be checked. Therefore, the following condition must be fulfilled

$$\tilde{\mathbf{a}}_i \mathbf{a}_j = \mathbf{0} \quad (4.13)$$

Bearing that in mind, Figure 4.8 represents a situation where the elements are aligned, and axial and radial contacts occur. These two contacts establish a superficial and linear contact zones, respectively, for the axial and radial interaction. Thus, the target is to determine the contact points in the center of each contact zone, which can be used to represent the whole contact and, where the forces can be applied.

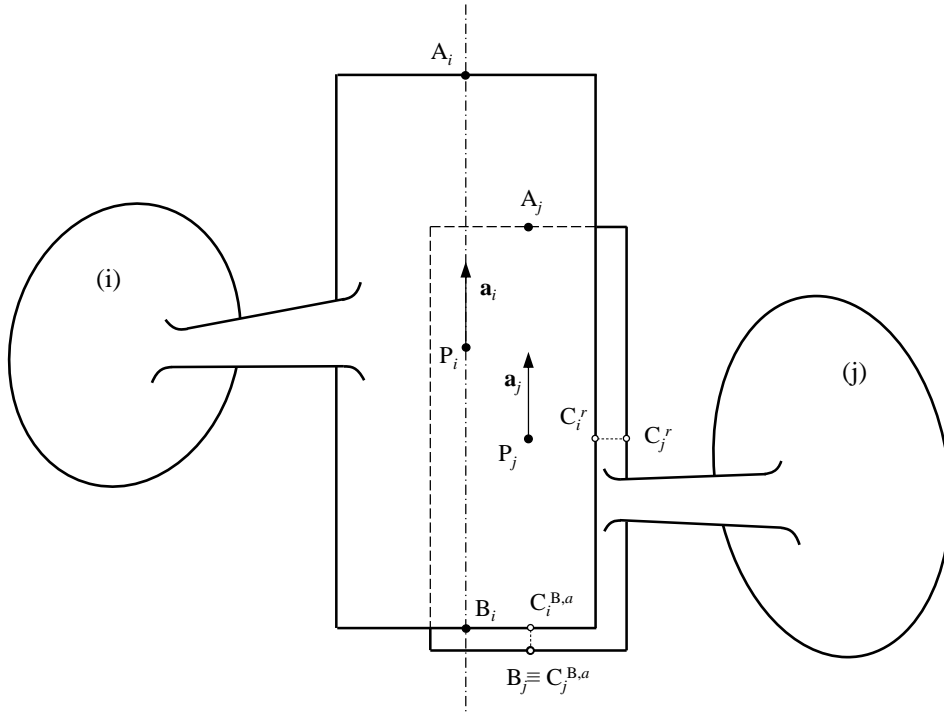


**Figure 4.8** - Configuration of a spatial revolute joint aligned with axial and radial contact.

The contact points are denoted by C, with the subscripts  $i$  and  $j$  for bearing or journal, respectively, and the superscripts  $a$  and  $r$  represent the type of contact, axial and

radial. For the axial contact, the superscript also includes the extremity where it occurs. For instance,  $C_i^{B,a}$  is the contact point of the bearing for axial contact in end B.

Regarding the radial contact, the center point of the contact line is at half of the length of the journal, as it is illustrated in Figure 4.8. The normal unit vector,  $\mathbf{n}_v$ , can be calculated as follows

$$\mathbf{n}_v = \frac{\left(\mathbf{r}^{P_j} - \mathbf{r}^{P_i}\right) - \left(\mathbf{r}^{P_j} - \mathbf{r}^{P_i}\right)^T \mathbf{a}_i \mathbf{a}_i}{\left\| \left(\mathbf{r}^{P_j} - \mathbf{r}^{P_i}\right) - \left(\mathbf{r}^{P_j} - \mathbf{r}^{P_i}\right)^T \mathbf{a}_i \mathbf{a}_i \right\|} \quad (4.14)$$

Thus, the contact points are determined with the following expressions

$$\mathbf{r}^{C_i^r} = \mathbf{r}^{P_i} + \left(\mathbf{r}^{P_j} - \mathbf{r}^{P_i}\right)^T \mathbf{a}_i \mathbf{a}_i + R_i \mathbf{n}_v \quad (4.15)$$

$$\mathbf{r}^{C_j^r} = \mathbf{r}^{P_j} + R_j \mathbf{n}_v \quad (4.16)$$

In order to analyze the axial contact, it will be considered the situation represented in Figure 4.8 which exhibits contact in end B, similar calculations are performed for the other extremity. In this case, the contact area is a circle and the center point is the center of the base of the journal as it is identified in Figure 4.8. Therefore, the contact points are given by

$$\mathbf{r}^{C_i^{B,a}} = \mathbf{r}^{B_j} + \left(\mathbf{r}^{B_i} - \mathbf{r}^{B_j}\right)^T \mathbf{a}_i \mathbf{a}_i \quad (4.17)$$

$$\mathbf{r}^{C_j^{B,a}} = \mathbf{r}^{B_j} \quad (4.18)$$

When the condition specified by Eq. (4.13) is not verified, the alignment of the bearing and journal is not achieved. Thus, the contact detection turns into a more complex assignment. In that sense, four types of contact have to be checked, namely axial and radial, in both ends. The combination of these contacts results in the different scenarios previously presented (see Figure 4.7), in which they are point contacts.

A generic contact configuration is represented in Figure 4.9, where there is axial contact in end B and radial contact in end B. Again, it will be exemplified the calculation of the contact points for the presented example.

Taking into account the axial contact detection, it can be simplified as that intersection of a circumference (base of the journal) and a plane (base of the bearing) which can be defined, respectively, as

$$\left\| \mathbf{x} - \mathbf{r}^{B_j} \right\|^2 = R_j^2 \wedge \mathbf{a}_j^T \mathbf{x} = \mathbf{a}_j^T \mathbf{r}^{B_j} \quad (4.19)$$

$$\mathbf{a}_i^T \mathbf{x} = \mathbf{a}_i^T \mathbf{r}^{B_i} \quad (4.20)$$

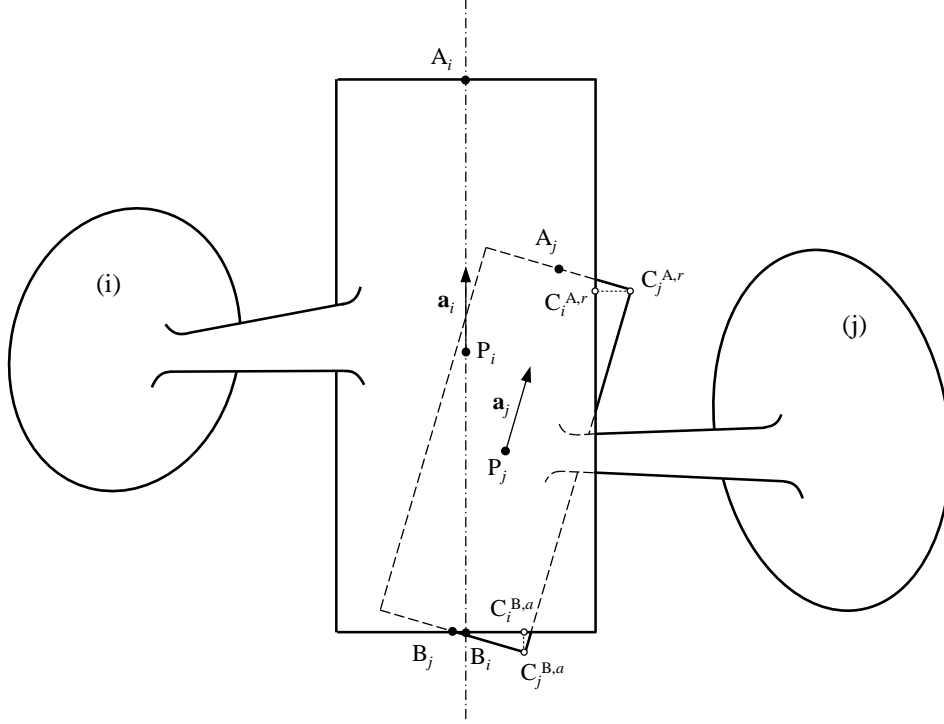


**Figure 4.9** - Configuration of a spatial revolute joint misaligned with axial and radial contact.

Both Eq. (4.19) and Eq. (4.20) can be solved together in order to find the intersection points analytically. The solution can hold the empty set, one or two solutions, respectively, no contact, tangent contact or penetration. If the solution is given by two points,  $I_1$  and  $I_2$ , their middle point and the center of the base of the journal form a vector, that define the direction of the contact point, as

$$\mathbf{n}_d = \frac{\frac{1}{2}(\mathbf{r}^{I_1} + \mathbf{r}^{I_2}) - \mathbf{r}^{B_j}}{\left\| \frac{1}{2}(\mathbf{r}^{I_1} + \mathbf{r}^{I_2}) - \mathbf{r}^{B_j} \right\|} \quad (4.21)$$

Thus, the contact point of the bearing can be given as

$$\mathbf{r}^{C_j^{B,a}} = \mathbf{r}^{B_j} \pm R_j \mathbf{n}_d \quad (4.22)$$

where the sign is chosen after the evaluation of the position of each point, i.e., the correct sign returns a point outside of the bearing. Hence, the contact point in the journal is calculated with the following expression

$$\mathbf{r}^{C_i^{B,a}} = \mathbf{r}^{C_j^{B,a}} + \left( \mathbf{r}^{B_i} - \mathbf{r}^{C_j^{B,a}} \right)^T \mathbf{a}_i \mathbf{a}_i \quad (4.23)$$

In the case of radial contact, the problem can be converted into the intersection of a circumference (base of the journal) and a cylindrical surface (lateral wall of the bearing) which can be defined, respectively, as



$$\|\mathbf{x} - \mathbf{r}^{A_j}\|^2 = R_j^2 \wedge \mathbf{a}_j^T \mathbf{x} = \mathbf{a}_j^T \mathbf{r}^{A_j} \quad (4.24)$$

$$\|\tilde{\mathbf{a}}_i(\mathbf{x} - \mathbf{r}^{P_i})\|^2 = R_i^2 \quad (4.25)$$

Contrary to the previous case, in this situation, the intersection points cannot be calculated analytically, since it involves the resolution of a nonlinear system. Thus, the intersection points have to be determined recurring to an iterative procedure, such the Newton-Raphson technique. This intersection can have from zero until four solutions, although, considering that the angle between the bearing and the journal is small, the maximum number of solutions is two. The method converges easily, since, at least, one solution exists and the initial approximation does not hold any singular position as a point equidistant of two solutions. When penetration occurs, similarly to the axial contact, the intersection is given by two points,  $I_1$  and  $I_2$ , and the contact point of the journal is calculated in the same way as Eq. (4.21) and Eq. (4.22), that is

$$\mathbf{n}_d = \frac{\frac{1}{2}(\mathbf{r}^{I_1} + \mathbf{r}^{I_2}) - \mathbf{r}^{A_j}}{\left\| \frac{1}{2}(\mathbf{r}^{I_1} + \mathbf{r}^{I_2}) - \mathbf{r}^{A_j} \right\|} \quad (4.26)$$

$$\mathbf{r}^{C_j^{A,r}} = \mathbf{r}^{A_j} \pm R_j \mathbf{n}_d \quad (4.27)$$

As before, the correct sign is the one that corresponds to a position outside of the bearing. The normal unit vector can be expressed as

$$\mathbf{n}_v = \frac{\left( \mathbf{r}^{C_j^{A,r}} - \mathbf{r}^{P_i} \right) - \left( \mathbf{r}^{C_j^{A,r}} - \mathbf{r}^{P_i} \right)^T \mathbf{a}_i \mathbf{a}_i}{\left\| \left( \mathbf{r}^{C_j^{A,r}} - \mathbf{r}^{P_i} \right) - \left( \mathbf{r}^{C_j^{A,r}} - \mathbf{r}^{P_i} \right)^T \mathbf{a}_i \mathbf{a}_i \right\|} \quad (4.28)$$

With this vector, the contact point of the bearing is given by

$$\mathbf{r}^{C_i^{A,r}} = \mathbf{r}^{P_i} + \left( \mathbf{r}^{C_j^{A,r}} - \mathbf{r}^{P_i} \right)^T \mathbf{a}_i \mathbf{a}_i + R_i \mathbf{n}_v \quad (4.29)$$

It should be reminded that the contact points were determined for axial contact in end B and radial contact in end A, as it is exemplified in Figure 4.9. For contacts in the opposite extremities, analogous equations should be employed.

#### 4.2.2 Contact Kinematics

At this point, it was defined the methodology for the evaluation of the contact points for all types of contacts. Therefore, it is possible characterize the contact kinematics for each collision as function of the contact points in the bearing and journal,

respectively,  $C_i$  and  $C_j$ .

The normal unit vector of the contact was already defined for some cases, but it can be, generically, given as

$$\mathbf{n}_v = \frac{(\mathbf{r}^{C_j} - \mathbf{r}^{C_i})}{\|(\mathbf{r}^{C_j} - \mathbf{r}^{C_i})\|} \quad (4.30)$$

The penetration depth,  $\delta$ , can be expressed by

$$\delta = \|(\mathbf{r}^{C_j} - \mathbf{r}^{C_i})\| \quad (4.31)$$

Moreover, the penetration velocity,  $\dot{\delta}$ , can be determined as it follows

$$\dot{\delta} = (\dot{\mathbf{r}}^{C_j} - \dot{\mathbf{r}}^{C_i})^T \mathbf{n}_v \quad (4.32)$$

where  $\dot{\mathbf{r}}^{C_i}$  and  $\dot{\mathbf{r}}^{C_j}$  are the linear velocities of the bearing and journal in the contact points which can be calculated as

$$\dot{\mathbf{r}}^{C_k} = \dot{\mathbf{r}}_k + \tilde{\boldsymbol{\omega}}_k \mathbf{s}_k^{C_k}, \quad (k=i,j) \quad (4.33)$$

Finally, the relative tangential velocity can be obtained recurring to the following expression

$$\mathbf{v}_T = (\dot{\mathbf{r}}^{C_j} - \dot{\mathbf{r}}^{C_i}) - (\dot{\mathbf{r}}^{C_j} - \dot{\mathbf{r}}^{C_i})^T \mathbf{n}_v \mathbf{n}_v \quad (4.34)$$

### 4.2.3 Contact Force Evaluation

For modelling revolute joints with clearance, it is of paramount importance to select a suitable contact force model. The contact model should properly define the forces acting in the journal and bearing during the contact-impact events.

In Section 1.2.2, it was provided a general overview of the most significant methodologies to deal with contact problems. Thus, for this application, it will be employed a model based on Hertzian theory, which, in its genesis, considered elastic impacts. Hunt and Crossley (1975) proposed a methodology to take into account the energy dissipation through the inclusion of a damping term, and it can be expressed in a general form as

$$F_N = K\delta^n + \chi\delta^n\dot{\delta} \quad (4.35)$$

where  $K$  is the contact stiffness,  $\chi$  is the hysteresis damping factor, and  $n$  is an exponent that defines the degree of nonlinearity. This approach was the basis for the development of other contact force models, as the work of Lankarani and Nikravesh (1990) which is

here utilized. In this model,  $n$  is  $3/2$ , and the hysteresis damping factor is given by

$$\chi = \frac{3(1-c_e^2)}{4} \frac{K}{\dot{\delta}^{(-)}} \quad (4.36)$$

where  $c_e$  is the coefficient of restitution, and  $\dot{\delta}^{(-)}$  is the initial impact velocity.

Introducing Eq. (4.36) into Eq. (4.35), the expression to determine the contact force can be rewritten in the following form

$$F_N = K \delta^n \left[ 1 + \frac{3(1-c_e^2)}{4} \frac{\dot{\delta}}{\dot{\delta}^{(-)}} \right] \quad (4.37)$$

This contact model exhibits a good numerical stability for low impact velocities, and shows an accurate damping effect for impacts with high coefficient of restitution. Normally, the contact stiffness can be calculated as a function of the geometry and material properties.

As it was aforementioned, this approach consists in utilization of force constraints. Thus, the contact forces are added to the equations of motion of a constrained multibody system, Eq. (2.44), as external forces. According to Eq. (2.23), the generalized external forces in each body are divided in forces and moments, which, in this case, can be calculated for the body that contains the bearing as

$$\mathbf{f}_i = F_N \mathbf{n}_v \quad (4.38)$$

$$\mathbf{n}_i = \tilde{\mathbf{s}}_i^{C_i} \mathbf{n}_v F_N \quad (4.39)$$

and, for the body of the journal as

$$\mathbf{f}_j = -F_N \mathbf{n}_v \quad (4.40)$$

$$\mathbf{n}_j = -\tilde{\mathbf{s}}_j^{C_j} \mathbf{n}_v F_N \quad (4.41)$$

These forces replace the effect of a clearance joint when a frictionless contact is taking into account.

#### 4.2.4 Simulations and Results

In order to implement this methodology to simulate the behavior of a revolute joint with clearance, it is considered the same example as in the previous section, a spatial slider-crank mechanism represented in Figure 4.2. The revolute joint with clearance is located at the connection between the crank and the ground. The bearing is placed in the crank, while the journal belongs to the ground.

For the frictionless case, three different simulations were performed in order to

understand the influence of the clearance size in the dynamic response of the system. In Table 4.2, the dimensions of the journal and bearing are displayed together with the resulting axial and radial clearances. The simulation 1 will be considered the standard case, and the remaining situations consist on variations of axial and radial clearance size, respectively, simulations 2 and 3.

**Table 4.2** – Geometric parameters of the joint for each simulation

<b>Simulation</b>	$R_i$	$R_j$	$c_r$	$L_i$	$L_j$	$c_a$
1	0.01	0.0095	0.0005	0.02	0.019	0.001
2	0.01	0.0095	0.0005	0.02	0.0195	0.0005
3	0.01	0.00975	0.00025	0.02	0.019	0.001

The general parameters that are common for all the simulations can be found in Table 4.3. For sake of simplicity, the contact properties were assumed to be equal for the different types of collisions. These simulations were carried with a fourth-order Runge-Kutta integrator, and the time step had to be significantly decreased due to the importance of an accurate detection of the beginning of the contacts.

**Table 4.3** - General parameters for simulation

<b>Parameter</b>	<b>Symbol</b>	<b>Value</b>	<b>Parameter</b>	<b>Value</b>
Contact stiffness	$K$	$6.71 \times 10^{10} \text{ N/m}^{3/2}$	Time step	$5 \times 10^{-7} \text{ s}$
Coefficient of restitution	$c_e$	0.9	Simulation time	1 s

This example shares the dimensional and inertial properties, and the initial condition with the example presented in Section 2.4, in which this information is displayed in Tables 2.1 and 2.2, respectively.

Figure 4.10 shows the position, velocity and acceleration of the slider for simulation 1. The results are compared with the situation of an ideal joint. The motion of the slider is highly affected by the impacts of a clearance joints, which results in peaks of acceleration displayed in Figure 4.10c. These peaks produce sudden changes in the mechanism motion. From the position plot, it is possible to conclude that the energy loss does not allow the mechanism to reach a full revolution of the crank, since the slider does not achieve its minimum position. The phase portrait presented in Figure 4.11 indicates that the global motion of the slider-crank is nonlinear. This phenomenon is more evident in Figure 4.11b due the dense overlapping lines.

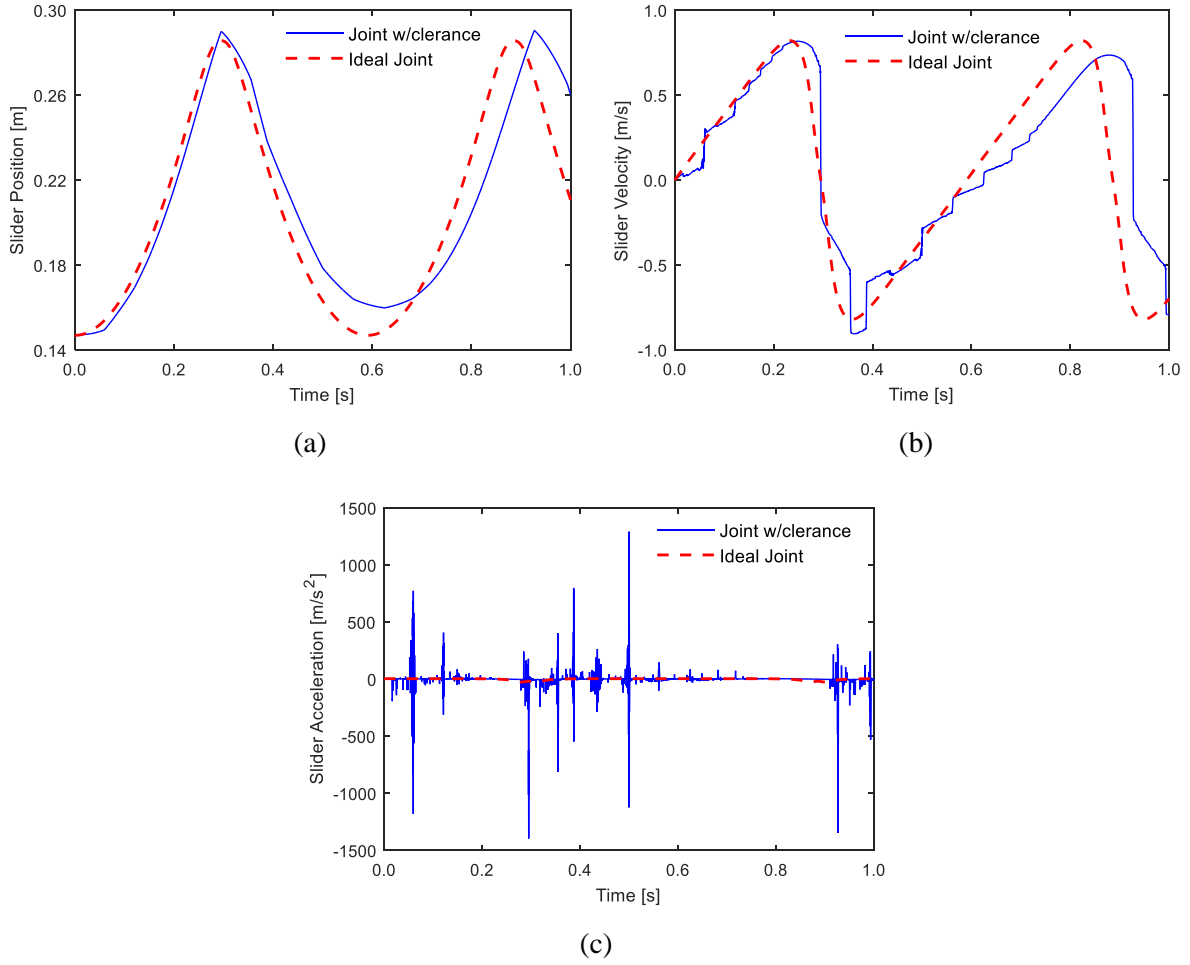


**Figure 4.10** - Motion of the slider for simulation 1: (a) position; (b) velocity; (c) acceleration.

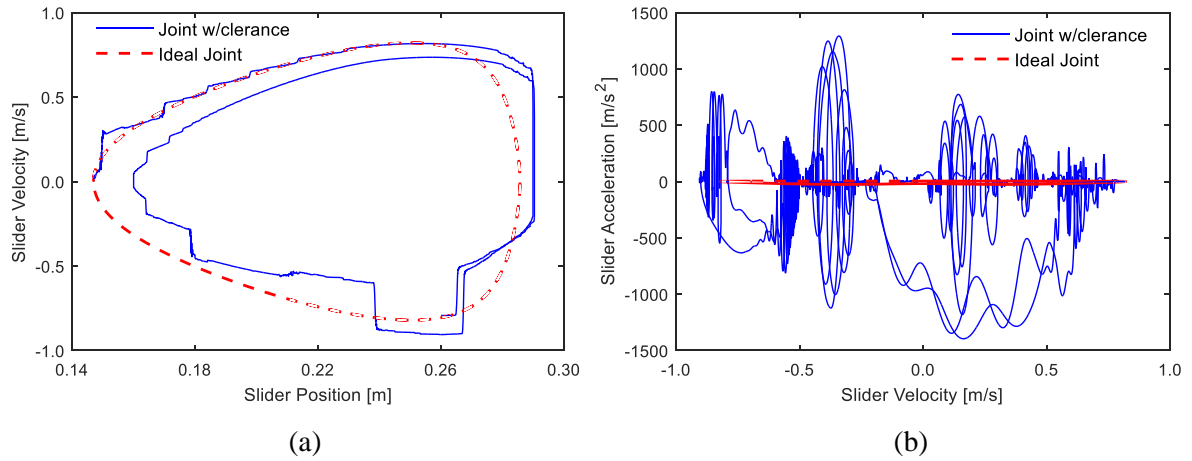


**Figure 4.11** – Phase portraits for simulation 1: (a) Position-Velocity; (b) Velocity-Acceleration.

The same analysis was performed for simulation 2, which considers a smaller axial clearance size (half of the preceding experiment). The motion of the slider is displayed in Figure 4.12. In this case, the mechanism shows a slightly smoother motion, the peaks of the acceleration achieve lower values compared with the previous case. For

this situation, the mechanism is able to perform a full crank revolution which indicates less energy loss. The phase portraits suggest a more stable motion, mainly Figure 4.13a, where the similarities with the results for ideal joint are more evident.

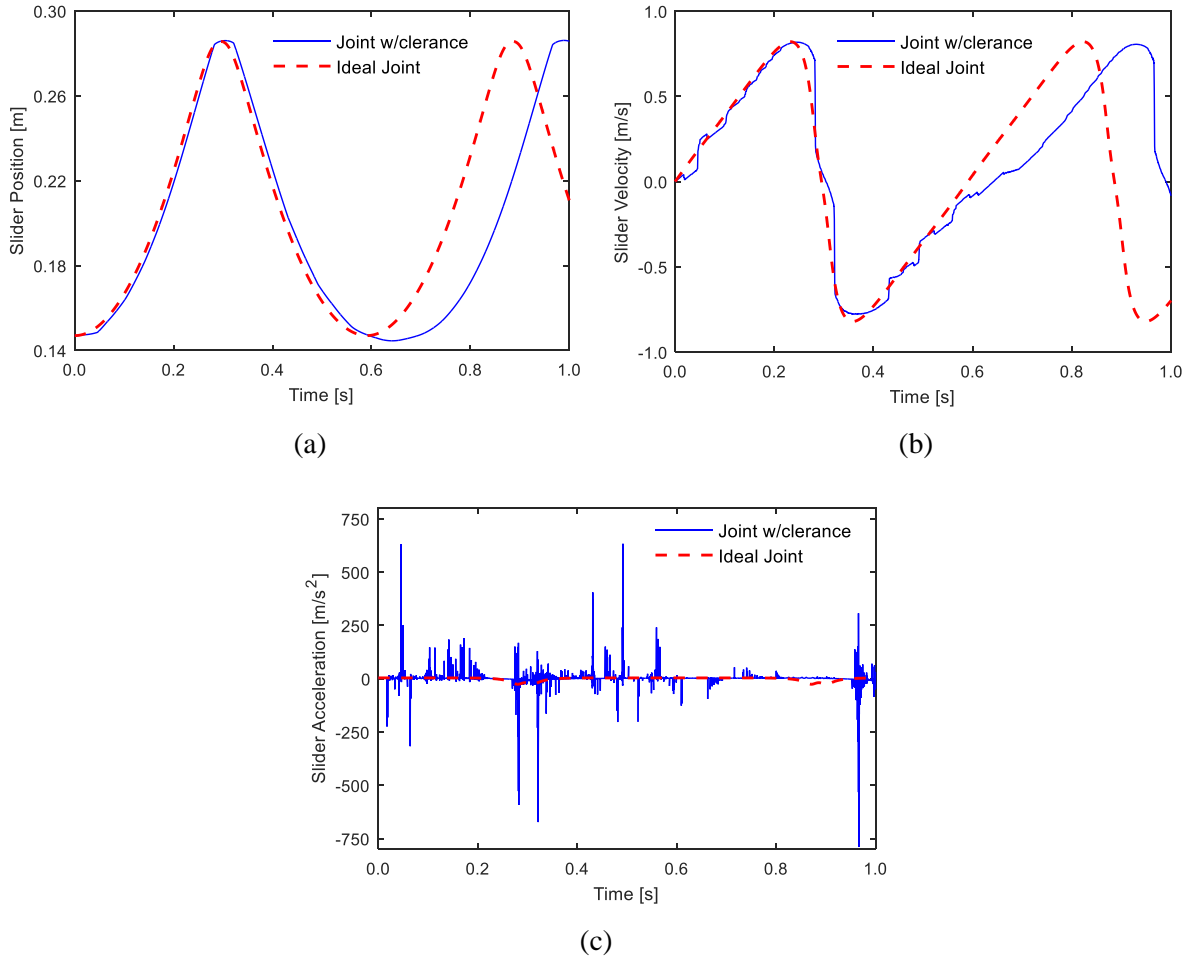


**Figure 4.12** - Motion of the slider for simulation 2: (a) position; (b) velocity; (c) acceleration.

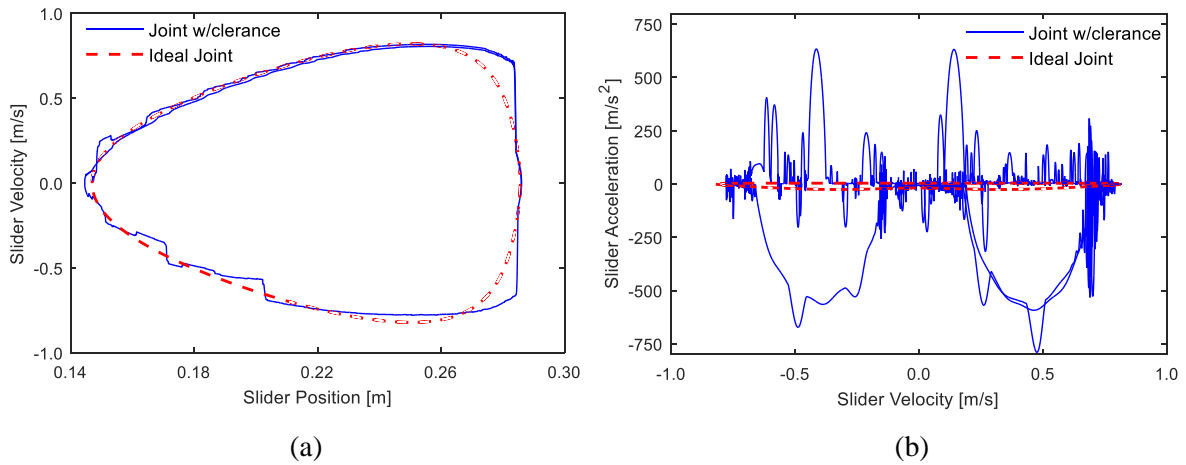


**Figure 4.13** – Phase portraits for simulation 2: (a) Position-Velocity; (b) Velocity-Acceleration.

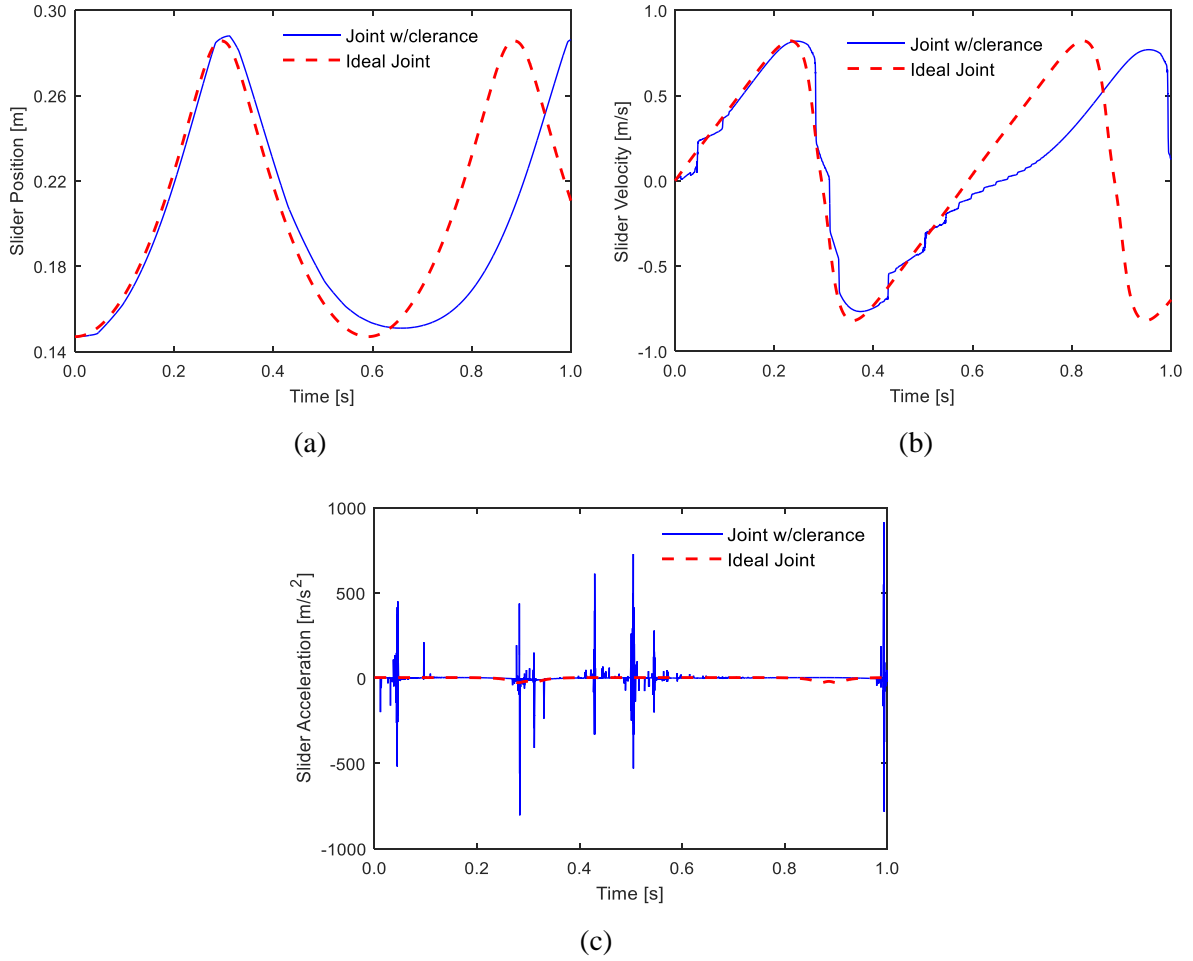


**Figure 4.14** - Motion of the slider for simulation 3: (a) position; (b) velocity; (c) acceleration.

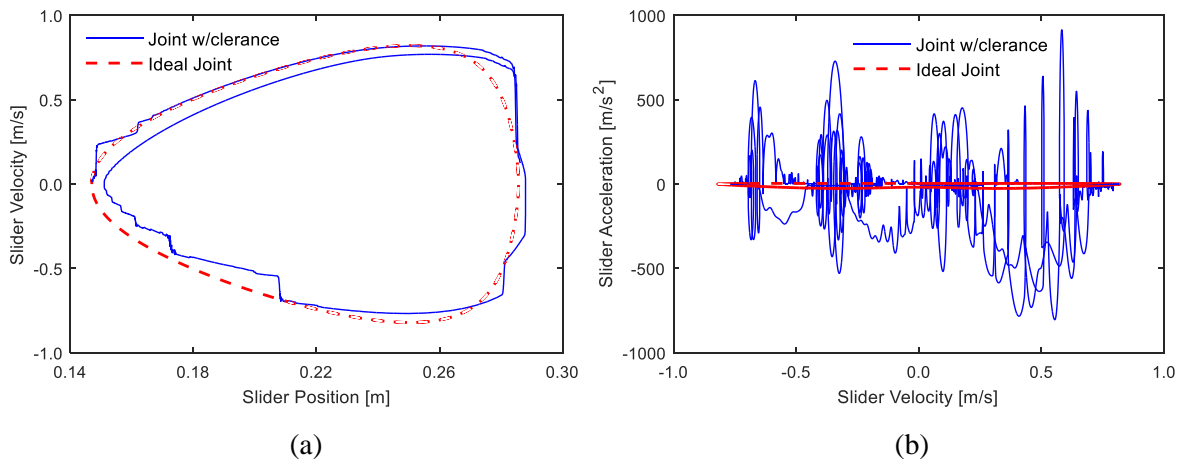


**Figure 4.15** – Phase portraits for simulation 3: (a) Position-Velocity; (b) Velocity-Acceleration.

In simulation 3, the geometric properties are identical to simulation 1, except for the radius of the journal, which, in this situation, was increased in order to reduce by half the radial clearance. The resultant motion of the slider is represented in Figure 4.14. The results shows that the reduction of the clearance has a significant impact in the dy-

dynamic response of the mechanism. As in the previous case, the reduction in clearance caused the decrease of the slider acceleration peaks. Although, this time, the differences were not so considerable. The mechanism also presents a nonlinear behavior, as it is shown by Figure 4.15.

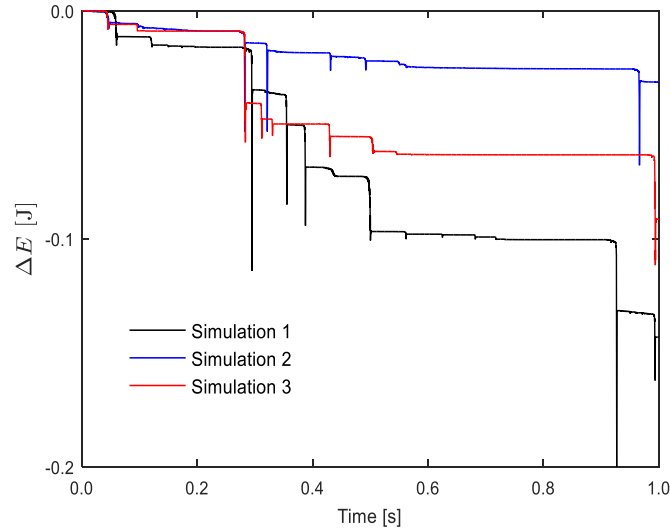


**Figure 4.16** - Comparison of the variation of mechanical energy for the three simulations.

The variation of the mechanical energy of the whole mechanism is presented in Figure 4.16. The results exhibit the energy loss for each simulation. The simulation 1, which considers both axial and radial clearance sizes larger, has the highest energy dissipation. This phenomenon is explained by higher impact velocities between the bearing and journal. The axial and radial clearance sizes were halved in simulations 2 and 3, respectively, and simulation 2 presents a lower energy dissipation, which seems to suggest that the axial clearance have more influence in energy loss for this mechanism.

### 4.3 Spatial Revolute Joint with Clearance and Friction

Similarly to the previous section, a revolute joint with clearance is considered. The joints description and the methodology for contact detection closely follows the steps already presented. The main difference is the employment of some of the friction models described in Chapter 3 rather than considering frictionless contacts.

In order to evaluate the friction force, it is necessary to introduce the relative tangential velocity and the normal contact force, which are given by Eq. (4.34) and Eq. (4.37), respectively. The friction force,  $\mathbf{f}_F$ , should be included in the generalized external forces vector. Thus, Eq. (4.38) and Eq. (4.39) are rewritten as



$$\mathbf{f}_i = F_N \mathbf{n}_v + \mathbf{f}_F \quad (4.42)$$

$$\mathbf{n}_i = \tilde{\mathbf{s}}_i^{C_i} \mathbf{n}_v F_N + \tilde{\mathbf{s}}_i^{C_i} \mathbf{f}_F \quad (4.43)$$

and, Eq. (4.40) and Eq. (4.41) can be replaced by

$$\mathbf{f}_j = -F_N \mathbf{n}_v - \mathbf{f}_F \quad (4.44)$$

$$\mathbf{n}_j = -\tilde{\mathbf{s}}_j^{C_j} \mathbf{n}_v F_N - \tilde{\mathbf{s}}_j^{C_j} \mathbf{f}_F \quad (4.45)$$

For this study, the same example will be considered, and the geometric properties of the imperfect joint follows simulation 1 of the previous section (see Table 4.2). From that case, it will be analyzed the influence of four friction force models. Bearing that in mind, two static models, Coulomb friction (1785) and Stribeck (Bo and Pavelescu, 1982), and two dynamic models, Dahl (1968) and LuGre (Canudas de Wit et al., 1995), will be considered.

The parameters necessary for the correct implementation of the referred friction models are established in Table 4.4. The remaining parameters of the simulation are equal to the preceding section.

**Table 4.4** - Parameters considered for the different friction models.

Parameter	Symbol	Value
Static coefficient of friction	$\mu_s$	0.2
Kinetic coefficient of friction	$\mu_k$	0.1
Stribeck velocity	$v_s$	0.001 m/s
Geometry factor	$\delta_\sigma$	2
Stiffness coefficient	$\sigma_0$	$10^5$ N/m
Damping coefficient	$\sigma_1$	$\sqrt{10^5}$ Ns/m
Coefficient of viscosity	$\sigma_2$	0 Ns/m

Coulomb's law is the most simple friction model, although, its implementation has a paramount influence in the resultant motion of the slider-crank when compared with frictionless behavior. Figure 4.17 delivers the position, velocity and acceleration of the slider, which suggest a much higher energy dissipation, since the slider has more cycles with less amplitude. The phase portrait represented by Figure 4.18a also shows this phenomenon. The acceleration peaks seems to decrease with the introduction of this friction model.

The model with the Stribeck curve is equal to Coulomb friction, except when the relative tangential velocity is lower than the Stribeck velocity. Thus, the main differ-

ences occur when the impact is almost frontal. From the analysis of the position and velocity plots in Figure 4.19, it has a similar behavior of the Coulomb friction. In the acceleration plot, some differences are can be evidenced. The phase portrait show a nonlinear behavior as expected.

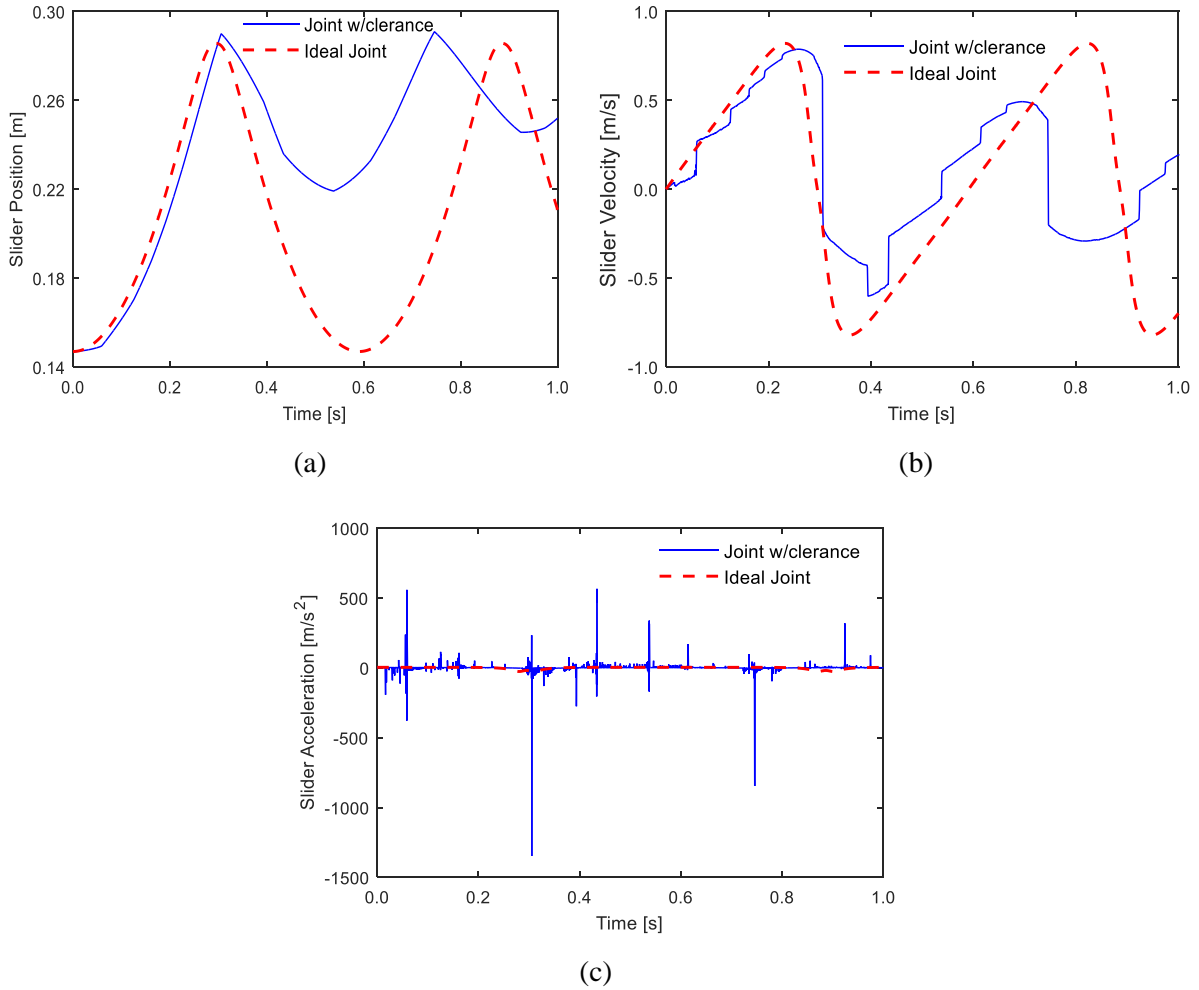


**Figure 4.17** - Motion of the slider for Coulomb friction: (a) position; (b) velocity; (c) acceleration.

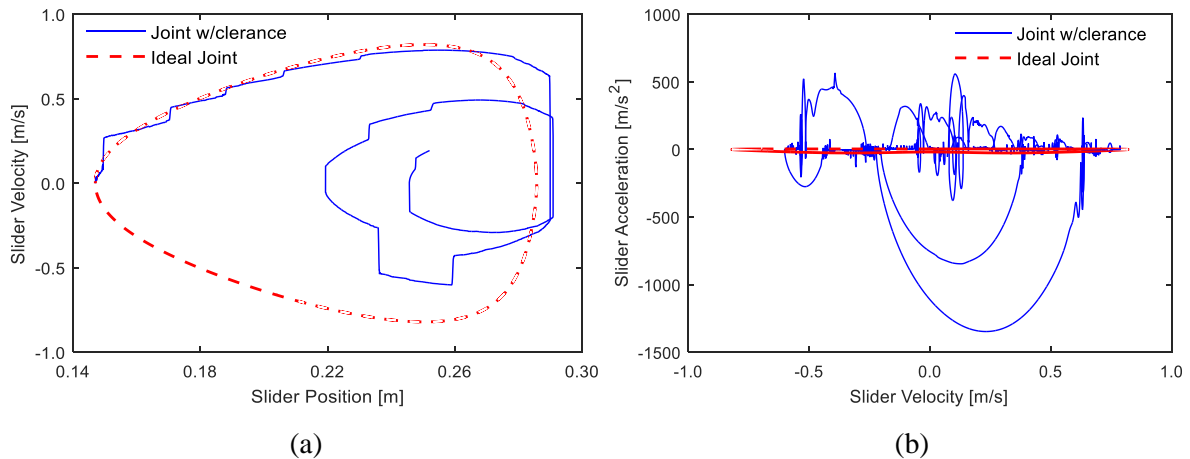


**Figure 4.18** – Phase portraits for Coulomb friction: (a) Position-Velocity; (b) Velocity-Acceleration.

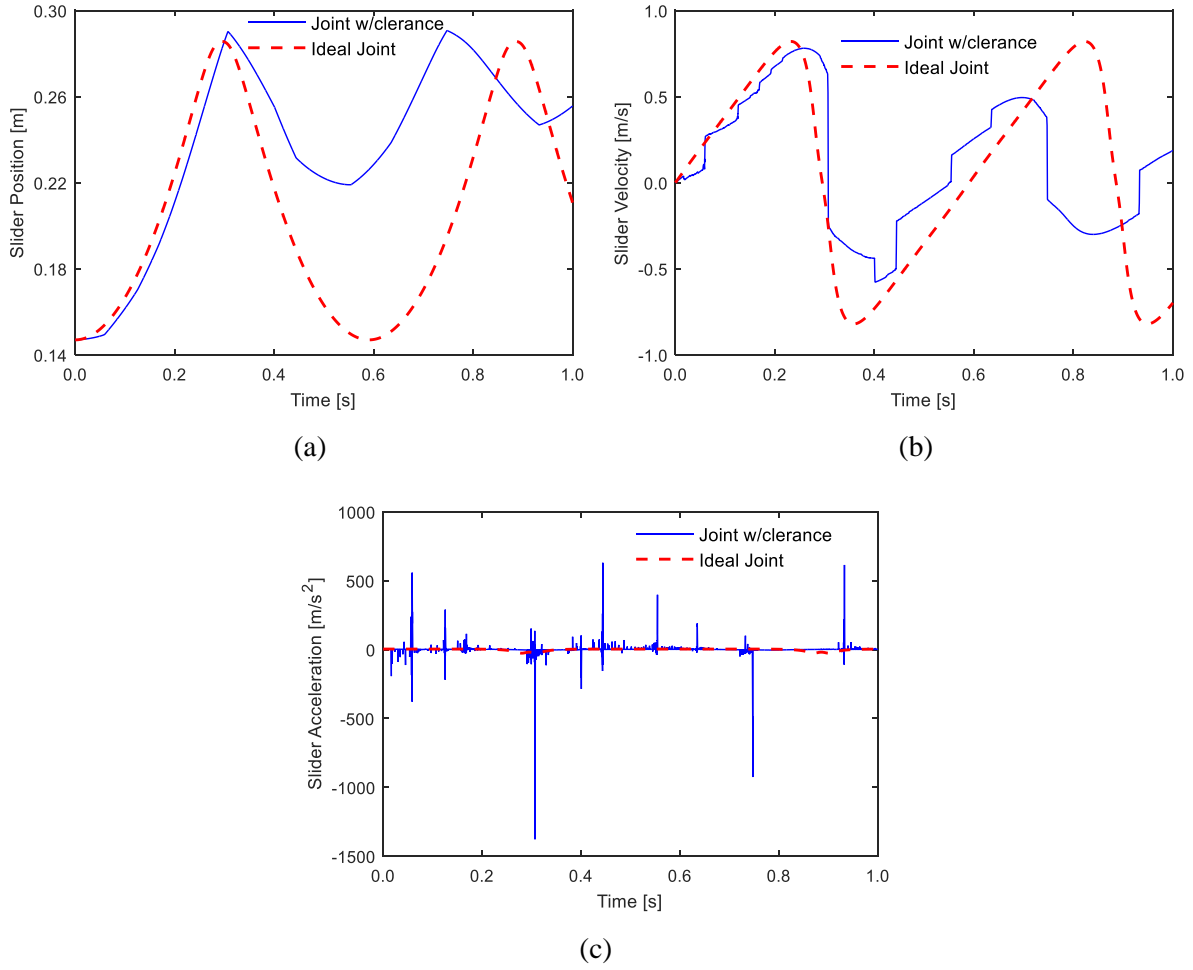


**Figure 4.19** - Motion of the slider for Stribeck model: (a) position; (b) velocity; (c) acceleration.

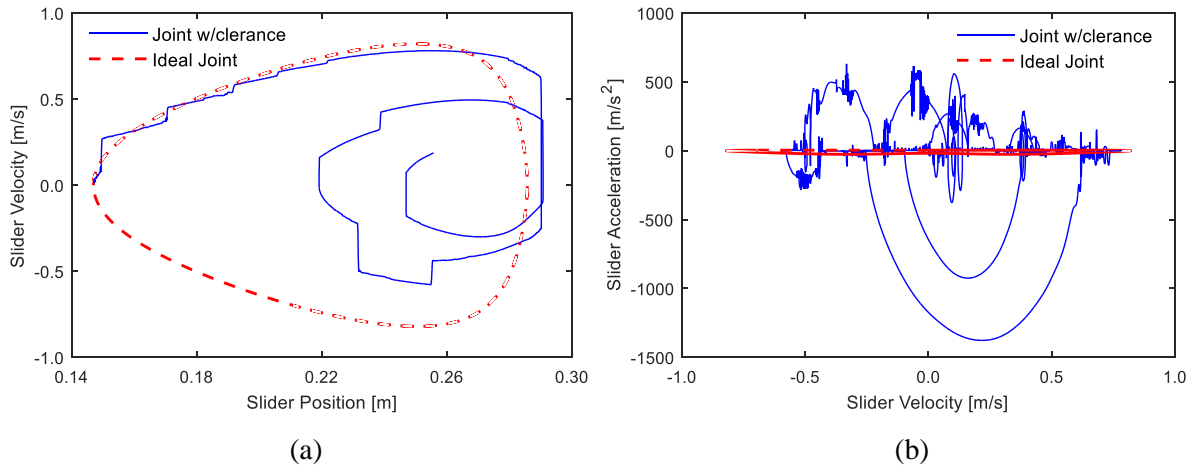


**Figure 4.20** – Phase portraits for Stribeck model: (a) Position-Velocity; (b) Velocity-Acceleration.

For the Dahl model, it is expected to have a performance similar to Coulomb's law with the exception of the beginning of the contact and in changes of the velocity direction. In these two situation, this models takes into account the pre-sliding displacement which consider a progressive increase of friction force. The outcome of the

mechanism in terms of the slider motion presents some differences to the Coulomb and Stribeck approaches, as it is represented in Figure 4.21. This model seems to create more oscillations on the slider acceleration when it is moving forward, as it shows the nonlinear behavior Figure 4.22b.

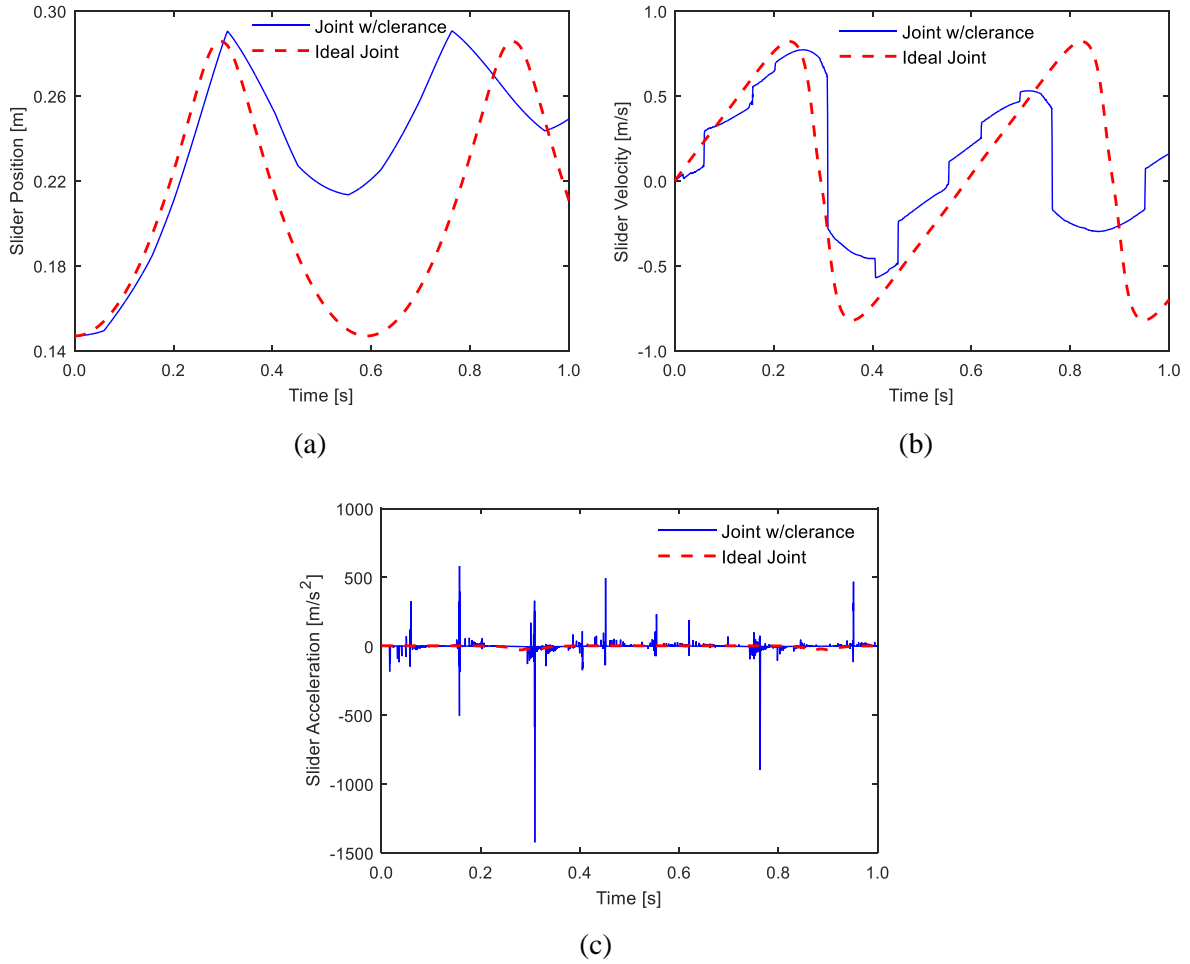


**Figure 4.21** - Motion of the slider for Dahl model: (a) position; (b) velocity; (c) acceleration.

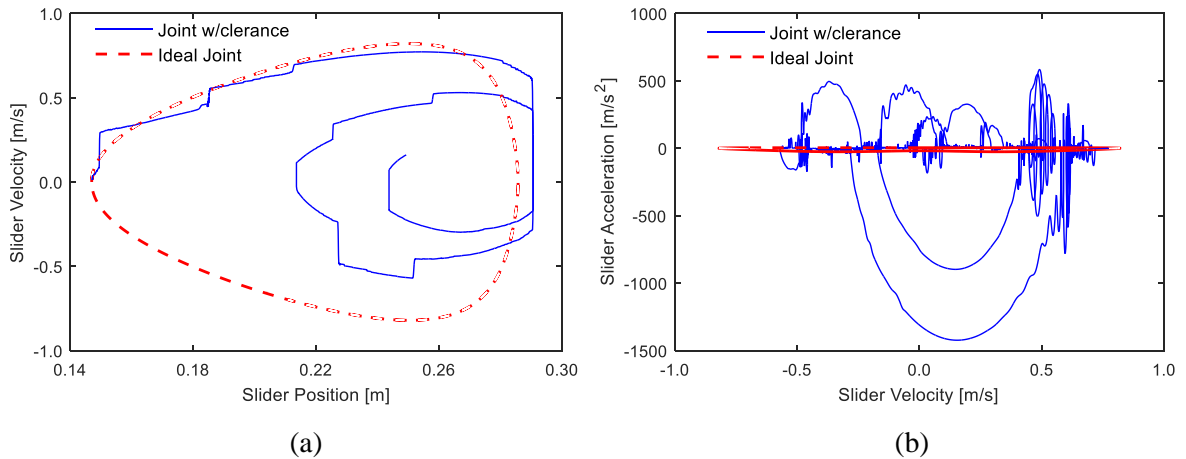


**Figure 4.22** – Phase portraits for Dahl model: (a) Position-Velocity; (b) Velocity-Acceleration.

This problem was also modelled by LuGre friction model, which is clearly the model that presents the most chaotic motion. For this case, the acceleration reaches higher values and has more significant peaks (see Figure 4.23c). Figure 4.23a displays the slider position which indicates that in this simulation the amplitude of its motion is even lower.

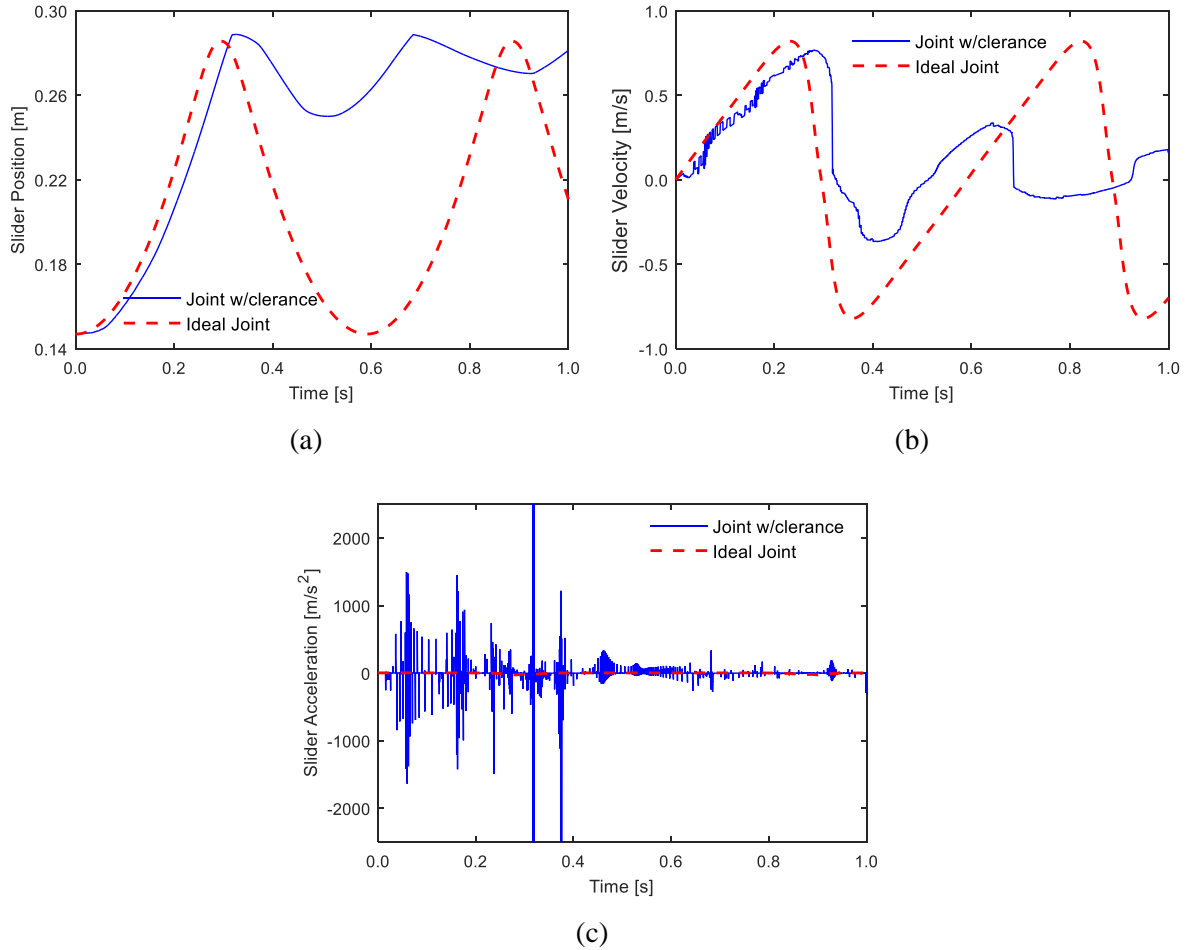


**Figure 4.23** - Motion of the slider for LuGre model: (a) position; (b) velocity; (c) acceleration.

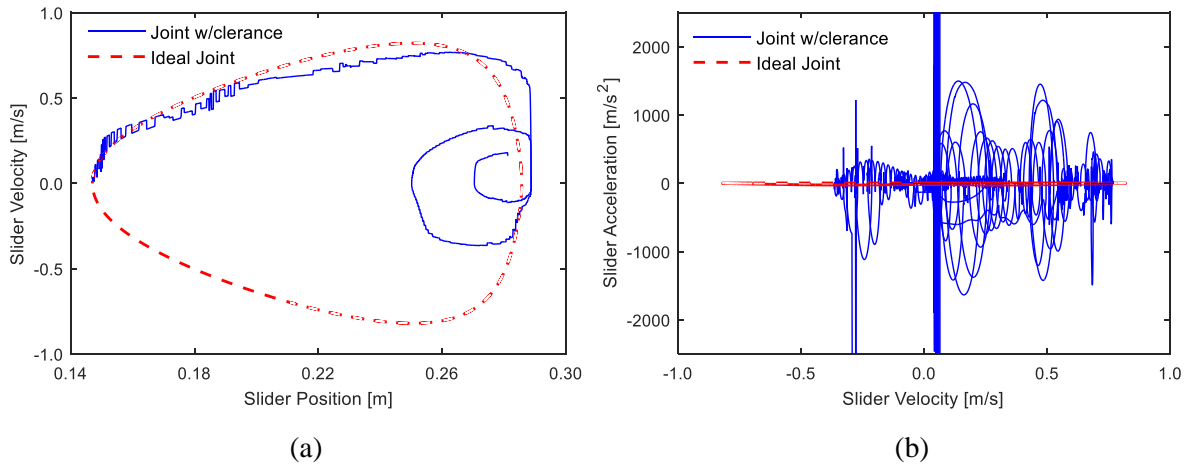


**Figure 4.24** – Phase portraits for LuGre model: (a) Position-Velocity; (b) Velocity-Acceleration.

The energy dissipation by each model is compared with the frictionless case, and the results are displayed in Figure 4.25 which contains the variation of mechanical energy of the system. From the analysis of the plot, it is possible to conclude that considering friction itself, regardless of the model, introduces a large amount of energy dissipation. The LuGre model presents a higher level of energy loss comparing to the remaining friction approaches. Figure 4.25 also shows that, for a frictionless model, the decreasing of mechanical energy only occurs by levels of energy which are result from the impacts, while, for frictional contacts, the energy dissipation can also happen in a continuous process.

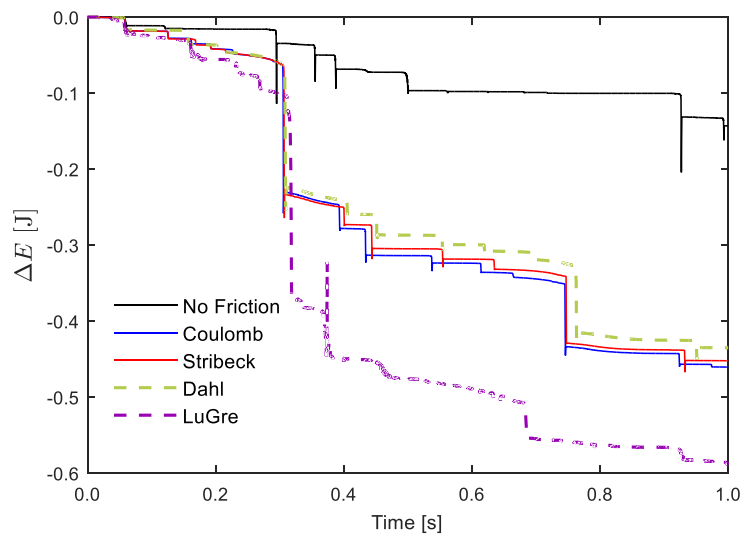


**Figure 4.25** - Comparison of the variation of mechanical energy for the different friction models.

## 4.4 Summary and Conclusions

In this chapter, it was performed a general study on the influence of friction implementation in the dynamic analysis of a mechanical systems with tridimensional motion. For this purpose, two different analyzes were conducted.

Firstly, the inclusion of friction in a kinematic translational joint was investigated. This implementation requires special attention in the construction of the equations of motion since the friction forces are calculated implicitly. This analysis was carried with the dynamic study of spatial slider-crank mechanism. The results showed that friction introduces a high energy dissipation, which have a huge impact in the velocity of the bodies. The friction models present more significant differences at the accelerations level, mainly when there are changes on the velocity direction. Since the main differences between friction models happens for small relative velocities, the time integrator

and the time step should be carefully chosen in order to be able to capture correctly those differences.

Secondly, a complete methodology for modelling a spatial revolute joint with axial and radial clearance was fully described. The different contact scenarios were identified and the procedure for the evaluation of the contact points was defined. The evaluation of the normal contact force during the impacts was held by the continuous contact force model proposed by Lankarani and Nikravesh (1990). The same mechanism was considered for the analysis of frictionless contacts in which the influence of clearance sizes were tested. The results show that larger clearance sizes emphasize the chaotic motion of the system and increase the energy dissipation.

The study of spatial revolute joints with clearance was naturally extended to the friction modelling. As in the case of the translational joint, the inclusion of friction itself provokes a significant increase in the energy dissipation. The models present some differences in their motion, and LuGre is the approach that yields the most chaotic motion.

It should be put in evidence the difficulties that the dynamic friction models have in capture some frictional properties, such as pre-sliding displacement or friction lag, when in the presence of impact motion. The dynamic models use extra state variables which have to be integrated together with the state properties of the system, and if their derivatives are not correctly captured, it might result in an inaccurate evaluation of the friction forces. The impacts produce rapid changes in the contacting kinematics and, therefore, provoke more difficulties to use properly a dynamic model.

This study provides a better understanding of the impact of some of the static and dynamic friction models in the analysis of a multibody systems.





*“Perfection is not attainable, but if we chase perfection we can catch excellence.”*

Vince Lombardi

## 5. CONCLUDING REMARKS

A comprehensive and broad study of the dynamic of multibody systems with frictional contacts has been delivered throughout this report. Several conclusions were drawn during the whole document, they will be summarized and presented in following paragraphs.

The Newton-Euler formulation to build the equations of motion for constrained multibody systems was concisely described in Chapter Two. This formulation uses Cartesian coordinates and it was presented in the context of the analysis of spatial motion of mechanical systems, therefore, the Euler parameters are used to describe rotational positions. The assemblage of the equations of motion involves the construction of the mass matrix, the definition of the kinematic constraints, and the gathering of the generalized external forces. In order to solve the equations of motion, the standard Lagrange multipliers technique can be employed, although it does not ensure the fulfillment of the constraints equations at position and velocity levels and does not handle redundant constraints. In this sense, several other methodologies to solve the equation of motion have been characterized. In the end, a comparative study between the different methodologies to eliminate constraints violation was provided. With a small increase in computational time, it is possible to apply a technique to keep the violation of the constraints under control, although the utilization of the direct correction approach completely vanishes the errors in the constraints.

In Chapter Three, the main phenomena associated with friction were detailed, and

a comparative study of several static and dynamic friction models was provided. It was also discussed the ability of each approach to capture frictional effects, such as pre-sliding displacement, stick-slip, Stribeck effect, viscous friction, among others. For sake of simplicity, the friction models were divided in two groups, the static and dynamic models. On the one hand, the static models are simpler, and only represent the steady-state behavior of friction force. Some of them also present problems due to having a discontinuity at zero velocity. On the other hand, the dynamic models use extra state variables which make them able to describe friction phenomena in more details. A simple multibody system, in which friction has preponderant role, was used to compare some of the presented models. For the analysis of results, the friction models were divided into three groups according their behavior, namely static models without stiction, static models with stiction and dynamic models. The ability to capture stick-slip motion showed to be the friction phenomenon with more impact in dynamic response of a multibody system. Although, the remaining characteristics also exhibited their influence in the results. It was seen that some of the dynamic models were capable of describing correctly most of frictional effects, nevertheless, the more advanced approaches need to define a large number of parameters. This becomes a significant limitation, since most of the parameters have to be determined experimentally.

The study of the influence of friction modelling in the dynamic analysis of a multibody system is extended in Chapter Four. For that reason, it is considered a more complex mechanical system, and two different approaches are utilized. The first example involves implementing friction in the continuous contact of kinematic translational joint, while the second situation consists in describing a methodology for modelling friction for a spatial revolute joint with axial and radial clearance which includes impacts. Both examples were performed only with four different friction models, and the implementation of friction introduces a high level of energy dissipation when compared with the respective frictionless cases. In the translation joint with friction, the main differences between the models occur at the acceleration level, mainly for low relative velocities. In the case of the revolute joint with clearance, the differences are also present at position and velocity levels. It was seen that the selection of the friction model has a significant impact in the system dynamics. The evaluation of friction forces during the resolution of equations motion does not introduce considerable extra computational time, although, since the main differences of the models are displayed for low velocities, the time integrator and the time step should be accurately selected to capture those

differences. The dynamic models usually require a more refined time step, since they use a differential equations to estimate the variation of the bristle deflection. This quantity must be correctly calculated to not generate unrealistic friction forces.

All the numerical simulations performed in the context of this work were carried in MATLAB. Some of them were done by implementing additional features in MUBODYNA (MUltiBOdy DYNAmics) which is a MATLAB code developed by Flores for the dynamic analysis of multibody systems. The remaining simulations were executed from dedicated codes.

One the most important statements of this work is that the dynamic modelling of frictional contacts in multibody systems is an open field of investigation and further developments will be certainly made in the upcoming years. Bearing that in mind, the author suggests some issues that can treated in future works. The establishment of a simple experimental procedure for the validation and comparison of any friction force model, the study the influence of friction modelling on the wear prediction in mechanical systems, and the employment of some of the previous presented models in the simulation of more complex multibody systems, such as railroad vehicles, are some of the proposed topics.



*“Someone is sitting in the shade today  
because someone planted a tree a long time ago.”*  
Warren Buffett

## REFERENCES

- Al-Bender, F., Lampaert, V., Swevers, J. (2004). A novel generic model at asperity level for dry friction force dynamics. *Tribology Letters*, 16(1), pp. 81-93.
- Al-Bender, F., Lampaert, V., Swevers, J. (2005). The Generalized Maxwell-Slip Model: A Novel Model for Friction Simulation and Compensation. *IEEE Transactions on Automatic Control*, 50(11), pp. 1883-1887.
- Alves, J., Peixinho, N., Silva, M.T., Flores, P., Lankarani, H.M. (2015). A comparative study of the viscoelastic constitutive models for frictionless contact interfaces in solids. *Mechanism and Machine Theory*, 85, pp. 172-188.
- Ambrósio, J.A.C. (2003). Impact of Rigid and Flexible Multibody Systems: Deformation Description and Contact Model. *Virtual Nonlinear Multibody Systems*, 103, pp. 57-81.
- Ambrósio, J., Verissimo, P. (2009). Improved bushing models for general multibody systems and vehicle dynamics. *Multibody Systems Dynamics*, 22(4), pp. 341-365.
- Amirouche, F.M.L. (1992). *Computational Methods for Multibody Dynamics*, Prentice-Hall, Englewood Cliffs, New Jersey.
- Amontons, G. (1699). On the resistance originating in machines. *Proceedings of the French Royal Academy of Sciences*, pp. 206-222.
- Andersson, S., Söderberg, A., Björklund, S. (2007). Friction models for sliding dry, boundary and mixed lubricated contacts. *Tribology International*, 40(4), pp. 580-587.

- Aoustin, Y., Formal'skii, A.M. (2013). Modeling, control and simulation of upward jump of a biped. *Multibody Systems Dynamics*, 29(4), pp. 425-445.
- Arabyan, A., Wu, F. (1998). An improved formulation for constrained mechanical systems. *Multibody Systems Dynamics*, 2(1), pp. 49-69.
- Armstrong-Hélouvry, B. (1991). *Control of machines with friction*, Kluwer Academic Publishers, Norwell, Massachusetts.
- Armstrong-Hélouvry, B., Dupont, P., Canudas de Wit, C. (1994). A survey of models, analysis tools and compensation methods for the control of machines with friction. *Automatica*, 30(7), pp. 1083-1138.
- Awrejcewicz, J., Olejnik, P. (2007). Occurrence of stick-slip phenomenon. *Journal of Theoretical and Applied Mechanics*, 35(1), pp. 33-40.
- Awrejcewicz, J., Grzelczyk, D., Pyryev, Y. (2008). A novel dry friction modeling and its impact on differential equations computation and Lyapunov exponents estimation. *Journal of Vibroengineering*, 10(4), pp. 475-482.
- Bai, Z.F., Zhao, Y. (2012). Dynamic behaviour analysis of planar mechanical systems with clearance in revolute joints using a new hybrid contact force model. *International Journal of Mechanical Sciences*, 54(1), pp. 190-205.
- Baumgarte, J. (1972). Stabilization of Constraints and Integrals of Motion in Dynamical Systems. *Computer Methods in Applied Mechanics and Engineering*, 1, pp. 1-16.
- Bayo, E., García de Jalón, J., Serna, M.A. (1988). A modified Lagrangian formulation for the dynamic analysis of constrained mechanical systems. *Computer Methods in Applied Mechanics and Engineering*, 71(2), pp. 183-195.
- Ben Horin, P., Djerassi, S., Sholam, M., Ben Horin, R. (2006). Dynamics of a six degrees-of-freedom parallel robot actuated by three two-wheel carts. *Multibody Systems Dynamics*, 16(2), pp. 105-121.
- Bengisu M.T., Akay, A. (1994). Stability of Friction-Induced Vibrations in Multi-Degree-of-Freedom Systems. *Journal of Sound and Vibration*, 171(4), pp. 557-570.
- Berger, E.J. (2002). Friction modeling for dynamic system simulation. *Applied Mechanics Reviews*, Vol. 55(6), pp. 535-577.
- Berger, E.J., Mackin, T.J. (2014). On the walking stick-slip problem. *Tribology International*, 75, pp. 51-60.

- Bicakci, S., Akdas, D., Karaoglan, A.D. (2014). Optimizing Karnopp friction model parameters of a pendulum using RSM. *European Journal of Control*, 20(4), pp. 180-187.
- Blajer, W. (1995). An orthonormal tangent space method for constrained multibody systems. *Computer Methods in Applied Mechanics and Engineering*, 121, pp. 45-57.
- Bliman, P.-A., Sorine, M. (1991). Friction modelling by hysteresis operators: application to Dahl, stiction and Stribeck effects. In *Proceedings of the Conference "Models of Hysteresis"*, Trento, Italy.
- Bliman, P.-A., Sorine, M. (1993). A system-theoretic approach of systems with hysteresis: Application to friction modelling and compensation. In *Proceedings of the second European Control Conference*, Groningen, The Netherlands, pp. 1844-1849.
- Bliman, P.A., Sorine, M. (1995). Easy-to-use realistic dry friction models for automatic control. *Proceedings of 3rd European Control Conference*, Rome, Italy, pp. 3788-3794.
- Bo, L.C., Pavelescu, D. (1982). The friction-speed relation and its influence on the critical velocity of stick-slip motion. *Wear*, 82(3), pp. 277-289.
- Borsotto, B., Godoy, E., Beauvois, D., Devaud, E. (2009). An Identification Method for Static and Coulomb Friction Coefficients. *International Journal of Control, Automation, and Systems*, 7(2), pp. 305-310.
- Bowden, F.P., Leben, L. (1939). The nature of sliding and the analysis of friction. *Proceedings of the Royal Society of London, Series A, Mathematical and Physical Sciences*, 169, pp. 371-391.
- Brutti, C., Coglitore, G., Valentini, P.P. (2011). Modeling 3D revolute joint with clearance and contact stiffness. *Nonlinear Dynamics*, 66(4), pp. 531-548.
- Canudas de Wit, C., Olsson, H., Åström, K.J., Lischinsky, P. (1995). A new model for control of systems with friction. *IEEE Transactions on Automatic Control*, 40(3), pp. 419-425.
- Chatelet, E., Michon, G., Manin, L., Jacquet, G. (2008). Stick/slip phenomena in dynamics: Choice of contact model. Numerical predictions & experiments. *Mechanism and Machine Theory*, 43(10), pp. 1211-1224.
- Coulomb, C.A. (1785). Théorie des machines simples, en ayant égard au frottement de leurs parties, et à la roideur des cordages. *Mémoire de Mathématique et de Physique*, Paris, France.

- Courtney-Pratt, J., Eisner, E. (1957). The effect of a tangential force on the contact of metallic bodies. *Proceedings of the Royal Society*, 238(1215), pp. 529-550.
- Dahl, P.R. (1968). *A solid friction model*, Technical Report, The Aerospace Corporation, El Segundo, California.
- Dahl, P.R. (1976). Solid friction damping in mechanical vibrations. *AIAA Journal*, 14(12), pp. 1675-1682.
- Dahl, P.R. (1977). *Measurement of Solid Friction Parameters of Ball Bearings*, Technical Report, The Aerospace Corporation, El Segundo, California.
- D' Alembert, J. (1743). *Traité de Dynamique*, Paris.
- Dankowicz, H. (1999). On the modelling of dynamic friction phenomena. *Journal of Applied Mathematics and Mechanics*, 79(6), pp. 399-409.
- De Moerlooze, K., Al-Bender, F., Van Brussel, H. (2010). A Generalised Asperity-Based Friction Model. *Tribology Letters*, 40(1), pp. 113-130.
- Derjaguin, B.V., Muller, V.M., Toporov, Y.P. (1975). Effect of Contact Deformations on the Adhesion of Particles. *Journal of Colloid and Interface Science*, 53(2), pp. 314-326.
- Dieterich, J. (1978). Time-Dependent Friction and the Mechanics of Stick-Slip. *Pure and Applied Geophysics*, 116(4), pp. 790-806.
- Do, N.B., Ferri, A.A., and Bauchau, O.A. (2007). Efficient Simulation of a Dynamic System with LuGre Friction. *Journal of Computational and Nonlinear Dynamics*, 2(4), pp 281–289.
- Dubowsky, S., Freudenstein, F. (1971). Dynamic Analysis of Mechanical Systems with Clearances, Part 1: Formulation of Dynamic Model. *Journal of Engineering for Industry, Series B*, 93(1), pp. 305-309.
- Dupont, P.E., Dunlap, E.P. (1993). Friction Modeling and Control in Boundary Lubrication. *Proceedings of the 1993 American Control Conference*, San Francisco, California, pp. 1910-1914.
- Dupont, P., Armstrong, B., Hayward, V. (2000). Elasto-Plastic Friction Model: Contact Compliance and Stiction. *Proceedings of the 2000 American Control Conference*, 2, pp. 1072-1077.
- Dupont, P., Hayward, V., Armstrong, B., Altpeter, F. (2002). Single State Elasto-Plastic Friction Models. *IEEE Transactions on Automatic Control*, 47(5), pp. 787-792.



- ESDU-78035 Tribology Series (1978). Contact Phenomena. I: stresses, deflections and contact dimensions for normally-loaded unlubricated elastic components. *Engineering Sciences Data Unit*, London, England.
- Euler, L. (1776). Nova methods motum corporum rigidarum determinandi. *Novi Commentarii Academiae Scientiarum Petropolitanae*, 20, pp. 208-238.
- Flores, P. (2004). *Dynamic analysis of mechanical systems with imperfect kinematic joints*, Ph.D. Thesis, University of Minho, Portugal.
- Flores, P., Ambrósio, J. (2004). Revolute joints with clearance in multibody systems. *Computers and Structures*, 82, pp. 1359-1369.
- Flores, P., Ambrósio, J., Claro, J.C.P., Lankarani, H.M. (2006a). Influence of the contact-impact force model on the dynamic response of multi-body systems. *Proceedings of the Institution of Mechanical Engineers. Part K: Journal of Multi-body Dynamics*, 220(1), pp. 21-34.
- Flores, P., Ambrósio, J., Claro, J.C.P., Lankarani, H.M. (2006b). Spatial revolute joints with clearances for dynamic analysis of multi-body systems. *Proceedings of the Institution of Mechanical Engineers. Part K: Journal of Multi-body Dynamics*, 220(4), pp. 257-271.
- Flores, P. (2009). Modeling and simulation of wear in revolute clearance joints in multibody systems. *Mechanism and Machine Theory*, 44, pp.1211-1222.
- Flores, P. (2010). A parametric study on the dynamic response of planar multibody systems with multiple clearance joints. *Nonlinear Dynamics*, 61(4), pp. 633-653.
- Flores, P., Ambrósio, J. (2010). On the contact detection for contact-impact analysis in multibody systems. *Multibody Systems Dynamics*, 24(1), pp. 103-122.
- Flores, P., Leine, R., Glocker, C. (2010). Modeling and analysis of planar rigid multi-body systems with translational clearance joints based on the non-smooth dynamics approach. *Multibody Systems Dynamics*, 23(2), pp. 165-190.
- Flores, P. (2011) A methodology for quantifying the position errors due to manufacturing and assemble tolerances. *Journal of Mechanical Engineering*, 57(6), pp. 457-467.
- Flores, P., Machado, M., Silva, M.T., Martins, J.M. (2011a). On the continuous contact force models for soft materials in multibody dynamics. *Multibody System Dynamics*, 25(3), pp. 357-375.
- Flores, P., Machado, M., Seabra, E., Silva, M.T. (2011b). A Parametric Study on the Baumgarte Stabilization Method for Forward Dynamics of Constrained Multibody Systems. *Journal of Computational and Nonlinear Dynamics*, 6(1), 9p.

- Flores, P., Koshy, C.S., Lankarani, H.M., Ambrósio, J., Claro, J.C.P. (2011c). Numerical and experimental investigation on multibody systems with revolute clearance joints. *Nonlinear Dynamics*, 65(4), pp. 383-398.
- Flores, P. (2012). MUBODYNA - A MATLAB program for dynamic analysis of spatial multibody systems. University of Minho, Guimarães, Portugal.
- Flores, P. (2013). A methodology to eliminate the violation of the constraint equations for forward dynamics of constrained multibody systems. *Congreso de Métodos Numéricos en Ingeniería*, Bilbao, Spain, 18p.
- Fréne, J., Cicone, T. (2001). Friction in Lubricated Contacts. *Handbook of Material Behavior Models*, Academic Press, pp. 760-767.
- Garcia, C. (2008). Comparison of friction models applied to a control valve. *Control Engineering Practice*, 16(10), pp. 1231-1243.
- García de Jalón, J., Bayo, E. (1994). *Kinematic and Dynamic Simulations of Multibody Systems*, Springer-Verlag, New York, New York.
- García de Jalón, J., Gutiérrez-López, M.D. (2013) Multibody dynamics with redundant constraints and singular mass matrix: existence, uniqueness, and determination of solutions for accelerations and constraint forces. *Multibody Systems Dynamics*, 30(3), pp. 311-341.
- Gilardi, G., Sharf, I. (2002). Literature survey of contact dynamics modelling. *Mechanism and Machine Theory*, 37, pp. 1213-1239.
- Glocker, C., Studer, C. (2005). Formulation and Preparation for Numerical Evaluation of Linear Complementarity Systems in Dynamics. *Multibody Systems Dynamics*, 13(4), pp. 447-463.
- Goldsmith, W. (1960). *Impact, The Theory and Physical Behaviour of Colliding Solids*, Edward Arnold Ltd., London, England.
- Gonthier, Y., McPhee, J., Lange, C., Piedboeuf, J.-C. (2004). A regularized contact model with asymmetric damping and dwell-time dependent friction. *Multibody System Dynamics*, 11(3), pp. 209-233.
- Haessig, D. A., Friedland, B. (1991). On the modeling and simulation of friction. *Journal of Dynamic Systems, Measurement, and Control*, 113(3), pp. 354-362.
- Hamaker, H.C. The London - van der Waals attraction between spherical particles. *Physica*, 4(10), pp. 1058-1072.
- Hassan, M.A., Rogers, R.J. (2005). Friction modelling of preloaded tube contact dynamics. *Nuclear Engineering and Design*, 235(22), pp. 2349-2357.

- Harnoy, A., Friedland, B. (1994). Dynamic Friction Model of Lubricated Surfaces for Precise Motion Control. *Tribology Transactions*, 37(3), pp. 608-614.
- Haug, E.J. (1989). *Computer-Aided Kinematics and Dynamics of Mechanical Systems - Volume I: Basic Methods*, Allyn and Bacon, Boston, Massachusetts.
- Hensen, R.H.A., van de Molengraft, M.J.G., Steinbuch, M. (2003). Friction induced hunting limit cycles: A comparison between the LuGre and switch friction model. *Automatica*, 39(12), pp. 2131-2137.
- Herbert, R.G., McWhannell, D.C. (1977). Shape and frequency composition of pulses from an impact pair. *Journal of Engineering for Industry*, 99(3), pp. 513-518.
- Hertz, H. (1881). Über die Berührung fester elastischer Körper. *Journal reine und angewandte Mathematik*, 92, pp. 156-171.
- Hess, D.P., Soom, A. (1990). Friction at a lubricated line contact operating at oscillating sliding velocities. *Journal of Tribology*, 112(1), pp. 147-152.
- Hsieh, C., Pan, Y.-C. (2000). Dynamic behavior and modelling of the pre-sliding static friction. *Wear*, 242(1), pp. 1-17.
- Hunt, K.H., Crossley, F.R.E. (1975). Coefficient of restitution interpreted as damping in vibroimpact. *Journal of Applied Mechanics*, 42(2), pp. 440-445.
- Huston, R.L. (1990). *Multibody Dynamics*, Butterworth-Heinemann, Boston, Massachusetts.
- Iurian, C., Ikhoulane, F., Rodellar, J., Griñó, R. (2005). *Identification of a system with dry friction*. Technical Report, Universitat Politècnica de Catalunya, Spain.
- Jackson, R.L., Green, I., Marghitu, D.B. (2010). Predicting the coefficient of restitution of impacting elastic-perfectly plastic spheres. *Nonlinear Dynamics*, 60(3), pp. 217-229.
- Johnson, K.L., Kendall, K., Roberts, A.D. (1971). Surface Energy and the Contact of Elastic Solids. *Proceedings of the Royal Society of London. Series A, Mathematical and Physical*, 324, pp. 301-313.
- Johannes, V.I., Green, M.A., Brockley, C.A. (1973). The role of the rate of application of the tangential force in determining the static friction coefficient. *Wear*, 24(3), pp. 381-385.
- Johnson, K.L. (1985). *Contact Mechanics*, Cambridge University Press, Cambridge, United Kingdom.

- Kale, K.G., Rampalli, R. (2011). On the application of the LuGre model to simulate joint friction in multi-body-systems. *Proceedings of the ASME 2011 International Design Engineering Technical Conferences & Computers and Information in Engineering Conference*, Washington, D.C., USA, 10p.
- Kane, T.R., Levinson, D.A. (1985). *Dynamics: Theory and Applications*, McGraw-Hill, New York, New York.
- Kalaba, R.E., Udwadia, F.E. (1993). Equations of Motion for Nonholonomic, Constrained Dynamical Systems via Gauss's Principle. *Journal of Applied Mechanics*, 60(3), pp. 662-668.
- Karnopp, D. (1985). Computer Simulation of Stick-Slip Friction in Mechanical Dynamic Systems. *Journal of Dynamic Systems, Measurement, and Control*, 107(1), pp.100-103.
- Kim, H.K., Guibas, L.J., Shin, S.Y. (2005). Efficient Collision Detection among Moving Spheres with Unknown Trajectories. *Algorithmica*, 43(3), pp. 195-210.
- Koshy, C.S., Flores, P., Lankarani, H.M. (2013). Study of the effect of contact force model on the dynamic response of mechanical systems with dry clearance joints: computational and experimental approaches. *Nonlinear Dynamics*, 73(1), pp. 325-338.
- Ksentini, O., Abbes, M.S., Abdessalem, J., Chaari, F., Haddar, M. (2012). Study of Mass Spring System Subjected to Dahl Friction. *International Journal of Mechanic Systems Engineering*, 2(1), pp. 34-41.
- Lagrange, J.-L. (1788). *Mécanique Analytique*, L'Académie Royal des Sciences, Paris, France.
- Lampaert, V., Swevers, J., Al-Bender, F. (2002). Experimental comparison of different friction models for accurate low-velocity tracking. *Proceedings of the 10th Mediterranean conference on control and Automation - MED2002*, Lisbon, Portugal, 9p.
- Lampaert, V., Al-Bender, F., Swevers, J. (2003). A generalized maxwell-slip friction model appropriate for control purposes. *Proceedings of IEEE International Conference on Physics and Control*, St. Petersburg, Russia, pp. 1170-1178.
- Lankarani, H.M., Nikravesh, P.E. (1990). A contact force model with hysteresis damping for impact analysis of multibody systems. *Journal of Mechanical Design*, 112(3), pp. 369-376.
- Lankarani, H.M., Nikravesh, P.E. (1994). Continuous contact force models for impact analysis in multibody systems. *Nonlinear Dynamics*, 5(2), pp. 193-207.

- Lee, T.W. Wang, A.C. (1983). On the dynamics of intermittent-motion mechanisms, Part 1: dynamic model and response. *Journal of Mechanisms, Transmissions, and Automation in Design*, 105(3), pp. 534-540.
- Leine, R.I., van Campen, D.H., de Kraker, A., van den Steen, L. (1998). Stick-Slip Vibrations Induced by Alternate Friction Models. *Nonlinear Dynamics*, 16(1), pp. 41-54.
- Liang, J., Fillmore, S., Ma, O. (2012). An extended bristle friction force model with experimental validation. *Mechanism and Machine Theory*, 56, pp. 123-137.
- Lin, M., Gottschalk, S. (1998). Collision detection between geometric models: A survey. *Proceedings of IMA Conference on Mathematics of Surfaces*, Birmingham, United Kingdom, pp. 602-608.
- Liu, L., Liu, H., Wu, Z., Yuan, D. (2009). A new method for the determination of the zero velocity region of the Karnopp model based on the statistics theory. *Mechanical Systems and Signal Processing*, 23(5), pp. 1696-1703.
- Liu, Y.F., Li, J., Zhang, Z.M., Hu, X.H., Zhang, W.J. (2015). Experimental comparison of five friction models on the same test-bed of the micro stick-slip motion system. *Mechanical Sciences*, 6(1), pp. 15-28.
- Machado, M. (2013). *A multibody approach to the contact dynamics: a knee joint application*, Ph.D. Thesis, University of Minho, Portugal.
- Machado, M., Moreira, P., Flores, P., Lankarani, H.M. (2012). Compliant contact force models in multibody dynamics: Evolution of the Hertz contact theory. *Mechanism and Machine Theory*, 53, pp. 99-121.
- Makkar, C., Dixon, W.E., Sawyer, W.G., Hu, G. (2005). A New Continuously Differentiable Friction Model for Control Systems Design. *Proceedings of the 2005 IEEE/ASME, International Conference on Advanced Intelligent Mechatronics*, pp. 600-605.
- Marques, F., Flores, P., Lankarani, H.M. (2015). On the Frictional Contacts in Multibody System Dynamics. *Proceedings of ECCOMAS 2015 Thematic Conference on Multibody Dynamics*, Barcelona, Catalonia, Spain, 12p.
- Maugis, D. (1992). Adhesion of spheres: The JKR-DMT transition using a dugdale model. *Journal of Colloid and Interface Science*, 150(1), pp. 243-269.
- Morin, A.J. (1833). New friction experiments carried out at Metz in 1831–1833. *Proceedings of the French Royal Academy of Sciences*, 4, pp. 1-128.

- Muvengei, O., Kihuu, J., Ikua, B. (2012). Dynamic analysis of planar multi-body systems with LuGre friction at differently located revolute clearance joints. *Multibody System Dynamics*, 28(4), pp. 369-393.
- Nassauer, B., Kuna, M. (2013). Contact forces of polyhedral particles in discrete element method. *Granular Matter*, 15(3), pp. 349-355.
- Neto, M.A., Ambrósio, J. (2003). Stabilization Methods for the Integration of DAE in the Presence of Redundant Constraints. *Multibody System Dynamics*, 10(1), pp. 81-105.
- Newton, I. (1687). *Philosophiae Naturalis Principia Mathematica*, Royal Society, London.
- Nikravesh, P.E. (1988). *Computer-Aided Analysis of Mechanical Systems*, Prentice Hall, Englewood Cliffs, New Jersey.
- Nikravesh, P.E. (2004). An Overview of Several Formulations for Multibody Dynamics. *Product Engineering*, 189-226.
- Oleksowicz, S., Mruk, A. (2011). A Basic Theoretical Model for Friction Process at Microasperity Level. *Tribology Transactions*, 54(5), pp. 691-700.
- Olsson, H., Åström, K.J., Canudas de Wit, C., Gäfvert, M., Lischinsky, P. (1998). Friction Models and Friction Compensation. *European Journal of Control*, 4(3), pp. 176-195.
- Qi, Z., Luo, X., Huang, Z. (2011). Frictional contact analysis of spatial prismatic joints in multibody systems. *Multibody System Dynamics*, 26(4), pp. 441-468.
- Park, C.J., Gschwendtner, G. (2015). Braking performance analysis of an escalator system using multibody dynamics simulation technology. *Journal of Mechanical Science and Technology*, 29 (7), pp. 2645-2651.
- Park, K.C., Chiou, J.C. (1988). Stabilization of Computational Procedures for Constrained Dynamical Systems. *Journal of Guidance, Control, and Dynamics*, 11, pp. 365-370.
- Pereira, C.M., Ramalho, A.L., Ambrósio, J.A. (2011). A critical overview of internal and external cylinder contact force models. *Nonlinear Dynamics*, 63(4), pp. 681-697.
- Pennestrì, E., Valentini, P.P., Vita, L. (2007). Multibody dynamics simulation of planar linkages with Dahl friction. *Multibody Systems Dynamics*, 17(4), pp. 321-347.
- Pfeiffer, F., Glocker, C. (1996). *Multibody Dynamics with Unilateral Contacts*, John Wiley & Sons, New York, New York.

- Pfeiffer, F. (2008). On non-smooth dynamics. *Meccanica*, 43(5), pp. 533-554.
- Piatkowski, T. (2014a). Dahl and LuGre dynamic friction models - The analysis of selected properties. *Mechanism and Machine Theory*, 73, pp. 91-100.
- Piatkowski, T. (2014b). GMS friction model approximation. *Mechanism and Machine Theory*, 75, pp. 1-11.
- Pombo, J.C., Ambrósio, J.A.C. (2008). Application of a wheel-rail contact model to railway dynamics in small radius curved tracks. *Multibody Systems Dynamics*, 19(1), pp. 91-114.
- Pombo, J.C., Ambrósio, J.A.C. (2012). An alternative method to include track irregularities in railway vehicle dynamic analyses. *Nonlinear Dynamics*, 68(1), pp. 161-176.
- Popp, K., Stelter, P. (1990). Nonlinear oscillations of structures induced by dry friction. *Nonlinear Dynamics in Engineering Systems*, pp. 233-240
- Rabinowicz, E. (1951). The Nature of the Static and Kinetic Coefficients of Friction. *Journal of Applied Physics*, 22, pp. 1373-1379.
- Rabinowicz, E. (1956). Stick and Slip. *Scientific American*, 194, pp. 109-118.
- Radzimovsky, E.I. (1953). *Stress distribution and strength conditions of two rolling cylinders pressed together*, University of Illinois Bulletin, Engineering Experiment Station, 408.
- Rhee, J., Akay, A. (1996). Dynamic Response of a Revolute Joint with Clearance. *Mechanism and Machine Theory*, 31(1), pp. 121-124.
- Roberson, R.E. and Schwertassek, R. (1988). *Dynamics of Multibody Systems*, Springer-Verlag, Berlin, Germany.
- Ruderman, M., Bertram, T. (2013). Two-state dynamic friction model with elasto-plasticity. *Mechanical Systems and Signal Processing*, 39, pp. 316-332.
- Schiehlen, W. (1990). *Multibody Systems Handbook*, Springer-Verlag, Berlin, Germany.
- Schwab, A.L., Meijaard, J.P., Meijers, P. (2002). A comparison of revolute joint clearance models in the dynamic analysis of rigid and elastic mechanical systems. *Mechanism and Machine Theory*, 37(9), pp. 895-913.
- Ścieszka, S.F, Jankowski, A. (1996). The Importance of Static Friction Characteristics of Brake Friction Couple, and Methods of Testing. *Tribotest*, 3(2), pp. 137-148.

- Seifried, R., Schiehlen, W., Eberhard, P. (2010). The role of the coefficient of restitution on impact problems in multi-body dynamics. *Proceedings of the Institution of Mechanical Engineers, Part K: Journal of Multi-body Dynamics*, 224, pp. 279-306.
- Shabana, A.A. (1989). *Dynamics of Multibody Systems*, John Wiley and Sons, New York, New York.
- Signorini, A. (1933). Sopra alcune questioni di elastostatica. *Atti della Societa Italian per il Progresso della Scienza*.
- Sousa, L., Verissimo, P., Ambrósio, J. (2008). Development of generic multibody road vehicle models for crashworthiness. *Multibody Systems Dynamics*, 19(1), pp. 133-158.
- Stribeck, R. (1902). Die wesentlichen Eigenschaften der Gleitund Rollenlager. *Zeitschrift des Vereines Deutscher Ingenieure*, 46(38), pp. 1342-1348, 1432-1438; 46(39), pp. 1463-1470.
- Swevers, J., Al-Bender, F., Ganseman, C.G., Projogo, T. (2000). An integrated friction model structure with improved presliding behavior for accurate friction compensation. *IEEE Transactions on Automatic Control*, 45(4), pp. 675-686.
- Teixeira, R.R., Moreira, S.R.D.S., Tavares, S.M.O. (2015). Multibody dynamics simulation of an electric bus. *Procedia Engineering*, 114, pp. 470-477.
- Threlfall, D.C. (1978). The inclusion of Coulomb friction in mechanisms programs with particular reference to DRAM au programme DRAM. *Mechanism and Machine Theory*, 13(4), pp. 475-483.
- Tian, Q., Zhang, Y., Chen, L., Yang, J. (2010). Simulation of planar flexible multibody systems with clearance and lubricated revolute joints. *Nonlinear Dynamics*, 60(4), pp. 489-511.
- Tian, Q., Liu, C., Machado, M., Flores, P. (2011). A new model for dry and lubricated cylindrical joints with clearance in spatial flexible multibody systems. *Nonlinear Dynamics*, 64(1), pp. 25-47.
- Tjahjowidodo, T., Al-Bender, F., Van Brussel, H. (2005). Friction identification and compensation in a DC motor. *Proceedings of the 16th IFAC World Congress*, Prague, Czech Republic, 6p.
- Tustin, A. (1947). The effects of backlash and of speed-dependent friction on the stability of closed-cycle control systems. *Journal of the Institution of Electrical Engineers*, 94(1), pp. 143-151.



- Wehage, R.A., Haug, E.J. (1982). Generalized coordinate partitioning for dimension reduction in analysis of constrained systems. *Journal of Mechanical Design*, 104, pp. 247-255.
- Weijia, Z., Zhenkuan, P., Yibing, W. (2000). An automatic constraint violation stabilization method for differential/algebraic equations on multibody system dynamics. *Applied Mathematics and Mechanics*, 21(1), pp. 103-108.
- Wittenburg, J. (1977). *Dynamics of Systems of Rigid Bodies*, Teubner, Stuttgart, Germany.
- Wojewoda, J., Stefański, A., Wiercigroch, M., Kapitaniak, T. (2008). Hysteretic effects of dry friction: modelling and experimental studies. *Philosophical Transactions of the Royal Society A*, 366, pp. 747-765.
- Wu, X.D., Zuo, S.G., Lei, L., Yang, X.W., Li, Y. (2011). Parameter identification for a LuGre model based on steady-state tire conditions. *International Journal of Automotive Technology*, 12(5), pp. 671-677.
- Xu, W., Meng, D., Chen, Y., Qian, H., Xu, Y. (2014). Dynamics modeling and analysis of a flexible-base space robot for capturing large flexible spacecraft. *Multibody Systems Dynamics*, 32(3), pp. 357-401.
- Yan, S., Xiang, W., Zhang, L. (2015). A comprehensive model for 3D revolute joints with clearances in mechanical systems. *Nonlinear Dynamics*, 80(1), pp. 309-328.
- Ylinen, A., Marjamäki, H., Mäkinen, J. (2014). A hydraulic cylinder model for multibody simulations. *Computers and Structures*, 138, pp. 62-72.
- Yoon, S., Howe, R.M., Greenwood, D.T. (1994). Geometric elimination of constraint violations in numerical simulation of Lagrangian equations. *Journal of Mechanical Design*, 116, pp. 1058-1064.
- Yu, Q., Chen, I.-M. (2000). A direct violation correction method in numerical simulation of constrained multibody systems. *Computational Mechanics*, 26, pp. 52-57.
- Zhiying, Q., Qishao, L. (2006). Analysis of impact process based on restitution coefficient. *Journal of Dynamics and Control*, 4, pp. 294-298.
- Zhuang, F., Wang, Q. (2013). Modeling and simulation of the nonsmooth planar rigid multibody systems with frictional translational joints. *Multibody Systems Dynamics*, 29(4), pp. 403-423.
- Zhuang, F.-F., Wang, Q. (2014). Modeling and analysis of rigid multibody systems with driving constraints and frictional translation joints. *Acta Mechanica Sinica*, 30(3), pp. 437-446.